REMOTE SENSING TECHNIQUES FOR MONITORING AQUATIC VEGETATION

by

Alfonso Blanco

A Dissertation
Submitted to the
Graduate Faculty
of
George Mason University
in Partial Fulfillment of
The Requirements for the Degree
of
Doctor of Philosophy
Earth Systems and Geoinformation Sciences

Committee:

_____ Dr. John J. Qu, Dissertation Director

_____ Dr. Ruixin Yang, Committee Member

_____ Dr. Daniel Carr , Committee Member

_____ Dr. Alan Falconer, Committee Member

_____ Dr. William Roper, Committee Member

_____ Dr. Peggy Agouris, Department Chair

_____ Dr. Timothy L. Born, Associate Dean for Student and Academic Affairs, College of Science

_____ Dr. Vikas Chandhoke, Dean, College of Science

Date: _____ Spring Semester 2013

George Mason University

Fairfax, VA

Remote Sensing Techniques for Monitoring Aquatic Vegetation

A Dissertation submitted in partial fulfillment of the requirements for the degree of Doctor of Philosophy at George Mason University

by

Alfonso Blanco
Master in Science
Tufts University, 1981

Director: John J. Qu, Professor
Department of Earth Systems and Geoinformation Sciences

Spring Semester 2013
George Mason University
Fairfax, VA

DEDICATION

I dedicate this Dissertation to my sister Esq. Patricia Fernandez who passed away in 2001; to my mother Dinorah B. Fernandez who has encouraged me to obtain a higher education and to achieve scholastic achievement; to my uncle Professor Emeritus Ernesto E. Blanco who taught Mechanical Engineering for 40 years at MIT, who was my father figure throughout my entire life and who also encouraged me to continue my education; to my wife who has been very patient and supportive and understood the importance of completing this work; and finally I am dedicating this Dissertation to my daughters, sons-in-law, grandson and granddaughter for their support.

ACKNOWLEDGEMENTS

After many years of studying and researching the science of remote sensing, it is a great accomplishment for me to finish this research. I am very proud of myself because I completed my research while working full time, but I am very grateful to those persons who have helped me along the way for whom I could not have done without. My family made me who I am and supported me all these years. I will always be grateful to them for their unconditional and overwhelming love. They were the ones that supported my ideas and dreams to continue my doctoral degree. I would like to thank Dr. John J. Qu and the rest of the Committee members who unconditionally agreed to be in my Committee and gave me suggestions, together with their perspectives toward my research. I am grateful to them for their valuable time, patience, and support. I would like to thank Dr. Xianjun Hao and the rest of the EastFire personnel for uploading the hydrilla database into the EastFire website. I would like to thank Dr. William Roper, who embarked me on this journey twelve years ago and has been my pillar all these years as my Advisor at George Washington University, and as a personal friend. I would like to thank Dr. Terence Slonecker of USGS for assisting me in collecting the in-situ field measurements. I would like to thank the personnel at the Anita Leight Center for providing access to the study site,and specifically Dr. Patricia Delgado who made available the ground survey data for the validation of hydrilla. Mr. Larry Ong from NASA GSFC for tasking the Hyperion satellite, Mr. Richard Perk for providing the AISA airborne image, Robert Orth and David Wilcox of the Virginia Institute of Marine Sciences (VIMS) for providing the aerial photos of the study area, and Dr. Foudan Salem who worked with me countless hours making sure that the image processing and analysis was accurate. Also, I would like to thank the Technical Support Group at ITT-Exelis for providing the necessary training and technical support, answering questions and resolving issues with the image processing techniques. I would like to thank the US Environmental Protection Agency for providing partial financial support for my training and especially my Supervisor Kellie Kubena for being so understanding and supportive. Finally, I would like to thank the Department of Geography and Geoinformation Sciences for providing me access to the software license in order to perform the image analysis. Without the cooperation of these individuals and entities, I could not have prepared this Dissertation.

TABLE OF CONTENTS

Page

LIST OF TABLES

Table Page

LIST OF FIGURES

Figure Page

LIST OF EQUATIONS

LIST OF ABBREVIATIONS OR SYMBOLS

Area Under the Curve……AUC
Airborne Spectrometer for Applications..... AISA
Analytical Spectral Device .....ASD
Center for Advanced Land Management Information Technologies ..... CALMIT
Chlorophyll Absorption Ratio Index .....CARI
Colored Dissolved Organic Matter .....CDOM
Chlorophyll a .....Chl a
Digital Numbers .....DN
Dissolved Inorganic Nitrogen ..... DIN
Dissolved Inorganic Phosphorus.....DIP
Dissolved Organic Matter ..... DOM
Electromagnetic Spectrum ..... EMS
Environmental Systems Research Institute……...ESRI
Environment for Visualizing Images .....ENVI
Fast Line-of-Sight Atmospheric Analysis of Spectral Hypercube .....FLAASH
Geographic Information System .....GIS
Global Positioning System…… GPS
Goddard Space Flight Center……...GSFC
Hydrilla vertillicata……...Hv
Inherent Optical Properties .....IOP
Minimum Noise Fraction.....MNF
Maryland Department of Environment.....MDE
Maryland Department of Natural Resources……..MDDNR
National Aeronautics and Space Administration.....NASA
Near Infrared Region .....NIR
Nephetolometric Turbidity Units……...NTU
New Millennium Program .....NMP
Normalized Difference Vegetation Index .....NDVI
Otter Point Creek .....OPC
Pixel Purity Index .....PPI
Quick Atmospheric Correction ..... QUAC
Receiver Operating Characteristics Curves……...ROC
Region of Interest.....ROI
Shortwave Infrared……...SWIR
Spectral Hourglass Wizard……SHW
Standard Operating Procedure ..... SOP

Spectral Angle Mapper ..... SAM
Submerged Aquatic Vegetation ..... SAV
Total Suspended Matter ..... TSM
Total Suspended Solids ..... TSS
United States Geological Survey ..... USGS
Virginia Institute of Marine Sciences ..... VIMS
Visible Near-Infrared ..... VNIR

ABSTRACT

REMOTE SENSING TECHNIQUES FOR MONITORING AQUATIC VEGETATION

Alfonso Blanco, Ph.D.

George Mason University, 2013

DissertationDirector: Dr. John J. Qu

This research addresses the need for a more accurate, efficient, large–scale and timely methods for identifying and mapping hydrilla infestation in coastal estuaries and other water bodies, as nutrient loadings continue to exert pressures on estuarine habitats. The majority of hydrilla infestations surveys are presently completed through ground surveys and manual aerial photograph interpolation which is time consuming, costly and subject to inconsistencies. Remote sensing has been used for assessing wetlands and other non-invasive aquatic species, but there is limited information on the detection of hydrilla using hyperspectral sensors. The first objective of this research was to establish a database of hydrilla spectral signatures from an experimental tank and from a field setting using a spectrometer. These spectral signatures will be used to identify the optimal spectral and spatial characteristics that are required to identify and classify the distribution of hydrilla canopies in a coastal estuary.

The second objective is to process the Hyperion satellite images with workflow process in ENVI version 4.8, named the Spectral Hourglass Wizard. This processing technique analyzes the hyperspectral images using several evaluation algorithms such as the Minimum Noise Fraction (MNF), Pure Pixel Index, n- D Visualization and the 2 D Scatter plot. Another image analysis tool the Spectral Angle Mapper (SAM) was applied to the hyperspectral images for classifying the hydrilla canopy and then matching the endmember collected spectra with the spectral library profiles that were developed from the in-situ field measurements.

The third objective was to process the airborne image collected with the AISA sensor with the same Spectral Hourglass Wizard workflow process.

The fourth objective was to validate the satellite and airborne hyperspectral images with the spectral signatures collected from the experimental tank and the field measurements. In addition, the Hyperion and AISA imaging results were compared with the aerial photos collected by the Virginia Institute of Marine Sciences (VIMS) and the ground survey data collected by Maryland Department of Natural Resources (MDDNR) for verifying the extent and the location of the hydrilla canopies.

The spectral signatures from the experimental tank and the field were compared to the spectral signatures resulting from the MNF and SAM spectral profiles which showing that the Hyperion image produced a spectral reflectance averaging 18% which can be interpreted that the hydrilla canopy was floating or partly submerged. The results of the AISA image were similar to the Hyperion with an average spectral reflectance of 18%. It can be concluded that when reflectance is below 10% the hydrilla canopy is submerged

and when it is above 10 % the hydrilla canopy is floating; however, the higher the reflectance, the more exposed the canopy is above the water surface. The analysis also showed that the average spectral reflectance from the hydrilla tank resulted in a 16 % reflectance compared to the field measurements which was only 6% reflectance. The hyperspectral analysis of both sensors provided for dual results, one is the identification and classification of hydrilla from hyperspectral imaging sensors and secondly the identification of blue-green algae in very productive waters. Accuracy assessment for Hyperion was almost the same as with the AISA sensor. The major contribution of this research was the development of a hydrilla spectral library and remotely identify and classify infestations of hydrilla in productive waters using hyperspectral sensors and simultaneously detect the presence of blue-green algae. The spectral library was established for hydrilla could be used by academia, other researches, as well as consultants to be used on future studies. The achievement of such mapping techniques will provide a more cost-effective (eventually), timely, and repeatable method for creating accurate baseline maps for water resource managers that are less subjective and will benefit the Federal, State and County agencies, as well as the coastal community programs at the national and international level.

CHAPTER ONE: INTRODUCTION

1.1 Background

Executive Order 13112, 1999, defines an invasive species such as *Hydrilla vertillicata* as "any species of plant or animal that is not native to that ecosystem and whose introduction does or is likely to cause economic or environmental harm or harm to human health." Invasive aquatic plant species can have severe ecological and economic impacts and can adversely impact navigation, nutrient cycling in wetlands, water quality, drinking water supplies, hydropower facilities, irrigation, fisheries, recreation, wildlife, and native vegetation diversity (Jakubauskas et al., 2002; Laba et al., 2008; Madden, 2004; Underwood et al., 2006). Federal and state agencies spend millions of dollars annually on aquatic plant management programs. Major portions of these budgets are targeted towards the monitoring and control of invasive aquatic plant species.

The National Invasive Species Council defines an invasive species as non-native to the ecosystem under consideration and whose introduction causes or is likely to cause economic or environmental harm or harm to human health. The Nature Conservancy/University of Florida, ranks hydrilla as the second most invasive plant after water hyacinth, out of 129 aquatic plants in the U.S. evaluated in their risk assessment.

The name hydrilla is derived from the Latin word "hydro" and "illa" meaning something that lives in the water. Verticillata is the Latin word for whorled and refers to

the leaf arrangement of this plant. Hydrilla is an aggressive, invasive, non-native aquatic weed that originated in Southeast Asia. An aquarium business dealer from Tampa, Florida imported this submersed aquatic plant in 1951 (Schmitz et al., 1991). It was first discovered in the wild in a canal in South Florida during the early 1960's (Chadwell and Engelhardt, 2008). Hydrilla was marketed under the name 'Indian star-vine' indicating its origin; it originally shipped to the U.S. from Ceylon, currently Sri Lanka. In 1960, a severe infestation of Indian star-vine was reported in Snapper Creek, southeast of Miami. The plant was incorrectly identified as *Elodea canadensis* until 1965. *Elodea canadensis* does not produce subterranean tubers and the plant was then correctly identified as *Hydrilla verticillata* (Blackburn et al. 1969). *Hydrilla verticillata* (L.F.) Royle is either monoecious or dioecious with both male and female flowers. The monoecious strain is dominant in the Chesapeake Bay area. Presently hydrilla has been found in 21 states across the US, as far north as Maine and Washington State (figure 1).

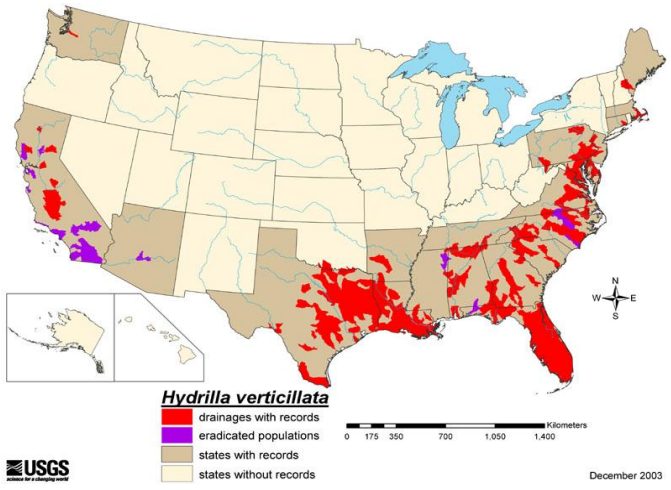

Figure 1 USGS Map of hydrilla coverage in the U.S. (Source: USGS, 2003)

USGS first reported hydrilla in the Chesapeake Bay in August 1982, specifically in the Potomac River (Haller 1982), south of Alexandria, VA and in Kenilworth Aquatic Gardens Ohio (C & O) Canal near Seneca, Marylend. This infestation began in the spring of 1980 when floating cages of hydrilla were incorrectly identified as *Elodea canadensis* and were placed in the Potomac River in order to restore the aquatic grasses.

There is an increased need by governmental agencies, consultants, and private groups for mapping submerged aquatic vegetation (Madden 2004; Shuman and Ambrose 2003).

Satellite imagery is a cost effective method for collecting information and mapping aquatic vegetation in coastal freshwater habitats; satellite imagery costs one half the amount of field surveys (Valta-Hulkkomen et al., 2005).

1.2 The importance of hydrilla

Hydrilla is an important component of wetland and coastal ecosystems, playing a key role in ecological function. Many macrophyte communities are characterized by high growth rates, rapid biomass accumulation, and, in seasonal ecosystems such as wetlands and floodplains, by connection to the flooding pattern of the landscape (Junk 1997). Aquatic plants like hydrilla have a large capacity to absorb harmful substances and pollutants and can be indicators of the eutrophic status of a water body (Onaindia et al., 1996). Monitoring and restoring is a key element for preservation of the Chesapeake Bay. Hydrilla is important to the overall restoration effort because of the various roles it plays in the ecosystem, including the following:

It provides for a nursery habitat, food, and shelter for juvenile fish, blue crabs, and other commercially and ecologically important species.

It serves as a vital food source for resident and migratory waterfowl, some of which are endangered, that consumes both its vegetative material and seeds.

It enhances water clarity by buffering shorelines, reducing sediment resuspension, and trapping suspended particles.

It reduces erosion by stabilizing the sediment with its roots and rhizomes.

It improves water quality by removing toxins and nutrients, such as nitrogen and phosphorus, from the water column.

It produces detritus as it decomposes, which serves as a valuable food source for zooplankton, thereby contributing to energy transfer up the food chain.

It oxygenates the surrounding water column, enhancing water quality for other aquatic organisms.

1.3 Statement of the problem

Waterways can be impaired by infestations of hydrilla, which create several problems for the transportation industry. Dense hydrilla mats can block commercial and recreational traffic through navigable waterways, ports, and passenger ferry terminals. Figure 2 shows the hydrilla invasion on the Potomac River under the Woodrow Wilson Bridge.

Figure 2 Hydrilla infestations on the Potomac River near the Woodrow Wilson Bridge (Source: Washington Suburban Sanitary District)

Floating mats of hydrilla have also been known to exert large amounts of pressure on bridge piers, locks, and docks. The weight of large mats of hydrilla pushed by water currents can scour bridge abutments, weakening infrastructures and thereby requiring costly repairs and/or replacements. This damage to the transportation system caused by hydrilla infestation is a significant and costly problem in southern and coastal states. Hydrilla has an annual maintenance cost of about $110 million, which includes the cost of losses, damages, and management costs associated with the infestations and invasion control (Pimentel et al., 2000). In the Upper Chesapeake Bay hydrilla has spread very rapidly, causing problems in cooling ponds for power generating utility companies. Similar to problems caused in canals, hydrilla mats can clog and damage dams, power plants, and other water control structures. In 1991, hydrilla mats blocked the intake structures at the St. Stephen hydroelectric facility on Lake Moultrie, South Carolina,

forcing the shutdown of the dam and the loss of $4 million in power generation. In addition, the infestation cost $1.2 million for emergency treatment alone (Richardson 2008).

1.4 General description of the study area

The Otter Point Creek is located in the Bush River watershed. This watershed is becoming increasingly urbanized with the densest development located in Harford County's residential and industrial development envelope (figure 3). This envelope was established by Harford County in 1977 in order to direct development towards areas served by water and sewer infrastructure. North of the development area is classified as an agriculture zone. Presently about 35 percent of the Bush River is along developed land, however, the north side of Otter Point Creek, where the Anita Leight Center is located, is undeveloped land. This means there have been little change in the water quality. The Maryland Department of the Environment (MDE) cites this sub watershed in the Bush River basin as an impaired water body because it contains high nutrient loadings, suspended sediments, and toxic substances (Delgado 2011). The Otter Point Creek (OPC) study area is located in the Chesapeake Bay National Estuarine Research Reserve system in Maryland's upper western shore of the Chesapeake Bay Watershed at a latitude of 39.4508 N and longitude of 76.2746 W. OPC is located in Harford County, east of the intersection of U.S. Route 40 and Maryland Route 24, and north of the town of Edgewood as shown in (figures 3, 4) (Pasternak and Hinnov). The creek flows into the Bush River and subsequently drains into the Chesapeake Bay in southeastern Baltimore County. OPC covers 672 acres of open water, tidal marshes, forested wetlands, and

upland hardwood forests surrounded by highways, residential, and commercial development in relatively natural and undisturbed condition. Bush River is located near the U.S. Army Aberdeen Proving Grounds site and is classified as oligohaline (low salinity or brackish waters). The creek is one of the few large tidal freshwater marshes in the upper Chesapeake Bay, which is still in a relatively natural and undisturbed condition (Delgado 2011). OPC consists of an estuarine wetland complex located near the headwaters of the Bush River. Figure 5 is an aerial view of OPC showing upland vegetation, creeks, mudflats, wetlands, and submerged aquatic vegetation.

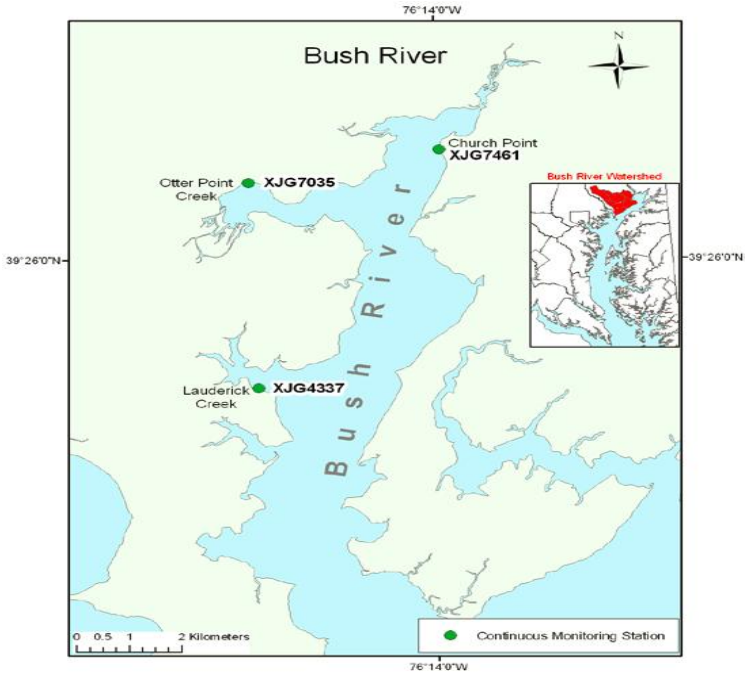

Figure 3 General location map of study area (Source: Pasternak and Hinnov, 2003))

Figure 4 Study area (Source: Pasternak and Hinnov, 2003)

Figure 5 Aerial view of Otter Point Creek (Source: Delgado 2011)

From 2005 thru 2011 the dominant SAV species in Otter Point Creek has been *Hydrilla verticillata* as indicated on Table 1. In 2005, Otter Point Creek had 116 acres covered by hydrilla[21]

Table 1 Ground Survey Data Otter Point Creek (Source: Delgado 2011)

Date	Surveyor	Lat.	Long.	Location	Species
8/23/2007	Delgado	39.444167	-76.275	Otter Point Creek	Hv
10/30/2007	Delgado	39.444167	-76.275	Otter Point Creek	Hv
4/29/2008	Delgado	39.444167	-76.275	Otter Point Creek	Hv
6/20/2008	Delgado	39.444167	-76.275	Otter Point Creek	Hv
10/16/2008	Delgado	39.444167	-76.275	Otter Point Creek	Hv
6/16/2009	Delgado	39.444167	-76.275	Otter Point Creek	Hv, Cd
8/6/2009	Delgado	39.444167	-76.275	Otter Point Creek	Hv
10/8/2009	Delgado	39.444167	-76.275	Otter Point Creek	Hv
6/14/2010	Delgado	39.444167	-76.275	Otter Point Creek	Hv
8/13/2010	Delgado	39.444167	-76.275	Otter Point Creek	Hv
6/6/2011	Delgado	39.444167	-76.275	Otter Point Creek	Hv
8/9/2011	Delgado	39.444167	-76.275	Otter Point Creek	Hv, Nm
10/13/2011	Delgado	39.444167	-76.275	Otter Point Creek	Hv

Hv = Hydrilla
Cd= Elodeas canadensis
Nm- Najas minor

web.VIMS.edu/bio/SAVSAV05/Tble/quadrate_page.htm[2]

1.5 Hydrilla characteristics

Once hydrilla invades an aquatic ecosystem, it competes with other native species for oxygen and can spread very rapidly, growing up to 1 inch per day and forming dense mats (Langeland 1996). Hydrilla reproduces using four mechanisms: fragmentation, turions, tubers, and seeds (figure 6). Hydrilla beds play an important role in supplying fishery habitats, a food source for aquatic and non-aquatic wildlife, slope stabilization, enhancement of sedimentation, and a reduction in wave energy. When hydrilla invades an aquatic ecosystem, it drives out native aquatic plants, creating a pure hydrilla canopy. This noxious weed can impact the aquatic environment by blocking sunlight to other native species. It can survive in a depth of nearly 10 m, anchoring itself in soft sediments along coastal, estuarine, and freshwater habitats (Dennison et al., 1993).

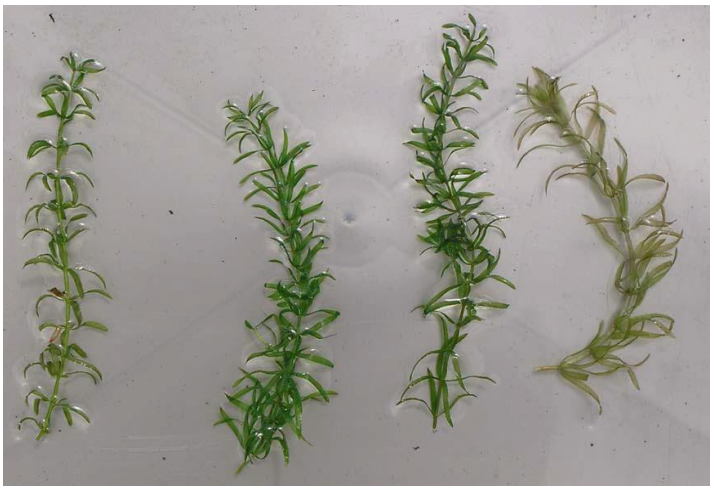

Figure 6 Hydrilla stems (Source: Chadwell, 2004)

Hydrilla's ability to use low light allows it to start photosynthesizing earlier in the morning than other plants. Hydrilla's speed of growth is also impressive. The plant is composed of 93-95 percent water, allowing it to create huge volumes of biomass with very few resources. As a result, it can grow very rapidly, doubling its biomass every two weeks in summer conditions. Hydrilla also branches profusely as it approaches the water surface, densely filling the entire water column up to 10 m deep and shading out other plants. Hydrilla grows very aggressively in a wide variety of water conditions and temperatures; so few habitats are safe from it. Many times hydrilla has been referred as the perfect aquatic weed because it survives in many aquatic environments (Langeland 1996).

1.6 Research objectives

This research effort will identify and classify hydrilla canopies in a coastal estuary using satellite and airborne measurements and validating the results. The specific objectives proposed herein are as follows:

1) The first objective was to build a hydrilla spectral library from in-situ field measurements collected from an experimental tanks and field setting in order to establish a baseline for validation purposes
2) The second objective was to identify and classify hydrilla aquatic vegetation using spaceborne platform (Hyperion) for validation of target identification
3) The third objective was to identify and classify hydrilla aquatic vegetation using an airborne platform (AISA) for validation of target identification

4) The fourth objective was to validate the Hyperion and AISA remote sensing measurements with the in-situ field measurements. Finally a comparison of the image results will be made with VIMS aerial photos and MDDNR ground surveys

1.7 Structure of dissertation

This dissertation consists of eight chapters.

Chapter 1 presents background information on hydrilla and various explanations for the importance of Submerged Aquatic Vegetation (SAV), a statement of the problem, research objectives, structure of the dissertation, and major data sources.

Chapter 2 presents a literature review and addresses previous research in aerial photography, field measurements, and remote sensing of aquatic vegetation.

Chapter 3 discusses theory of aquatic optics and remote sensing of aquatic vegetation.

Chapter 4 presents the field measurements collected in-situ and the procedures for the data collection from the experimental tanks and from the estuary. The data was analyzed and the results shown.

Chapter 5 covers remote sensing techniques for processing a Hyperion image with the Environment for Visualizing Software (ENVI) version 4.8 software and covers the procedures which includes preprocessing techniques, band removals, atmospheric correction, and algorithms such as Minimum Noise Fraction (MNF), Pixel Purity Index (PPI), 2 D Scatter plot, n-Dimensional Visualizer, and Spectral Angle Mapper (SAM).

Chapter 6 covers remote sensing techniques for processing an AISA image using ENVI with the same preprocessing and processing techniques as in Chapter 5

Chapter 7 Validation of the satellite and airborne hyperspectral images with the in situ field measurements collected from the experimental hydrilla tank and field settings, and aerial photos. The images that resulted from the hyperspectral processing techniques were compared to the aerial photos collected by VIMS and the ground surveys collected by the Maryland Department of Natural Resources (MDDNR).

Chapter 8 Conclusions and Discussion of the in-situ field measurements, remote sensing techniques, and validation procedures. In addition, it includes a discussion and comparison of results of the airborne sensor AISA and the satellite sensor Hyperion and the differences in endmember collection spectra collected from both sensors. The in-situ field measurements will be compared to spectra collected by both sensors. Also the aerial photos collected by the Virginia Institute of Marine Sciences (VIMS) will be validated against the resulting images from both sensors. This chapter will summarize the entire dissertation and it will discuss major contributions to the science of remote sensing, limitations, and future research needs.

1.8 Major data sources

This section describes the procedure for collecting and processing the aerial photographs by the Virginia Institute of Marine Sciences (VIMS), the in-situ field measurements of the experimental tank and the field, and the collection of hyperspectral images from the satellite and airborne sensors. The experimental tanks and field measurements were collected at the Anita Leight Center on August 8, 2008 and the field

measurements at the Otter Point Creek coastal estuary on August 9,2009. The experimental tank and field measurements were collected using an ASD Field SpecPro field spectrometer. The AISA image was atmospherically corrected with FLAASH and provided by the University of Nebraska CALMIT and FAMU as the sensor was flown on July 15, 2005 and the satellite hyperspectral image from Hyperion was downloaded from the Earth Explorer website for a flyover of July 20, 2011. Both images were processed and analyzed with the Environment for Visualizing Software (ENVI®) version 4.8. The aerial photography was provided by VIMS taken on July 15, 2011.

1.8.1 Protocol for the collection and processing of aerial photographs

Black-and-white photographs at a scale of 1:24,000 were collected by VIMS for identifying all visible aquatic vegetation beds by the VIMS for several ideal conditions, such as low tide, when maximum delineation of aquatic vegetation is observed; when phenologic stage overlap was the greatest; when surface reflectance from sun glint did not cover more than 30 percent of the frame; when the sun angle was generally between 20° and 40° to minimize water surface glitter; when the clarity of water ensured complete delineation of grass beds; during periods of no or low wind; and during periods of no or low haze and/or clouds below aircraft in the vertical mode with less than a 5° tilt. Scale/altitude/film/focal length combination permitted resolution and identification of one square meter area of aquatic vegetation at the surface (Moore et al., 2009; 2000). Each flight line included sufficient identifiable land area to assure accurate plotting of grass beds. The procedures established were that aerial photography negatives covering aquatic vegetation beds were scanned and orthorectified to create orthophoto mosaics.

The outlines of the beds were then interpreted on-screen, providing a digital database for analysis of bed areas and locations. Ground survey information was collected in 2011 by MDDNR tabulated and entered into a Geographic Information System (GIS) by VIMS (Moore et al., 2009; 2000). USGS 7.5 minute quadrangle maps were used to organize the mapping process, which included interpreting the beds from aerial photography, mapping ground survey data, and compiling SAV bed area measurements in OPC. The negatives from the aerial photos were scanned, georectified and orthographically corrected to produce a seamless series of aerial mosaics in accordance to VIMS Standard Operating Procedures (SOP). The SAV beds were interpreted on-screen from the orthophoto mosaics using Environmental Research Institute, Inc. (ESRI) Arc Info GIS software (Moore et al., 2009; 2000). The identification and delineation of aquatic vegetation beds by photo interpretation utilizes all available information including: knowledge of aquatic grass signatures on film, distribution of aquatic vegetation in 2010 from aerial photography, 2010 ground survey information, and aerial site surveys (Moore et al., 2009; 2000). In addition to delineating SAV bed boundaries, an estimate of SAV density within each bed was made by visually comparing each bed to an enlarged crown density scale similar to those developed for estimating crown cover of forest trees from aerial photography (Paine 1981). Bed density of seventy to one hundred percent was characterized for the Otter Point Creek aerial photo.

1.8.2 Experimental tank and field measurements

The experimental tank spectral measurements were collected from a hydrilla tank on August 5, 2008 that grows hydrilla for harvesting to the estuary during the summer

months. Field spectral measurements were collected on August 9, 2009 at the Otter Point Creek pier when hydrilla was at its maximum annual growth. The instrument used to collect the spectra was a FieldSpec® Pro spectroradiometer (ASD Inc, Boulder, CO, USA). A more detailed description of the experimental tank and field spectral collection is detailed in Chapter 4.

1.8.3 Hyperion data acquisition and characteristics

The Hyperion satellite was tasked by NASA Goddard Space Flight Center (GSFC) to fly over the study area on July 20, 2011 at a twenty to twenty-nine percent cloud cover. The image was downloaded from the Earth Explorer website.managed by USGS The acquisition date for Hyperion was collected the same month and year as the VIMS aerial photo, July 2011. Hyperion was NASA's first hyperspectral imager aboard NASA's Earth Observing-1 (EO-1) under the New Millennium Program (NMP) of November 2000. Hyperion is the first civilian hyperspectral image sensor in space having a sun-synchronous, circular orbit inclined at 98.2^0 and at an altitude of 705 km, a swath of 7.5 km by 185 km. Hyperion is a push broom-type imaging spectrometer that follows the same track as Landsat-7 satellite at only about one minute behind. Hyperion sensor has 220 spectral bands with the spectral range of 400 to 2500 nm at 30 m spectral resolution.

1.8.4 AISA data acquisition and characteristics

The acronym AISA stands for Airborne Imaging Spectrometer and it is capable of acquiring continuous data within many narrow bands, up to 244 spectral bands, at a spectral resolution of approximately 10 nm from the Visible and Near-Infrared regions of

the electromagnetic spectrum (EMS). Spatial resolution that can be achieved range from less than 1 m to 10 m. The hyperspectral imagery acquired by AISA provides for an attractive alternative to aerial photographs and broad–based images acquired by space borne sensors because of its high spectral and high spatial resolution in the same image, and its increased dynamic range (Staenz 1992). An AISA image was acquired of the study site onboard an aircraft managed by the University of Nebraska's Center for Advanced Land Management Information Technologies (CALMIT) remote sensing center and Florida Agricultural and Mechanical University (FAMU). AISA was flown on July 10, 2005 at 6:13 PM over the Otter Point Creek estuary at an altitude of 3.07 km above sea level under clear skies. The ground surface was relatively dry. AISA is a push-broom imaging spectrometer with a spectral resolution of 2.5 nm and a spatial resolution of 2.0 x 2.0 nm. The AISA imagery acquired for this research has a spectral resolution of ninety-seven (97) bands within a range of 498 nm to 819 nm. The AISA image was atmospherically corrected by CALMIT taking into consideration the solar irradiance, interaction of the electromagnetic energy with the atmospheric absorption, reflectance, and scattering, and the sensor geometry using the Fast Line-of-Sight Atmospheric Analysis of Spectral Hypercube (FLAASH) in ENVI version 4.8.

CHAPTER TWO: LITERATURE REVIEW

2.1 In - situ field surveys of aquatic vegetation

Presently conventional methods of mapping aquatic vegetation beds consist in ground surveys, which are sampling and field surveys along quadrants and transects. These methods tend to be expensive and time consuming. Maryland Department of Natural Resources (MDDNR) uses this method for collecting SAV data at Otter Point Creek. Collection of field data in areas of dense aquatic vegetation can be difficult to gain access making these conventional methods impractical (Jakubauskas et al., 2002; Jensen et al., 1986). One drawback of field surveys and mapping techniques is that they can disturb the aquatic vegetation beds and aquatic life (Shuman and Ambrose, 2003). The inventorying of large geographical areas of aquatic vegetation can be impractical to use**.** These conventional mapping techniques can be challenging to implement when there is a need for accounting for changes in density, especially when looking at a seasonal or interannual time scale (Jakubauskas et al., 2002).

2.2 Mapping by aerial photography

Application of aerial photography has been successful in marine and littoral environments (Marshall and Lee, 1994; Valta-Hulkkonen et al., 2004). The advantages of conventional film based methods are the very fine resolution (0.1 to 1.0 m, dependent on scale) (Jensen et al., 1986) and cost-effective data acquisition compared to airborne

multispectral scanner data. However the results have been shown to be somewhat inaccurate as aerial photographs require careful geo-correction to overcome geometric distortions introduced by aircraft instability and the camera lens (Chauvaud et al., 1998). If manually undertaken, photo-interpretation of such media is more often than not a subjective process and, applied as an operational tool, can be time consuming and limited in temporal coverage (Valta-Hulkkonen et al., 2004). Digital images are an improvement over manual ones in that they provide better geographical positioning and can be superimposed upon and compared with other geographical data in order to study the interactions between parameters and temporal changes. As much of the interpretation of aerial photography is based upon brightness, shallow submerged aquatic vegetation appears dark and is often indistinguishable from deep water. Variable water clarity, bottom sediments, macroalgae, and epiphytes add to the uncertainty in photographic identification of benthic vegetation habitats (Werdell and Roesler, 2003). Despite high spatial resolution, the poor spectral resolution of aerial photography is insensitive to subtle spectral variations and is certainly a limiting factor for successfully discriminating submerged features; however, the relatively high spatial resolution of aerial photographs can be suitable for terrestrial vegetation and emergent aquatic vegetation where the signal is not influenced by an overlying water column.

Presently, color aerial photographs combined with image analysis successfully have mapped SAV in the Lower Chesapeake Bay, Maryland (Orth and Moore, 1983). Aerial photography had poor spectral resolution when compared to remote sensors. Aerial photography can identify homogenous emergent submerged aquatic vegetation

beds, but is not adequate to map most submerged aquatic vegetation (Jensen et al., 1986; Moore et al., 2000). Visual interpretation of aerial photography is a labor-intensive process (Marshall and Lee, 1994; Nelson et al., 2006). Aerial photography has limited use when assessing aquatic vegetation distributions across small water bodies spread across a large geographical area (Nelson et al., 2006). This is because even high-resolution cameras mounted on an aircraft do not have a great field of view as a remote sensor on a satellite (Madden, 2004). Aerial photography requires multiple passes by an airplane to cover the same area acquired at one point in time by a satellite as shown in Figure 7. These additional passes can introduce changes in light and atmospheric conditions, which in turn can affect classification attempts (Jensen, 2005). A zoom of the Otter Point Creek study area is shown in Figure 8.

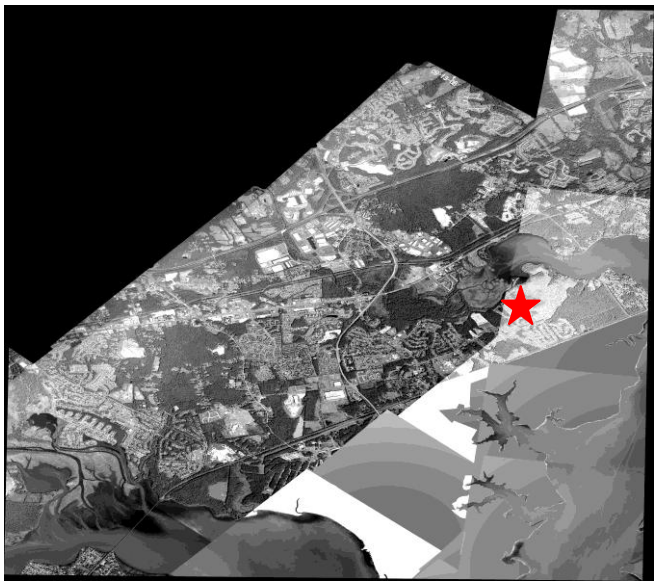

Figure 7 Main image mosaic (Source: VIMS, 2011)

Figure 8 Aerial photo of study area
(Source: VIMS, 2011)

Presently color aerial photographs combined with image analysis successfully have mapped Submerged Aquatic Vegetation (SAV) in the Lower Chesapeake Bay, Maryland (Orth and Moore, 1983). Current approaches for mapping aquatic vegetation in coastal estuary areas have been primarily done thru visual interpretation of photographs or satellite image data sets in combination with field-surveys. Recent reviews of databases and approaches for mapping, monitoring and modeling of aquatic vegetation show that accurate image are aerial photos that have been restricted to coastal areas which are shallow and have moderate to high levels of aquatic vegetation mats with densities greater than 40 percent (VIMS 2005).

2.3 Field spectroscopy of aquatic vegetation

Spectral libraries as the basis for developing routine methods of applying remote sensing to aquatic vegetation surveys are a fundamental part of many hyperspectral image classification and radiative transfer modeling procedures, including atmospheric and water column correction, spectral unmixing and endmember mapping (Jupp et al., 1985). Spectral libraries will ultimately have the potential to serve as valuable tools for identifying characteristic wavelengths that can be incorporated into bottom classification and bathymetry algorithms. Spectral libraries also provide information needed to make an informed choice about the spectral resolution required of a sensor and the wavebands that will be most useful for a particular application. After spectral libraries are obtained, analysis of the data for identifying significant components of the signal must be made.

Aquatic vegetation reflects a strong spectral signature that can be tracked using satellite and airborne remote sensors (Armstrong, 1993; Mumby et al., 1997; Dierssen et al., 2003).

Spectral differences between aquatic plants are difficult to detect, because most aquatic plants have essentially the same biochemical and spectral characteristics, which remain, unchanged (Jakubauskas et al., 2000). To date there has been little or no analysis of the different processing techniques suitable for mapping spectrometry data for identifying hydrilla using hyperspectral image analysis (Jakubauskas et al., 2000).

Jakubauskas et al., (2000) studied the effects of canopy coverage on the spectral signature of the emergent macrophyte spatterdock or yellow pond lily (*Nuphar polysepalum*). As the coverage of emergent macrophyte decreased, the amount of

reflectance decreased in the green and infrared parts of the spectrum. Similar results were also found using water hyacinth (*Eichornia crassipes*) and percent coverage in Texas waterways (Jakubauskas et al., 2002). The researchers concluded that even though this work was done at close range with hand-held hyperspectral sensors, the high correlations between vegetation cover and infrared reflectance should be transferable to satellite sensors with broader bandwidths (Jakubauskas et al., 2000).

Blanco et al., (2012) collected and analyzed spectral signatures of hydrilla from a tank and field settings at Otter Point Creek, Edgewood, Maryland in August 8, 2008 and on August 9, 2009 and determined that the field spectra collected from the field had a lower reflectance than the tank spectra because the hydrilla was submerged and was affected by turbidity and other constituents in the water column. The tank spectra from hydrilla vegetation were emergent which resulted in an average peak reflectance of 16 percent while the field peak reflectance was only 6 percent. Therefore, it was concluded that the reflectance of hydrilla depended on the water depth.

It is known that different types of aquatic vegetation have subtly different spectral reflectance signatures, which differ greatly from open water and clear vegetative areas (Ozesmi and Bauer, 2002; Underwood et al., 2003). However, in the case of mixed beds, the varying contribution of each emergent macrophytes species to the total coverage remains difficult to detect (Underwood et al., 2006; Vis et al., 2003). Mapping submerged aquatic vegetation with remote sensing can be problematic because water absorbs much of the electromagnetic spectrum used. A major complication of remotely sensing submerged vegetation is depth of the macrophyte canopy in the water column (Han and

Rundquist 2003). Non-canopy forming aquatic vegetative species are the most commonly misclassified submerged vegetation (Valta-Hulkkonen et al., 2005; Vis et al., 2003; Wolter et al., 2005). It has been reported in studies that the mapping of aquatic vegetation can be remotely sensed and classified to a maximum depth between 2 m and 3 m (6.5 ft. and 9.8 ft.) (Han, 2002; Sawaya et al., 2003). However, aquatic vegetation is harder to remotely sense when concentrations of algae and turbidity increase (Underwood et al., 2006; Valta-Hulkkonen et al., 2005; Vis et al., 2003). When aquatic vegetation is mapped, researchers often label it only as "submerged" with no attempt to differentiate between species or plant structure types (Sawaya et al., 2003; Wolter et al., 2005). For this reason, researchers have primarily used remote sensing to detect dense homogenous clusters of submersed vegetation (Nelson et al., 2006; Underwood et al., 2006; Vis et al., 2003; Zhu et al., 2007). Han and Rundquist (2003) studied the effects of depth on the spectral signatures of coontail (*Ceratophyllum demersum*), a submerged, freshwater macrophyte. They also considered the effects of depth in both clear and algae-laden waters. They found that as depth increases the amount of reflectance from the submerged macrophyte decreased, particularly in the infrared and green parts of the spectrum. Another study on aquatic vegetation examined a type of eel grass (*Vallisneria spiralis),* but focused on coverage as opposed to depth in both a laboratory and in algae-laden waters in the field (Yuan and Zhang, 2007). As the amount of coverage of the submerged macrophyte decreased, the amount of reflectance decreased; again, most heavily in infrared and green wavelengths. Of particular interest is that Yuan and Zhang (2007) found that the "green peak" was more evident in algae-laden waters and did not decrease

as quickly with a decrease in coverage in algae-laden waters as in clear waters. The presence of algae emphasizes the green portion of the spectrum and masks the decrease in the spectral signature with respect to coverage that is normally seen in non-algae laden waters. Several studies have shown the capability of hyperspectral imaging to detect and map vegetation types and their cover (Asner et al., 2002, Lass et al., 2005).

2.4 Remote sensing for monitoring aquatic vegetation

The study of aquatic macrophytes using remote sensing techniques has been less comprehensive than that of terrestrial vegetation because of the additional challenges associated with water reflectance, differentiating between different macrophyte species, and the small scale of freshwater aquatic environments compared to the resolution of most sensors (Nelson et al., 2006; Underwood et al., 2006).

Airborne and space borne imagery has been researched for mapping terrestrial invasive species (Williams and Hunt, 2002; DiPietro et al., 2002; Underwood et al., 2003); however, the application of remote sensing techniques to invasive aquatic vegetation has been limited. In order to overcome conventional satellite sensor limitations and to accurately monitor small-scale macrophyte dynamics (<10 m), airborne remote sensing has been used. The recent advances in computer and detector technology has generated imaging spectroscopy (Green et al., 1998; Vane et al., 1993), as airborne sensors usually have higher spatial and spectral resolution than satellite sensors. This provides more spectral information on more pure targets, and thus greater spectral accuracy in detailed benthic habitat mapping (Mumby et al., 1997). Instrumentation and technique development in the 1990's was somewhat limited, with macrophyte species

discrimination by absorption spectrum largely dependent on water column depth. Several studies successfully used airborne digital sensors to examine benthic vegetation, (Malthus and George, 1997; Mumby et al., 1997). Recent mapping applications of hyperspectral technology include an analysis of coastal seagrass. To date, only a few studies have reported spectra from a variety of macrophyte species and growth habits (Penuelas et al., 1993; Malthus and George, 1997). The spectral reflectance characteristics of features within a submerged coastal environment are optically similar, so confusion can arise in identification. The results indicated that airborne remotely sensed data have good potential for monitoring freshwater macrophyte species. In comparison to conventional spaceborne sensors such as Landsat TM and SPOT, airborne hyperspectral sensor data is more accurate and precise (Jakubauskas et al., 2000). AVIRIS, HyMap, and CASI airborne hyperspectral sensors show highly accurate results in mapping aquatic vegetation. Hyperspectral sensors increase the spectral resolution of mixed pixels and together with spectral libraries, improve the ability to unmix the signal and resolve the make-up of each mixed pixel scene. Until recently, airborne sensors were the only way to acquire hyperspectral images of aquatic vegetation.

Remote sensing technology not only can be applied for mapping vegetation covers over land areas, but also in underwater areas focusing on mapping aquatic vegetation which is regarded as a powerful indicator of environmental conditions in marine and freshwater ecosystems (Lathrop et al., 2006; Wolter et al., 2005). Remote sensing can be an effective method for mapping SAV in saltwater, brackish water, and freshwater environments (Ciraolo et al., 2006; Everitt et al., 2008). However, as the

spatial resolution of the satellites improve, a change from aerial photography to satellite imagery for mapping aquatic vegetation has taken place (Everitt et al., 2008; Olmanson et al., 2002; Ozemi and Bauer, 2002). Satellite imagery is more effective than aerial photography when high spatial resolution is needed for covering a large geographical area. Using satellite imagery generates maps, which can be used to prioritize areas for removal of aquatic vegetation, such as an invasive aquatic species (hydrilla) and allows for evaluating the effectiveness of aquatic plant control efforts (Jakubauskas et al., 2002; Madden, 2004). Satellite imagery has been used to track and monitor the spread of invasive aquatic vegetation, which can facilitate the early detection of new or spreading species that eradication efforts could be successful (Laba et al., 2008).

Remote sensing techniques of aquatic vegetation has been less comprehensive than that of terrestrial vegetation because of additional challenges associated with water reflectance, differentiating between aquatic vegetation species, and the small scale of freshwater aquatic environments compared to the resolution of most sensors (Nelson et al., 2006; Underwood et al., 2006). Aquatic vegetation from coastal waters have different spectral signatures, which differ greatly from ocean waters and non-vegetated areas (Marshall and Lee, 1994; Ozesmi and Bauer 2002; Peñuelas et al., 1993; Underwood et al., 2003). At least one study has shown that it is possible to differentiate between submerged macrophyte using remote sensing. Pinnel et al. (2004) was able to distinguish between the two submerged macrophytes groups *(Chara and Potomageton)* using hyperspectral sensors. Satellite imagery with high spectral and spatial resolution provides more detailed spectral information relatively to traditional photography that can be used

to classify aquatic macrophytes species (Jensens et al., 1986). Early satellites like Landsat TM, with moderate spatial and spectral resolutions were unable to identify mixed beds unless they dominated the beds (Laba et al., 2008). Coarser resolutions have also been linked to lower accuracies in classifications (Everitt et al., 2008) and are not suited to mapping most submerged aquatic vegetation (Underwood et al., 2006).

Hyperspectral satellites and airborne scanners have been used to map aquatic vegetation in shallow waters (Ciraolo et al., 2003). While hyperspectral imagery can be useful in discriminating between vegetation and exotic species, the large data volume inherent in this method makes it challenging for use by water resource managers without sufficient expertise and data processing capabilities (Madden, 2004). Recently, hyperspectral imagery, consisting in many contiguous bands, has been applied to mapping aquatic vegetation, Eurasian watermilfoil and wild celery, in the lower Potomac River of the Chesapeake Bay (Williams et al., 2003).

Hyperspectral imaging has been used to remotely delineate wetland areas and classify hydrophytes vegetation characteristics and promoted the use of high spectral and spatial resolution for improving the mapping of salt marsh vegetation of similar structural characteristics. The analysis identified regions in the electromagnetic spectrum, which discriminated between wetland species (Schmidt and Skidmore, 2003). The study also focused on the importance of hyperspectral imaging systems for the Visible and Near-Infrared regions (Becker et al., 2005). Several studies have investigated the potential of providing timely date for mapping and monitoring aquatic vegetation which has been identified as one of the most important aspects of ecosystems restoration and

reconstruction (Lin and Liquan, 2006; Pengra et al., 2007) tested the applicability of AVIRIS hyperspectral satellite imagery for mapping phragmites, an invasive plant in coastal wetlands. Lobo et al,,2009 identified cyanobacterial blooms using Hyperion/EO-1 data in Patos Lagoon estuary located in Rio Grande do Sul state, Brazil. The Spectral Angle Mapper was used to identify the potential areas of cyanobacterial blooms. Li et al., 2008 applied the Hyperion sensor for detecting tidal flats in a coastal region. Demuro and Chisholm, assessed mangrove communities by using the Hyperion sensor for discriminating vegetation in coastal wetlands.

CHAPTER THREE: AQUATIC OPTICS AND REMOTE SENSING OF AQUATIC VEGETATION

3.1 Principles of aquatic optics

The water bodies in the Otter Point Creek estuary are classified as coastal estuarine waters. This creates some difficulty due to complexity of substance mixtures, unstable atmospheric residue and noise. Water-leaving radiances used for the extraction of upper ocean constituents represent no more than 10 percent of the total radiance captured by satellite optical sensors. Figure 9 shows the interaction of the different components, which interfere when a sensor collects an image from a water body.

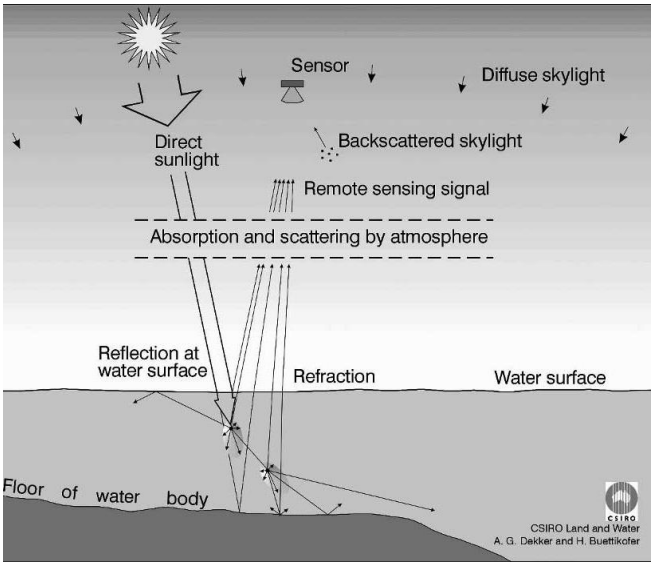

Figure 9 Aquatic Optics Processes Diagram (Source: Dekker and Buittikofer)

A schematic diagram of the various processes that contribute to the signal as measured by a remote sensor in optically shallow waters (class 2 waters) where the substrate has a significant effect on the water-leaving radiance (Dekker et al., 2001).

The overall brightness of the water surface will increase in the blue band, which is the visible region of the spectrum, so the water no longer appears as a dark object but instead becomes brighter as the concentration of the constituents in the water column increases, the wavelength then shifts from the blue to the green region of the electromagnetic spectrum. Aquatic optics is the branch of physics that deals with the interaction of spectral radiation and its propagation within molecular water and surrounding matter that is suspended or dissolved therein (Bukata 2005). Photons that pass thru the air water interface will attenuate in the water column. Attenuation results from absorption and back scattering. A spectrometer is an instrument that measures the amount of attenuation in the water column as a function of reflectance by measuring the apparent optical properties of the water body. These apparent properties are a function of inherent optical properties (IOP's). IOP's are a quality of the water body itself, which includes the organic and inorganic constituents (Bukata 2005). Remote sensing techniques applicable to class 2 waters are related to several relationships of surface reflectance, R (λ), where R is the reflectance and λ the wavelength. This property is directly related to Inherent Optical Properties (IOP's), total absorption a, and backscattering coefficients, b_b (Bukata, 2005).

Equation 1 Relationship of reflectance and inherent optical properties (Bukata, 2005)

$$R(\lambda) = \frac{\gamma b_b(\lambda)}{a(\lambda) + b_b(\lambda)}$$ v b

When sunlight penetrates the water column, the light intensity decreases exponentially as the depth increases and this is called attenuation. In the visible light region of the electromagnetic spectrum, the red portion attenuates more rapidly than the shorter wavelength of the blue region, illustrated in (figure 10).

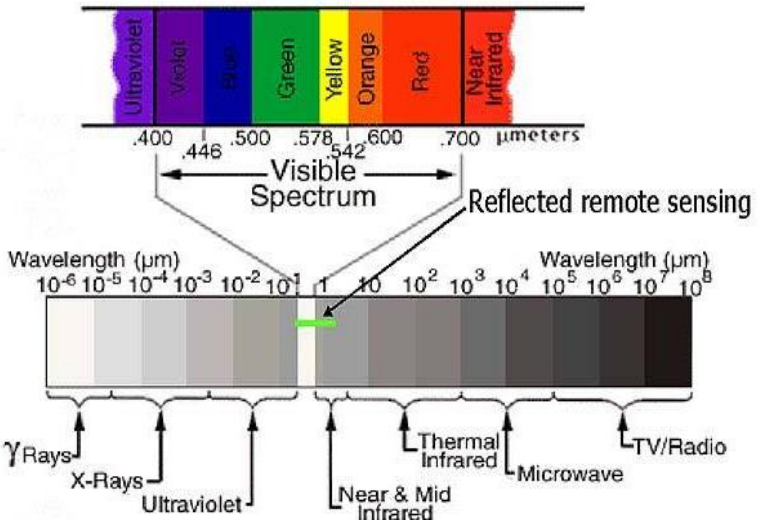

Figure 10 Electromagnetic Spectrum (Source: Sheppert 1998)

The spectral radiance recorded by a sensor is dependent on the surface reflectance and the depth. Phytoplankton in water converts the electromagnetic energy into photosynthesis. Other absorbers are inorganic and organic matter resulting from the

breakdown of plant tissue, and water itself, which absorbs red light and has a smaller effect on shorter wavelength. Chlorophyll in algae will look green because reflects in the central region of the visible spectrum, green, and absorbs strongly at either end of the spectrum. Dissolved organic compounds absorb at the shorter wavelengths, blue, and strongly reflect in the yellow-red end, impacting the gelbstoff. Electromagnetic radiation may interact with the Total Suspended Matter (TSM) in the water column and generate backscattering effects. This scattering process is caused by the inorganic and organic constituents in the water column and will increase with turbidity**.** In water quality applications, we do not have transmittance or reflectance. Waters in this tidal estuary of Otter Point Creek are not pure due to these organic and inorganic constituents, which cause interference of the sunrays, especially at the surface.

The waters in Otter Point Creek are highly turbid and very productive waters. This particular research only applies to Class 2 waters (productive waters), which are not pure like Class 1 waters, because they have organic and inorganic constituents contained in the water column, especially at the surface (Bukata 2005). Sunlight will reflect and diffract according to IOP's, but in open waters the sunlight scatters by absorption. These constituents will cause Near Infrared Region (NIR) surface reflectance and subsurface volumetric scattering so the amount of NIR radiant flux leaving the water surface will increase. The TSM will cause significant scattering and reflectance of the radiant flux to the sensor causing brightening. When light penetrates water, the intensity decreases exponentially as the depth increases (Green et al., 2000) and this is called attenuation and it exerts an effect on the remotely sensed data. In the region of visible light, the red part

of the electromagnetic spectrum attenuates more rapidly than the shorter wavelength (blue region). As the depth increases, the ability to differentiate substrate spectra declines. Spectral radiance recorded by a sensor is dependent on the reflectance and the depth of the location being imaged. Absorption involves converting the electromagnetic energy into photosynthesis in phytoplankton because it is one of the main absorbers in water. In addition, it has been well documented that the water bodies researched contain various organic matters like phytoplankton, Chlorophyll a, Colored Dissolved Organic Matter (CDOM) which result from the breakdown of plant tissue, inorganics like Total Suspended Matter (TSM), and water itself which absorbs red light and has a smaller effect on shorter wavelength blue light (causing the blue color of clear water). These constituents interfere with remote sensing data (Gitelson 1992). Figure 11 shows spectral signatures of case 1 (clea) and case 2 waters (algae-laden).

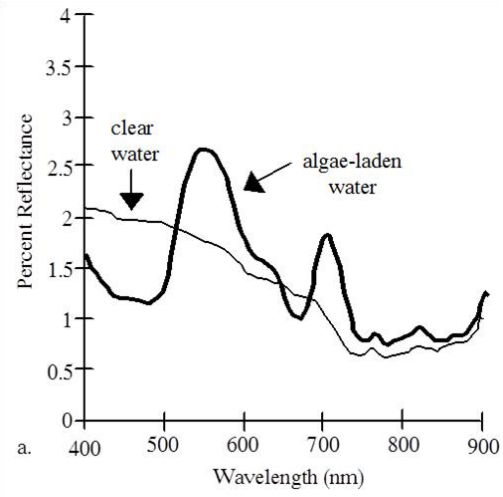

Figure 11 Percent reflectance of clear and algae-laden water based on in-situ measurements (Jensen, 1995)

3.2 Remote sensing characteristics for Class 2 waters

When performing water quality studies using remote sensing data, the most important data that we need to collect is the subsurface volumetric radiance. Water bodies are able to transmit significant amounts of radiation, but vary with the wavelength, so the direct observation in the visible spectrum is not transferred to other regions of the spectrum. For instance, shown on (figure 12), a red object absorbs most of the blue and green incident light and reflects most of the red light toward a sensor. In part b of figure 12 a red filter looks red because it selects the blue and green light while allowing the red light to go through it (Simmons et al., unpublished).

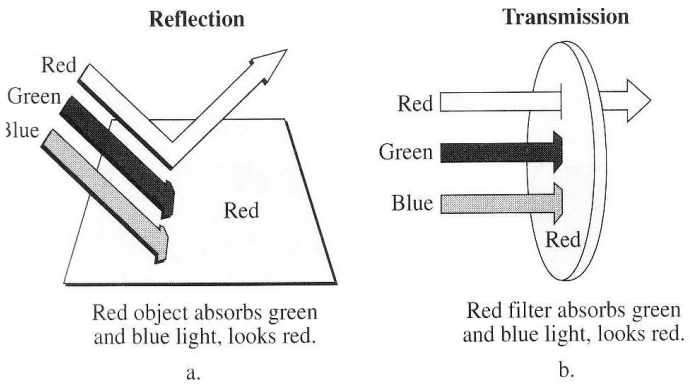

Figure 12 Concept of transmittance and reflectance (Source: Jensen 1995)

Other types of transmittance which will need to be considered is atmospheric transmittance in which the transmittance is dependent on the wavelength and the spatial data is limited to the areas which have not been blocked. Transmittance is important

because natural formed materials like vegetation are opaque to visible radiation, but vegetation transmits much of the infrared radiation. The relationship between transmittance and reflectance can be explained by Equation 2 as follows: transmittance is the radiation been transmitted when it passes through without significant changes. The capability of a material that has a depth and a thickness for transmitting energy is called transmittance.

Equation 2 Transmittance and radiation (Jensen ,2000)

$$Transmittance\ (t) = \frac{Radiation\ been\ transmitted}{Incident\ radiation}$$

Transmittance happens when radiation passes through a material without significant changes. When the light photons enter the water column, they are influenced by absorption and scattered by particles that are suspended on the water, such as in Class 2 waters. The color of the water is determined by volume scattering rather than by surface reflectance, and spectral properties are determined by transmittance rather than by surface characteristics alone. Maximum penetration of sunlight in the blue region is 400 to 446 nm, but at a slightly longer wavelength, the penetration is much greater for recording the bottom of the water body. However, at longer wavelengths, toward the red region, the absorption of sunlight is much greater, and only shallow features can be detected. Finally, in the Near Infrared Region (NIR) 700 nm absorption is so great that only a land-water distinction can be made. Coastal waters contain suspended sediments and dissolved

organic matter (Zhang 2005). Class 2 waters is the classification of the water bodies in the Otter Point Creek estuary, which creates some difficulty due to the complexity of substance mixtures, unstable atmospheric residue and noise. Water-leaving radiances used for the extraction of upper ocean constituents represent no more than 10 percent of the total radiance captured by satellite optical sensors. Atmospheric correction may be performed to remove the contribution of the atmosphere in satellite measurements. The interaction of the different optics takes place when a sensor collects an image from a waterbody (Rundquist et al., 1996). The overall brightness of the water surface will increase in the visible region so the water stops appearing as a dark object and becomes bright as the sediment concentration increases, the wavelength then shifts from the blue to the green region of the electromagnetic spectrum. For different classes of water depth the intensity of radiation will decrease exponentially with depth, in other words brightness decreases as depth increases. Dark waters mean an area is deep, brighter waters mean they are shallow. Equation 3 is interpreted as the reflected energy E_r is equal to the EI (λ)- EA that is either absorbed or transmitted. Water is capable of transmitting large quantities of radiation, which changes with wavelength, so the direct observation in the visible range of the electromagnetic spectrum does not transfer to other transmitting parts of the spectrum. When the energy from the sun hits the earth surface, basic interactions occur. Some portions of the energy is reflected, absorbed, and/or transmitted. If we apply the principles for energy conservation, we can show the following relationships can be show. Radiation from the sun, when incident upon the earth's surface, is reflected by the surface, transmitted into the surface or absorbed and emitted

by the surface (figure 13). These changes are detected by the remote sensor and enable the interpreter to obtain useful information about the object of interest. The remotely sensed data contain both spatial information such as size, shape and orientation, and spectral information such as tone, color and spectral signature.

Equation 3 Energy Equation (Jensen, 2000)

$$E_I = E_r + E_A + E_t$$

$E_I = \text{Incident Energy}$

$E_r = \text{Reflected Energy}$

$E_A = \text{Absorbed Energy}$

$E_t = \text{Transmitted Energy}$

EA that is either absorbed or transmitted**.** This equation is interpreted as the reflected energy Er is equal to the EI (λ). From the viewpoint of interaction mechanisms, with the object-visible and infrared wavelengths, from 300 to 1600 nm

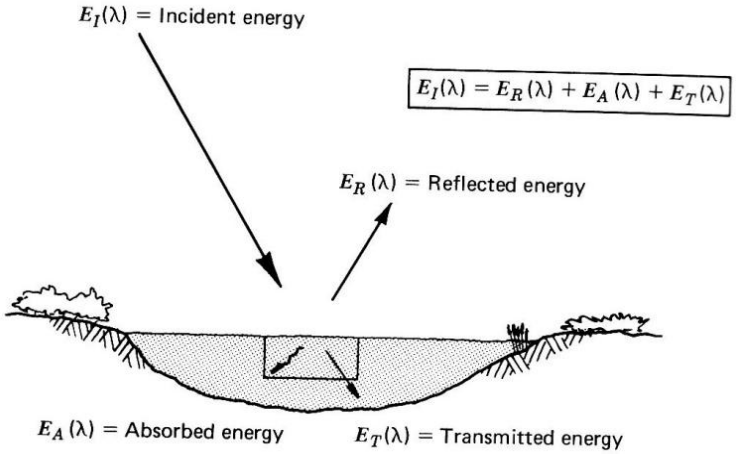

Figure 13 Energy Balance (Source: Liliesand and Kiefer, 1999)

Two important relationships can be observed from (figure 13) above. One is that the proportion of the energy reflected, absorbed, and transmitted changes with the different surface features that are directly dependent on type of materials and condition. This difference allows for the image analyst to distinguish different features found in the image. Secondly, the proportion of the different energies being reflected, absorbed, and transmitted vary at the different wavelengths, for instance, in the electromagnetic spectrum range, these different spectral variations will result in color which means that we can define certain objects as blue in color, when they reflect in the blue range of the spectrum, and green color in the green spectrum. Total radiance recorded by the sensor onboard an airborne or satellite platform is a direct function of the electromagnetic energy from the four sources shown in (figure 14).

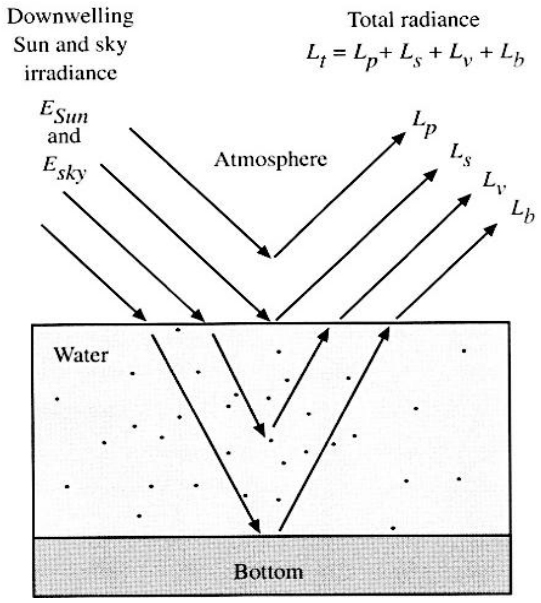

Figure 14 Water Leaving Radiances (Source: Bukata, 2005; Jensen, 2000)

In our research it is necessary to identify the organic and inorganic constituents in the water column such as Chl a and TSM by separating the subsurface volumetric radiance. This equation is interpreted as the reflected energy Er is equal to the EI (λ) - EA that is either absorbed or transmitted.

Equation 4 Total Radiance (Source: Jensen 2000)

$$L_t = L_p + L_s + L_v + L_b L_v = L_t - (L_p + L_s + L_b)$$

Equation 4 is requiring the atmospheric correction of the sensor data by removing the atmospheric attenuation (L_p) surface glint as previously mentioned other surface reflectance (L_s), and bottom reflectance (L_b). Subsurface volumetric radiance (L_v) is the

product of down swelling solar and sky radiation that actually penetrates the air-water interface, interacting with the water and organic/inorganic constituents and then going out of the water column towards the sensor without even reaching the bottom surface (Bukata 1995). L_v is a function of the concentration of pure water (w), inorganic suspended minerals (SM), organic Chlorophyll a (Chl a), dissolved organic material (DOM) and the total amount of attenuation of absorption and scattering taking place inside the water column.

Equation 5 Down swelling solar and sky radiation penetrating the air water interface (Source: Jensen 2000)

$$L_v = f[w_c(\lambda), SM_c\ (\lambda), Chl\ a_c(\lambda), DOM_c(\lambda)]$$

Equation 5 is the portion of the radiance which is been recorded at the sensor which results from the down swelling solar (Esum) and Sky (Esky) radiance which does not reach the water surface. Ls is the radiance from the down swelling solar and sky radiation that reaches air-water interface, at the surface layer or boundary layer, and only penetrates about 1 mm and is reflected back. The interface volumetric radiance shown on Equation 6 where Lv is from the down swelling solar and sky radiation that penetrates the air-water interface and intersects with the water constituents that exists in the water column without touching the bottom. This is called interface volumetric radiance and is important to collect.

Equation 6 Interface volumetric radiance (Jensen 2000)

$$L_v = L_t - (L_p + L_s + L_b)$$

L_b is the portion of the radiance been recorded which results from the down welling solar and sky radiation that penetrates the air-water interface and reaches the bottom and is propagated back through the water column, and finally exits. In aquatic remote sensing, the radiance is extracted from all of the radiance components, which are recorded by the sensor. In this approach, the organic and inorganic water column constituents' spectra will be collected. By correcting the sensor data radiometrically, the atmospheric attenuation (L_p), surface sunglint and bottom reflectance (L_b) can be removed (Bukata, 2005, Jensen 2000).

3.3 Water quality habitat requirements

The major parameters that control aquatic vegetation distribution is light attenuation (Batiuk et al., 2000). Light attenuation (reduction in light intensity) in the water column is due to light absorption by water molecules and suspended particles. Light attenuation can be measured in two ways: with a secchi depth disc or with a light meter for calculating the light attenuation coefficient (Kd) based on exponential decay function. Chlorophyll a (Chl a) and other suspended solids are responsible for the majority of the total light attenuation in the water column. Chl a is a pigment found in all photosynthetic phytoplankton. Measurements of Chl a concentrations are used as indicators of phytoplankton biomass and, therefore, indirectly provide a measure of nutrient loading. Total Suspended Solids (TSS) is a measure of suspended inorganic solids, plus microorganisms and organic detritus. Nutrients like nitrogen and phosphorus are important habitat parameters because they indirectly affect the light attenuation by

stimulating growth of phytoplankton in the water column and algal epiphytes on the SAV leaves and stems. These parameters are measured as Dissolved Inorganic Nitrogen (DIN) and Dissolved Inorganic Phosphorus (DIP) (Batiuk, 2000)**.** The principal relationships between water quality conditions and light regimes for growth of SAV is shown in (figure 15). Incident light is partially reflected at the water surface and is attenuated through the water column above SAV by particulate matter.

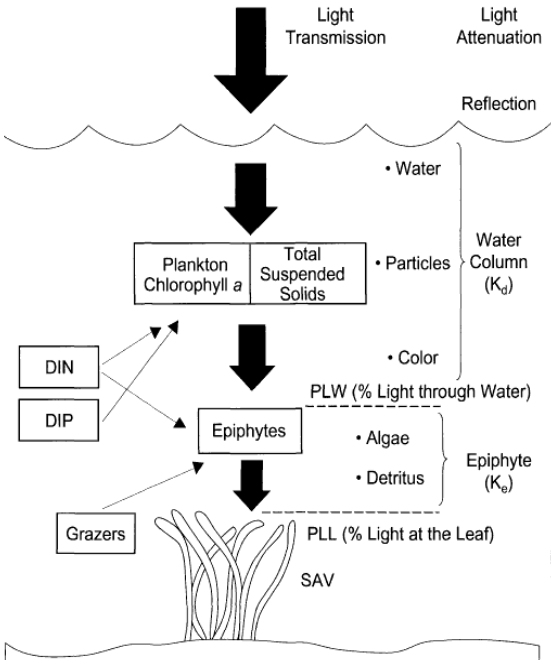

Figure 15 Conceptual model of light, nutrient effects on submerged aquatic vegetation habitat (Source: Chesapeake Bay Program 2000)

3.4 Class 2 waters

Class 2 waters contain suspended sediments, dissolved organic matter, and other particles. Coastal zones are mostly classified as Class 2 waters is the classification of

water bodies creates a difficulty due to complexity of substance mixtures, unstable atmospheric residue and noise. In Class 2 waters there is a significant water-leaving radiance in both the visible and near-infrared regions. It has been well documented that in Class 2 waters the extrapolation of aerosol path radiance into visible bands results in distorted or negative reflectance at visible wavelengths. Current operational ocean color algorithms are not suited to analyze Class 2 waters. Some algorithms additionally apply a turbid water test on 555 nm channel normalized water leaving radiances after the full atmospheric correction. They label isolated Class 2 waters because chlorophyll estimates in these waters are unreliable. Phytoplankton containing carbon sinks to the bottom of a water body once they die and other sediments will cover the carbon in the dead phytoplankton. Phytoplankton uses carbon dioxide (CO_2) and produces oxygen during the photosynthetic process.

3.5 Spectral behavior of submerged aquatic vegetation

The green region of the electromagnetic spectrum 570 to 578 nm is considered the most suitable for detecting submerged aquatic vegetation, followed by the red and red edge regions. Pigment concentrations and cellular structure are responsible for the main differences among aquatic vegetation species (figure 16). The green region provides greater light penetration in waters with higher concentrations of suspended and dissolved material (Kirk 1994). Water absorbs electromagnetic radiation in the optical spectral region, resulting in the dampening of the radiometric signal. Due to this effect, surface reflectance measurements for submerged aquatic vegetation is usually less than 10 percent reflectance (Pinnel et al., 2004). The principles behind aquatic vegetation spectral

characteristics are the same as land vegetation. The presence and concentrations of the leaf pigments determine the response in the visible region of the spectrum, and the leaf morphology and their water content are the main factors affecting the infrared wavelength.. Plants that grow vertically have a reduced leaf area, which have less of a surface area for interacting with the down swelling radiation; however, plants that have a canopy and broadleaved plants have more of an effective reflective area (Williams et al., 2003).

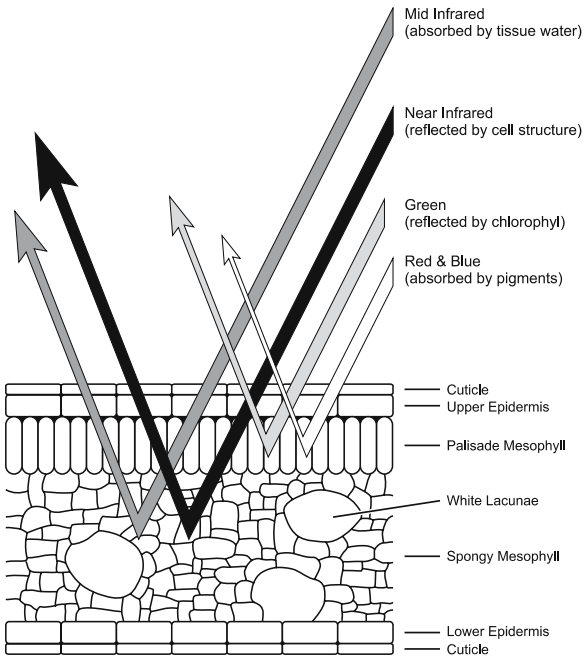

Figure 16 Leaf-radiation interactions at microscopic level.
Note: The thickness of the arrows are proportional to the magnitude of the radiation fluxes
(Source: Silva et al., 2008)

characteristics. It is useful to distinguish whether the aquatic vegetation is submergent and floating or emergent, as these factors act differently in each condition.

3.6 Spectral characteristics of aquatic vegetation

Figure 17 demonstrates how internal scattering of leaf pigments and leaf water content affect the reflectance and transmittance properties of the leaves (Peterson et al., 1989).

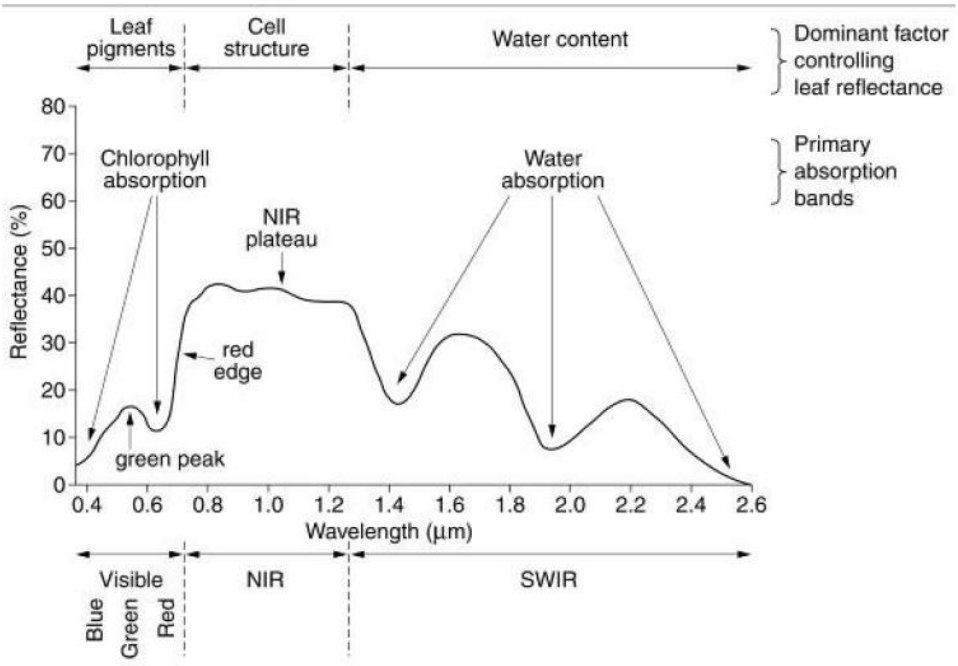

Figure 17 Spectral reflectance characteristics of healthy, green vegetation (Source: Jensen 2000)

The dominant factors controlling leaf reflectance are the various leaf pigments in the palisade mesophyll (e.g., chlorophyll a and b, and β-carotene), the scattering of near-

infrared energy in the spongy mesophyll, and the amount of water in the plant. The primary chlorophyll absorption bands occur at 430 to 450 nm and 650 to 660 nm in the visible region. The primary absorption occurs at 970, 1190, 1450, and 2700 nm. Other pigments present in the mesophyll region are usually masked by an abundance of chlorophyll pigments yellow carotenes and xanthophyll pigments with strong absorption in the blue band region. β Carotene absorption spectra absorbs in the 450 nm. Phycocyanin absorbs in the green and red regions at 620 nm, which allows most of the blue and some of the green light to be reflected. Chlorophyll a and b are the dominant pigments in the leaves because they absorb much of the blue and red wavelengths. It is important to understand the plant physiology and their pigmentation characteristics in order to appreciate how a plant will appear when chlorophyll absorption starts to decrease due to seasonal senescence or environmental stress. The lack of chlorophyll pigmentation usually causes the plant to absorb less in the chlorophyll absorption bands 430 to 450 nm 650 to 660 nm. Therefore, they will have a higher reflectance especially in the green and red regions. According to Carter (1993), increased reflectance in the visible spectrum is the most consistent leaf reflectance response to plant stress. Leaf spectral reflectance in the regions 535 to 640 nm and 685 to 700 nm visible light range indicates plant stress. The increased reflectance near 700 nm represents a blue shift of the red edge. This shift occurs in stressed plants when reflectance plots against wavelength (Cibula and Carter, 1992). The above ranges are the ones that may provide capability for detecting plant stress on leaves or on entire densely vegetated canopies (Carter, 1993; Carter et al., 1996). In a typical healthy green leaf, the NIR reflectance increases in the 700 to 1200

nm. The reason for the reflectance and transmittance of plant leaves increases while the absorbance falls to low values because in the NIR the direct sunlight incident on plants have the bulk of the energy. The mesophyll layer controls the amount of NIR energy reflected because this is where photosynthesis and respiration takes place. In the NIR, healthy green vegetation has high reflectance (40 to 60%), high transmittance (40 to 60%) thru the leaves onto underlying leaves, and low absorption (5 to 10%). Imaging spectrometers can identify small changes in absorption and reflectance because sensors like AISA and Hyperion have channels that are 10 nm apart (i.e., 10 channels from 600 to 700 nm). High reflectance of the NIR (700 to 1200 nm) energy from plant leaves is due to internal scattering at the cell wall-air interface within the leaf (Gausman et al., 1969; Peterson and Running, 1989).

CHAPTER FOUR: IN - SITU FIELD MEASUREMENTS

4.1 Study sites

The in-situ field measurements were collected from a hydrilla experimental tank site and a field setting on the waters adjacent to a fishing pier located behind the Anita Leight Estuary Center (39° 26′ 54”N, 76° 16′ 05”W) in Harford County, Edgewood, Maryland, USA (figure 18).

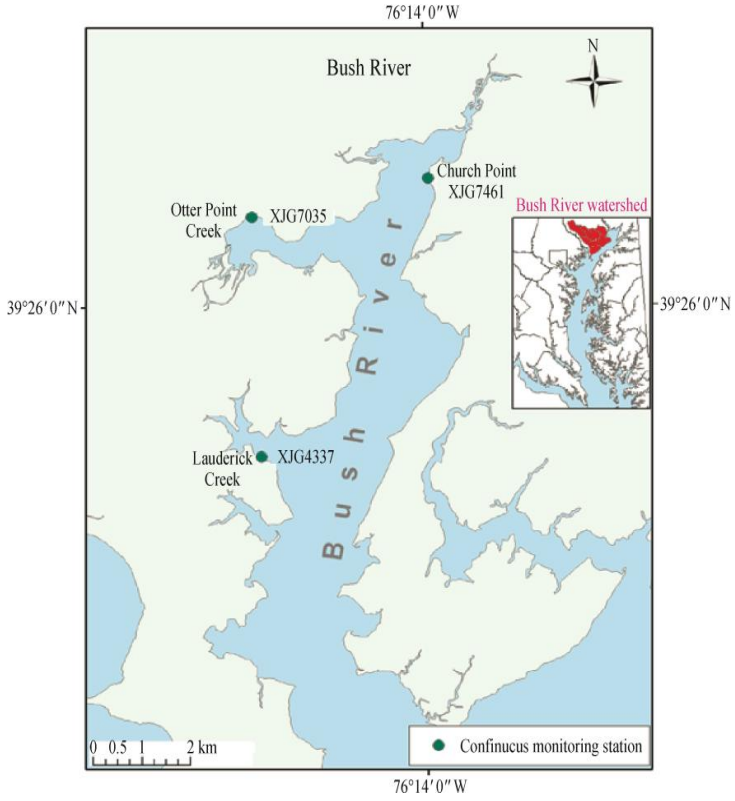

Figure 18 Study area (Source: Pasternack and Hinnov, 2003)

4.1.1Anita Leight Center

The Center grows hydrilla, wild celery, redhead grass, long leaf pondweed, slender pondweed, and water stargrass, in four experimental tanks as shown in (figure 19). The Center is located north of the Otter Point Creek estuary and it functions as an educational center for students to learn about aquatic vegetation, native animals, and history of the area.

4.1.2 Otter Point Creek estuary site

The second study site is located at the Otter Point Creek Estuary (39° 27′ 03”N, 76° 16′ 28”W), south of the Susquehanna River, in the upper Chesapeake Bay National Estuarine Research Reserve. Otter Point Creek is one of the last remaining freshwater tidal marshes in the Chesapeake Bay, classified as oligohaline (low salinity or brackish water) with a surface area of 672 acres consisting of open water, tidal marshes, forested wetlands, and upland hardwood forests which are ideal conditions for the growth of hydrilla.

4.2 Data collection

4.2.1 Experimental tank measurements

The experimental tank measurements of hydrilla were collected on August 5, 2008 behind the Anita Leight Center.

Figure 19 Anita Leight Center experimental tanks
(Source: Anita Leight Center)

A total of 35 reflectance measurements were collected at the surface and processed with an Analytical Spectral Devise (ASD) spectroradiometer FieldSpec Pro Full Range (FR). The spectroradiometer has three spectrometers recording wavelengths from 350 nm to 2500 nm with a spectral resolution of 1 nm. The instrument averaged the readings to compensate for noise and ten readings were analyzed. The hydrilla in the experimental tank was observed to be emergent without suspended matter or turbidity that could attenuate the light. The measurements were collected from 10:00 AM to 10:30 AM. The weather conditions at the time of collecting the data were partly cloudy, but there was no precipitation. In order to account for changes in light conditions and instrument drift, the ASD (Analytical Spectral Devices, Boulder, Colorado, 2013) instrument was calibrated every 10 min according to the instrument manufacturer by

taking measurements above-water down-welling irradiance with a Spectralon (Labsphere, North Sutton, NH, USA) white reference panel. The Spectralon panel has a high diffuse reflectance over a wide spectral range and converts it to percent reflectance. The Field SpecFR has a 1.5 m fore optic (25^{o} field of view) which was positioned at nadir approximately 46 cm above the vegetation as shown in (figure 20). The probe was positioned at several locations inside the tank to collect the highest reflectance values.

Figure 20 Collection of spectral signatures in the experimental tank

The spectral signatures collected were pre-analyzed on the ASD instrument computer to ensure accuracy of the data before processing it. The radiance measurements were converted to reflectance by dividing them with the Spectralon and recorded by the

instrument. A sample of hydrilla stem collected from the hydrilla tank is shown in (figure 21).

Figure 21 Sample of hydrilla collected from the tank

4.2.2 Field measurements collected at the estuary

Field measurements were collected on August 9, 2009 at the Otter Point Creek pier when hydrilla was at its maximum annual growth. Hydrilla spectral signatures were collected on the water surface next to the fishing pier, about 10 m from the shoreline. The study site was selected because of accessibility to the water from a fishing pier, abundant hydrilla species (e.g., dominant species), and obstructions which could interfere with the field measurements. Figure 22 shows the hydrilla been submergent in the study area.

Figure 22 Hydrilla mats submerged on the left side of the pier

At the time the field measurements were collected, there were dense hydrilla mats submerged on both sides of the fishing pier. The weather during collection activities was clear and sunny. It was recommended that the instrument manufacturer that field measurements should be collected between 10:00 AM and 2:00 PM because this is when the sunrays are at its maximum. Low tides occur in the early morning and late afternoon which are outside of the recommended times for spectra collection. Because of the strong absorption of NIR light by water, only the 400 to 900 nm range was used. The instrument used to collect the spectra was a FieldSpec® Pro spectroradiometer. The instrument measures spectral reflectance in the range between 350 and 2500 nm with a 1.4 nm bandwidth. The instrument was calibrated every 10 minutes with the Spectralon® (Labsphere, North Sutton, NH, USA) white reference panel to compensate for changes in

light conditions and instrument drift. Viewing and illumination geometries were standardized while obtaining signals from the hydrilla canopy. The spectral measurements were collected by holding the fiber-optic tip of the probe at approximately 40 cm above the hydrilla mats and the probe positioned at an angle where reflectance was the highest. Twenty-nine (29) readings were collected at different locations within 2 square meters (Blanco et al., 2012). The ASD instrument averaged the sampling to twelve (12) readings.

The Otter Point Creek site is optimum because hydrilla is the dominant species (i.e., monoecious). The density of hydrilla at the pier site was 100 percent, similar as to the hydrilla tank. No other aquatic plant species were identified within the hydrilla canopy. The spectral signatures were collected on August 9, 2009 at high tide from 10:00 AM to 11:00 AM. The conditions of the water in the pier area were turbid and the depth was about 0.8 feet at 10:47 AM. The weather conditions were excellent, sunny, no cloud cover and no precipitation. The ASD instrument was calibrated every 10 min with the Spectralon white reference panel for accounting for changes in light conditions and instrument drift. Twenty-nine readings were collected and processed by the ASD instrument at the site, but only twelve spectra were plotted for clarity. The spectral signatures were processed and converted from ASD format to text format, then graphed using Excel 2007 software program.

4.3 Summary of Results

Due to water absorption recorded by the ASD instrument above 900 nm, only wavelengths from 400 to 900 nm were used for comparing the hydrilla between the tank and the field measurements because this range covers the sensitivity of conventional color. A total of 35 spectral measurements were collected from the tank. The spectral measurements, as per instrument specifications, were averaged to ten spectra (figure 23) for compensating for noise 567 nm with a surface reflectance of 4.36 percent, and two in the NIR region, one at 716 nm and the other at 817 nm with a peak reflectance of 6.43 percent and 7.71 percent, respectively. The two absorption troughs shown on the graph are attributed to the absorption of chlorophyll a at a wavelength of 679 nm, with a 2.8 percent surface reflectance and at 740 nm, and 3.0 percent surface reflectance. As seen in figure 24, the field data generated two reflectance peaks which are assumed that the hydrilla leaves in the experimental tank were emergent and not exposed to turbidity, sediments, nutrients, or other elements contained in the water column, while the hydrilla mats in the field were submerged and exposed to the effects of light attenuation. The difference between the reflectance of hydrilla in the tank and in the field is 16 percent and 6 percent, respectively. The double peaks at 723 nm and 800 nm are the result of water absorption in the canopy. The spectral signatures of hydrilla observed in the tank and the field had similar characteristics, of low reflectance in the visible region of the spectrum from 400 to 700 nm, but high reflectance in the NIR region 700 to 900 nm.

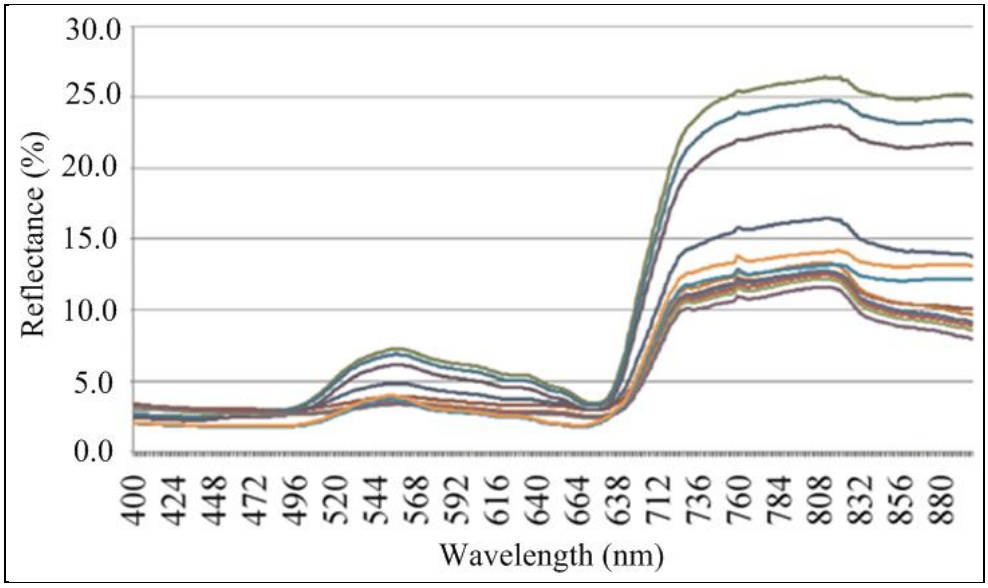

Figure 23 Results of spectral signatures in the experimental tank

Each colored spectra was extracted from the moist hydrilla leaves from a different location in the tank. A separation was noted between the third and fourth spectra due to the movement of the probe from one location to another. The surface reflectance of hydrilla was plotted against wavelengths between 400 nm and 900 nm and compared to the field measurements collected at the pier. The maximum reflectance in the experimental tank was observed in the NIR region at 26.5 percent and a wavelength 818nm. Chlorophyll absorbance was noted at a wave- length of 488 nm, 2.6 percent and 670 nm, and 3.26 percent. An irregular reflection was noted at 760 nm for all the spectral signatures, due to water absorption by the ASD instrument. A total of 29 measurements were collected from the pier, but only twelve were plotted for simplicity (figure 24). The spectral signatures for the tank and field measurements were averaged as shown on

(figure 25). The data shows that there were some differences in the spectral signatures collected from the experimental tank and from the field.

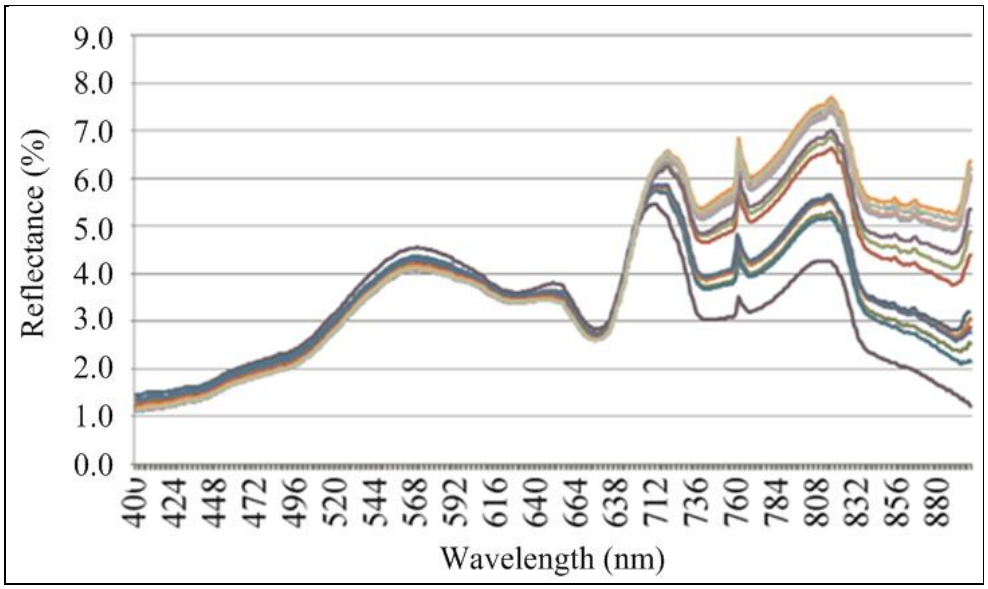

Figure 24 Results of spectral signatures in the field from the pier

The findings in this study showed that the reflectance measurements in the tank were higher than in the field because hydrilla in the tank was emergent. Both spectra collection were spectrally distinct over the NIR regions as shown on the figures. Similarly as in the experimental tank measurements, an irregular reflection was observed at 760 nm caused by water absorption registered in the ASD instrument. It is more noticeable on the spectra collected on the field than in the experimental tank. Hydrilla in the experimental tank were emergent, while the hydrilla in field were submerged. Hydrilla showed the typical vegetation reflectance pattern in the tank both sites; green

region peaking at a wavelength of 550 nm, red absorption near 670 nm, and NIR greater than 700 nm. Figure 25 above shows a reflectance difference between the tank and the field measurements from a wavelength of 685 to 839 nm. In the tank, hydrilla registered a peak reflectance at a wavelength of 818 nm and 16 percent and 6 percent for the field.

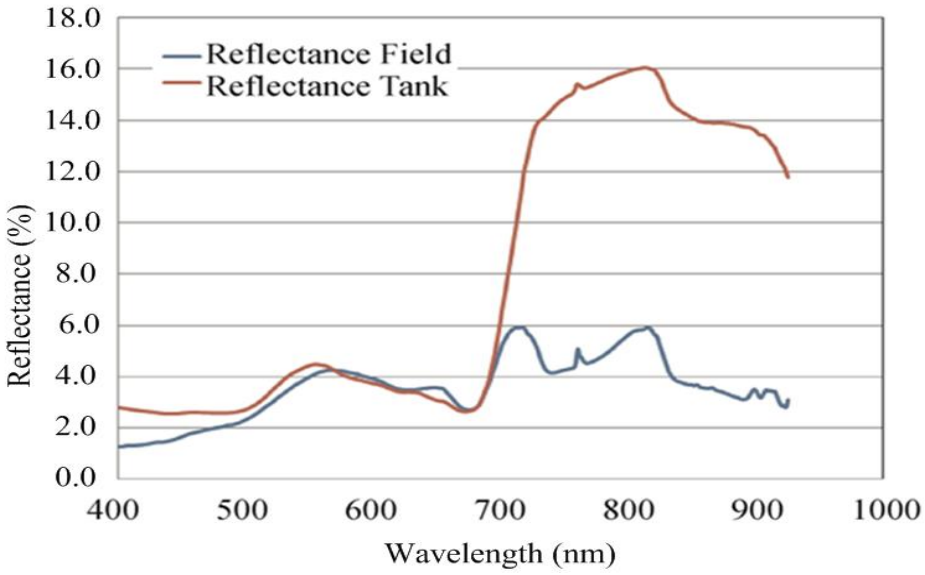

Figure 25 Results of the average measurements collected in the tank and the field

Results for the NDVI values for ten spectral measurements of hydrilla were calculated for the hydrilla in the experimental tank and are reported in an online library website[2]. The average NDVI for hydrilla was 0.695 for the experimental tank and 0.345 for the field. Kim et al. (1994) developed the Chlorophyll Absorption Ratio Index

[2] The results for the hydrilla spectral library can be found at the following website: http://estc.gmu.edu/database/Hydrilla/

(CARI), which measures the depth of chlorophyll absorption at 670 nm relative to the green reflectance peak at 550 nm and the reflectance at 700 nm. This ratio index was developed to reduce the changes of the active radiation due to the presence of different materials. The index uses bands which correspond to minimum absorption of the pigments which are centered at wavelength 550 nm and 700 nm, in conjunction with the maximum chlorophyll a absorption band which is at 670 nm. Wu et al. (2008) modified this chlorophyll ratio index (MCARI) as follows:

Equation 7 Modified Chlorophyll Absorption Ratio Index (CARI)

$$MCARI[670,700] = [(R700 - R670) - 0.2(R700 - R550)] * (\frac{R700}{R670})$$

The MCARI average values for ten spectral measurements of hydrilla were 0.026 for the experimental tank and 0.01665 for the field.

CHAPTER FIVE: REMOTE SENSING TECHNIQUES USING THE HYPERION SENSOR FOR MONITORING HYDRILLA

5.1 Background information

The Hyperion satellite was NASA's first hyperspectral imaging device aboard NASA's Earth Observing-1 (EO-1) under the New Millennium Program (NMP) of November 2000. Hyperion was the first civilian hyperspectral image sensor sent into space with a sun-synchronous, circular orbit inclined at 98.2^0 and at an altitude of 705 km. It covers an altitude swath of 7.5 km to 185 km. Hyperion is a push broom-type imaging spectrometer that follows about one minute behind the track of the Landsat-7 satellite. The Hyperion sensor has 220 spectral bands with the spectral range of 400 to 2500 nm at 30 m spectral resolution (Pearlman et al., 2003). The Hyperion satellite was tasked by NASA Goddard Space Flight Center (GSFC) to fly over the study area on July 20, 2011 at a twenty to twenty-nine percent cloud cover. The resulting image was downloaded from the Earth Explorer website. The acquisition date for the Hyperion data was collected the same month as the VIMS aerial photo. The objective of using the Hyperion sensor is to determine if hydrilla could be identified and classified in a waterbody by analyzing the spectral profiles processed using hyperspectral imaging techniques in the ENVI software.

5.1.1 Band selection

The Hyperion level 1R image, as previously mentioned, has up to 242 bands over an array of 256 pixels of which 182 bands are calibrated. There were sixty (60) noisy bands, which were not calibrated and were set to zero (Jupp et al., 2002). The reason for these non-calibrated bands was that Hyperion has a low signal to noise response (Felde et al., 2003). The 242 bands were viewed one by one for selecting noise-free bands for further processing. The noisy bands were 1–7, 58–78, 80–82, 120–132, 165–182, and 185–187. Bands corresponding to water absorption features were very noisy containing no spatial information and were subsequently removed from the data set. Also there is a spectral overlap between SWIR and VNIR sensors making two pairs of bands redundant.

5.1.2 Image acquisition and characteristics

The Hyperion image was downloaded from the Earth Explorer website[3], which was flown over the study site on July 20, 2011 area under a twenty to twenty-nine percent cloud cover. The acquisition date for the Hyperion data was collected the same month as the VIMS aerial photo. There was a spatial-temporal difference between the ground truth measurements collected on August 9, 2009 and the flyover of Hyperion on July 20, 2011. Figure 26 shows the Hyperion fly path over the study area. A subset of the Main Hyperion image is shown on (figure 27).

[3] The Earth Explorer website is available at the following link: *http://earthexplorer.usgs.gov/metadata/1854/EO1H0150322011201110K3_SGS_01*

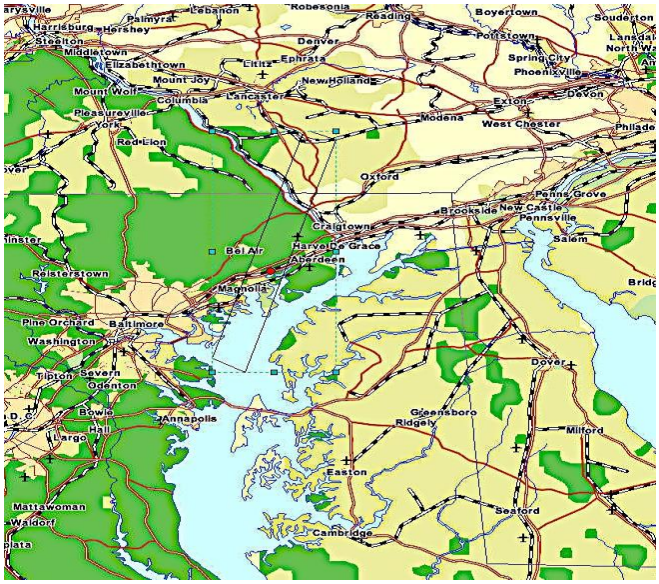

Figure 26 Hyperion flyover image highlighting the study area (Source: USGS, 2011)

Figure 27 Subset of Hyperion image downloaded from EarthExplorer website[1]

5.2 Data processing and analysis

The Hyperion image was atmospherically corrected using Quick Atmospheric Correction (QUAC), which is part of the Atmospheric Correction Module and is added to core ENVI version 4.8 (ITT-Exelis). QUAC is a Visible-Near Infrared through Shortwave Infrared (VNIR-SWIR) atmospheric correction method for hyperspectral imagery and is based on the empirical findings that average the reflectance of a collection of diverse material spectra. One example of this diverse spectra is the endmember spectra, which is essentially scene-independent.

QUAC provides for automated atmospheric correction of hyperspectral data in the solar reflective spectral region, between 400 and 2500 nm. QUAC creates an image of retrieved surface reflectance scaled into two-byte signed integers using a reflectance scale factor of 10,000. QUAC was selected because it performs an acceptable approximate atmospheric correction to FLAASH and other physics-based first-principle methods, generally producing reflectance spectra within an uncertainty of approximately +/-15 percent (Agrawal Gaurav et al., 2001).

5.3 Hyperspectral image analysis

The spectral Z profile was generated using ENVI, by opening a subset of a resized image, as shown in figure 28, and collecting the spectra from the green canopies in the water. Where there is surface vegetation on the water, typical vegetation spectra are generated on the graph. Figure 29 shows the spectral profile of the spectra collected from random pixels. The spectral signature of hydrilla begins to climb at the red edge, around 680 nm, and reaches a maximum reflectance at approximately eight percent. The spectral

range in the visible to the infrared regions decreases in surface reflectance as the signature increases in the spectrum; this could be due to certain attenuation in the water column such as algae or partial submersion of the hydrilla mats.

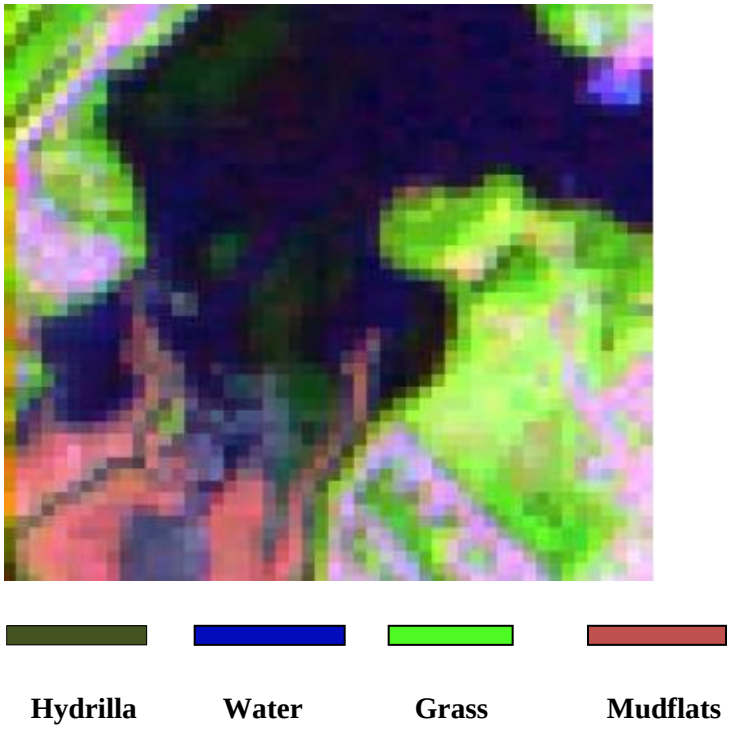

Figure 28 Subset of the raw image after atmospheric correction with QUAC

The spectral Z profile shows a water-vegetation spectrum with a high surface reflectance at 18 percent and a wavelength of 435 nm and declining to a wavelength of 680 nm with a surface reflectance of 6 percent. The hydrilla spectra begins to develop once it reaches the “Red Edge” at 680 nm, then it increases to a reflectance of about 8 percent. At 770 nm there is an irregularity, which is could be to water absorption.

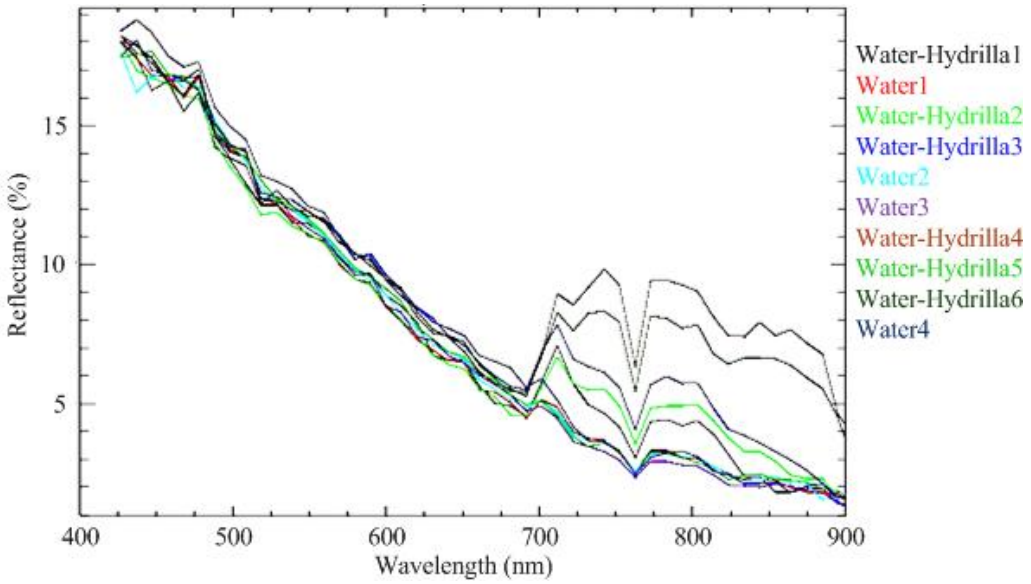

Figure 29 Spectral Z profile processed from the Hyperion image subset

5.3.1 Spectral Hourglass Procedure

The Spectral Hourglass Wizard (SHW) procedure derives endmembers from the hyperspectral image beginning with calibration of the imaging spectrometer radiance data, converting the data to reflectance, reducing the spectral and spatial dimensions to a few key endmembers for identification purposes, and then finally uses partial spectral unmixing to map the abundance and spatial distribution of the specific endmembers (Boardman and Kruse, 2011). SHW can extract spectral information without having previous knowledge or requiring the collection of referenced data. The SHW process flow diagram shown in (figure 30) uses the spectrally over-determined nature of hyperspectral data to find the most spectrally pure or spectrally unique pixels

(endmembers) within the dataset and to map their locations and sub-pixel abundances. This process flow begins with reflectance or radiance input data. The data can be spectrally and spatially subset, visualized in n-D space and the purest pixels can be clustered into endmembers. When the endmembers are located, the Spectral Analyst is used to identify them and for reviewing the mapping results. The SAM classification method was used in this study, which produced a classified image based on the value specified for the Maximum Angle (0.1 radian).

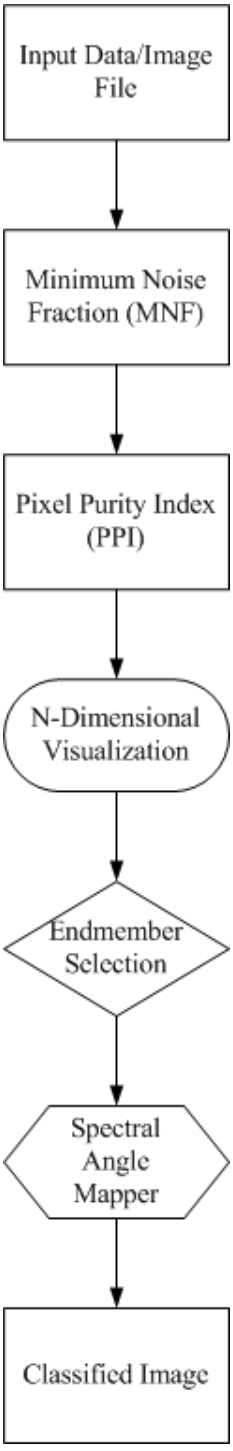

Figure 30 Flow process diagram of Spectral Hourglass Wizard (Source: Boardman and Krause, 2011)

5.3.2 Minimum Noise Fraction (MNF)

The MNF reduces the spectral variances of the data existent in the image so that the image can be displayed in a minimized form without changing the original data (Keshara and Mustard 2002). MNF reduced the number of bands to 33, and then produced an estimate of noise statistics. Higher order images have larger eigenvalues and spatially coherent MNF images (Jensen 2005). These larger eigenvalues correspond to most of the spectral data in an image. (ENVI Tutorials 2008. ITT-Exelis Inc, Boulder, CO). The eigenvalues range from 87.65 to 1.75 for bands 1 - 15. Figure 31 shows hydrilla and algae-laden productive waters at Otter Point Creek. The brighter red color defines the hydrilla area with the highest spectral reflectance. Figure 32 shows plot of MNF eigenvalues, showing the amount of covariance in each output MNF band. The output results of this data reduction process leaves 15 bands containing data.

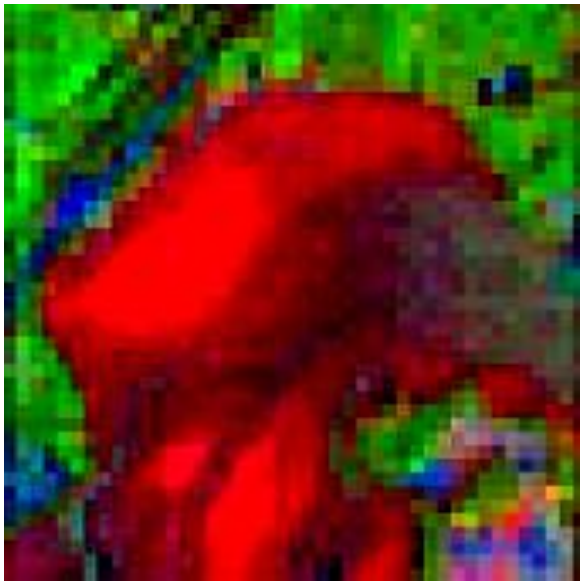

Figure 31 Subset of MNF image

Table 2 Hyperion Eigenvalues

Eigenvalues (Bands)	Eigenvalues
1	87.65
2	48.75
3	28.18
4	20.08
5	18.34
6	11.44
7	9.25
8	8.95
9	6.17
10	4.62
11	2.94
12	2.35
13	2.04
14	1.77
15	1.75

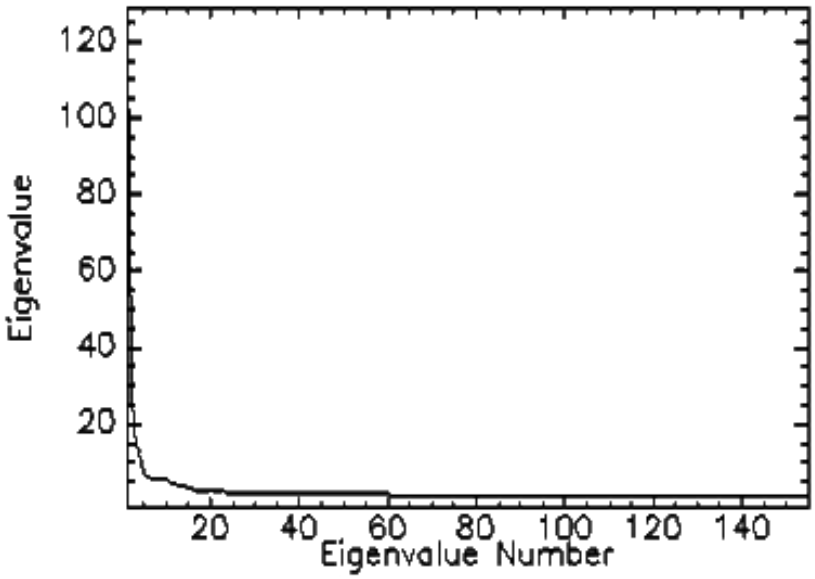

Figure 32 Plot of MNF eigenvalues

5.3.2.1 Minimum Noise Fraction statistics

ENVI will generate statistical reports and display plots of histograms (frequency distributions), mean spectra, eigen values, and other statistical information. It will also calculate basic statistics and/or tabulated histogram information. The minimum, maximum, and mean spectrum was calculated for multi-band images (figures 33, 34). Similarly the covariance statistics, including the eigen vectors and a correlation matrix, was only calculated for multi-band images.

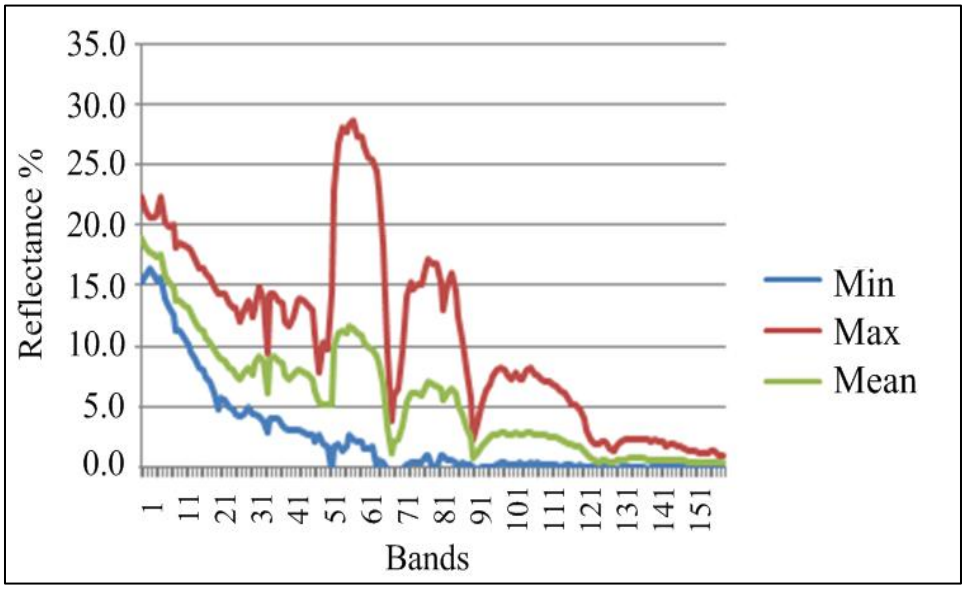

Figure 33 Hyperion Minimum Noise Statistics (Red)

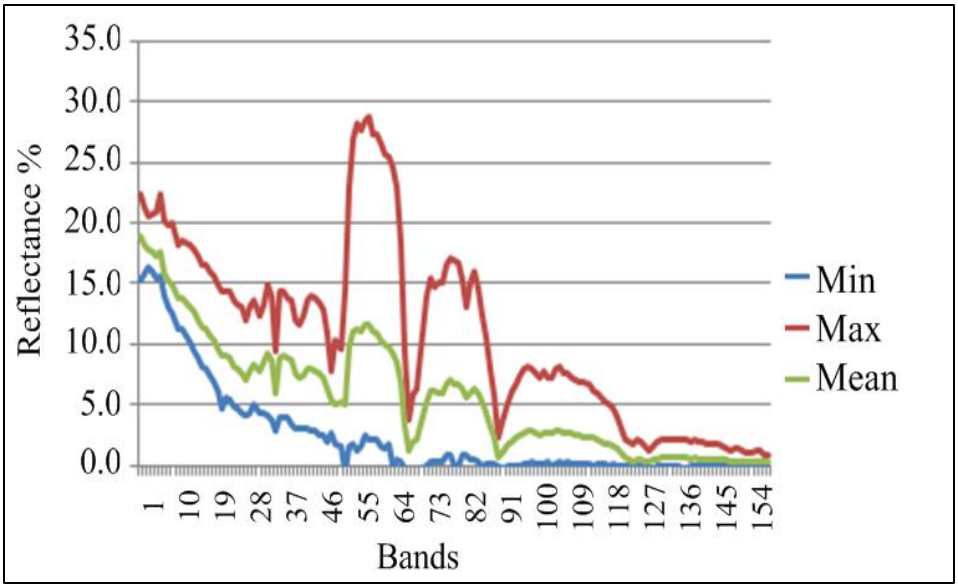

Figure 34 Hyperion MNF Noise Statistics (Green)

Definitions

- Basic statistics - these include minimum, max, mean, and standard deviation for all bands. ENVI does not calculate the band
- Covariance-The covariance calculates the covariance matrix, correlation matrix, eigen values, and eigen vectors

The MNF Transform produces two separate statistics; one is the MNF Noise Statistics and the other one MNF Statistics. ENVI Version 4.8 software computes the mean for each band of the raw Hyperion image for normalizing the data, the Covariance Statistics of the noise, for the noise rotation and normalization, and the Covariance Statistics. The first MNF rotation stores a complete set of covariances statistics in ENVI

file. The second rotation stores the eigen vector matrix and eigenvalues in the ENVI Statistics file. The ENVI program assumes that each pixel contains both signal and noise, and the adjacent pixels contain the same signal, but different noise. A shift difference is performed on the data differentiating adjacent pixels to the right and above each pixel being processed. The best noise estimate is collected using the shift-difference statistics from a homogenous area rather than an entire image. For the noise subset, the subset of the study area was used, most bands have little change in the subset; however, if any band in the data is set to zero (0) variance, a problem may occur where the covariance matrix cannot be inverted and the result would be too many (iterations) bands, by generating and receiving the statistics report on the same shift-difference subset of the raw image. If it is determined that any band has a zero variance, then a different or larger subset is chosen for the noise estimate. The shift-difference spatial subset needs to have more pixels than bands.

5.3.2.3 Interpreting the MNF eigenvalues plot

In the output is shown that the number of bands that were selected as the output. Bands with large eigenvalues greater than 1 contain data and bands with less than one contain noise. These compare the MNF band from the Available Band List in ENVI to the MNF eigenvalue plot to determine which bands have noise and which ones do not. After the processing is complete, the spectrally subset the MNF bands, so only include those bands where the images appear to be spatially coherent and the eigenvalues are above the break in slope of the MNF eigen value plot.

5.3.3 Cyanobacteria spectral profile

The spectral Z profile extracted from the MNF image (figure 35) derived a bell shaped curve which is recognized as a Cyanobacteria (blue - green algae) curve. Several pixels were selected at random from the MNF image which generated a series of spectral signatures. As noted, no water spectra was collected from the image.

Figure 36 shows the typical spectral profile of a cyanobacteria curve generated by several researchers. This pectral profile is similar as the one collected by the Hyperion sensor

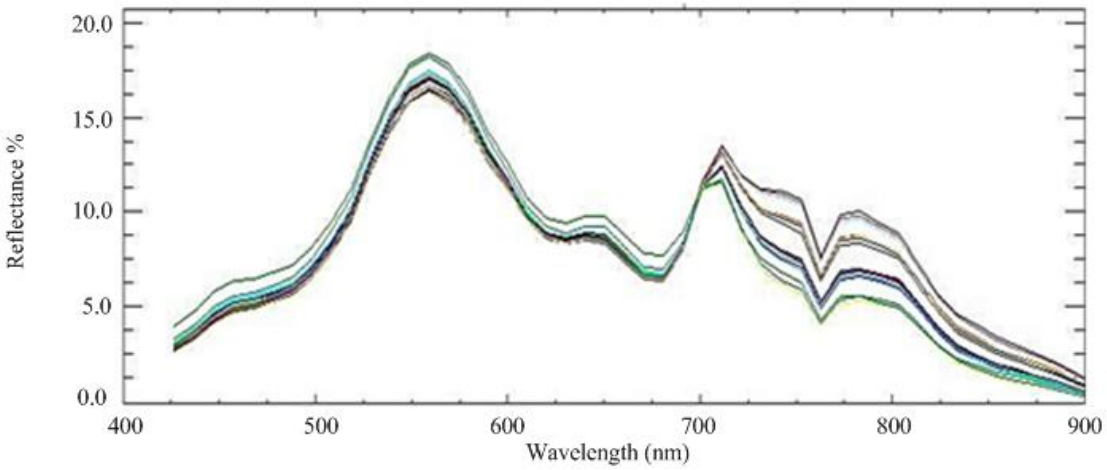

Figure 35 Endmember collected spectra from MNF image

Cyanobacteria is characterized by accesory pigments which favor the absorption of electromagnetic radiation in wavelengths other than that of Chlorophyll a, taking advantage of a wider range of the available photosynthetic radiation (Kirk 1994). The three main pigment groups affecting cyanobacteria optical properties are: chlorophyll a,

with absorption bands from 440 to 675 nm ; carortene, with absorption at the ultra-violet and blue region; and phycobiliproteins, which are exclusive of cyanobacteria and have an absorption band at 620 nm and a fluorescence band at 650 nm. The phycobiliprotein absorption band at 620 nm, produced by the phycocyanin pigment-protein complex in freshwater systems, is therefore a marker for cyanobacteria presence in eutrophic waters (Kutser 2004). Chlorophyll has two maximum absorption bands, one in the shorter blue light wavelengths and another in the longer red wavelength region. The maximum absorption bands for chlorophyll a is approximately 430 nm and 665 nm. Chlorophyll d absorbs at slightly higher bands, hitting maximums at approximately 448 nm and 690 nm (Rowan 1989). Phycoerythrin in cyanobacterial species can exhibit two absorption maximums, at about 559 nm and 569 nm. Phycocyanin exhibits an absorption maximum of about 620 nm. Allophycocyanin absorbs at a maximum of about 615 nm and 650 nm (Rowan 1989). The absorption band in the lower wavelengths of about 470 nm is likely due to a combination of Chla, carotenoids and dissolved matter (Rowan, 1989; Rundquist et al., 1996; Gitelson et al., 1999; Schalles and Yacobi, 2000). The green peak at 560 nm is present at the position of maximum reflectance caused by minimum absorption of algal pigments and scattering by non-organic particles and phytoplankton cell walls (Rundquist et al., 1996; Gitelson et al., 2000; Schalles and Yacobi, 2000). A trough at 628 nm represents the absorption maximum. At 650 nm, a small peak (d) represents a region of reduced pigment absorption and possibly fluorescence due to the PC (Rowan, 1989; Schalles and Yacobi, 2000). The second absorption peak of Chlorophyll a and cell wall competitively influence the spectra causing a trough at 675 nm (Rundquist et al., 1996;

Gitelson et al., 2000). This trough is followed by a peak at 704 nm which is caused by the interaction of suspended matter, including algal cells, and absorption due to water and Chlorophyll a (Gitelson et al., 1995; Gitelson et al., 2000; Schalles and Yacobi, 2000). Beyond this peak the spectra is strongly influenced by the absorption of water, causing low reflectance.

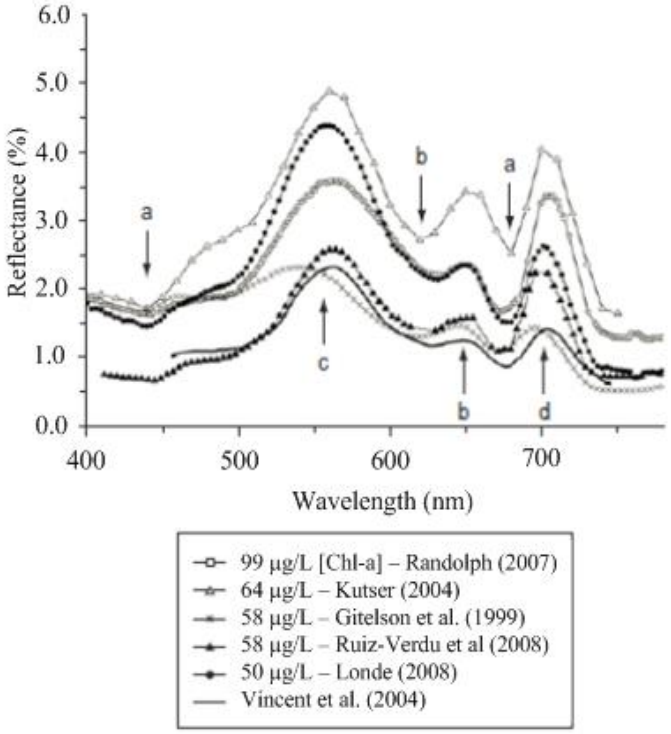

a) Chl-a absorption at 440 and 675 nm
b) Phycocyanin absorption at 620 nm and fluorescence at 650 nm
c) Scattering in the green region
d) NIR scattering by phytoplankton cells (Lobo et al., 2009)

Figure 36 Spectral curves presenting common cyanobacteria features (Source: Lobo et al., 2009)

The spectra collected from the subset of the raw image in the productive waters of Otter Point Creek resulted in a peak reflectance of 5 percent at a wavelength of

approximately 550 nm. This coincides with the cyanobacteria curves shown in (figure 37).

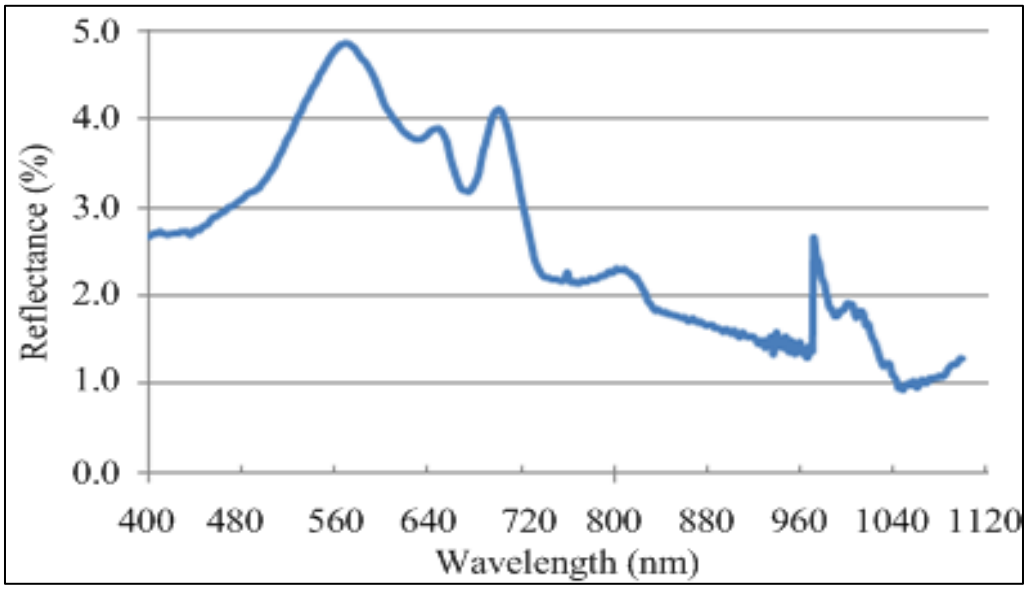

Figure 37 Spectral signature of algae-laden water (Source: Bukata 2005)

5.3.4 Pure Pixel Index

The PPI algorithm finds spectrally pure pixels in the hyperspectral image. A PPI image was created from the MNF image data set in which the Digital Numbers (DN) of each pixel represents the spectral pureness of the pixel. A threshold value of 2.5 was placed in the PPI image for segregating the pixels with high PPI values, which identifies the location of spectrally pure pixels. The resulting PPI had a number of iterations 5000 and 12,000 pixels. Figure 38 shows the PPI results with the number of iterations and the cumulative number of pixels. Once the iterations are completed, the PPI image (figure

36) is created in which the value of each pixel corresponds to the number of times that the pixel was recorded as spectrally extreme (ENVI version 4.8 ITT-Exelis 2008).

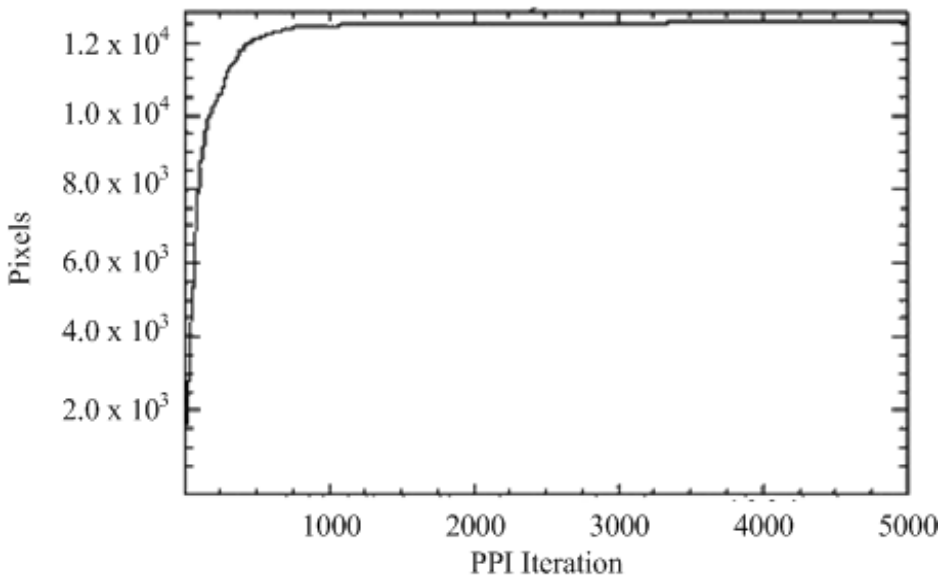

Figure 38 Pixel Purity Index curve

5.3.5 Two-dimensional scatter plot

A two-dimensional scatter plot was for used for testing the image data. Two bands were selected for identifying the training sites, including different classes such as water and aquatic vegetation. These training sites were used to identify the hydrilla mat on the water surface. The two-dimensional scatter plot method provides a two-band interactive classification of image data. Band 45 (803 nm) and 104 (1184 nm) were selected with minimum correlation to show high scattering for pixels as shown in (figure 39). Therefore, a good separation is shown between hydrilla, land vegetation, and water.

Pixels corresponding to the pixels colored on the two-dimensional scatter plot are highlighted. At the same time, the pictures and the composite image were used to identify the pixels that represent each class. The density distribution shows the density of the cloud of pixels at each location in the scatter plot. Regions of interest (ROIs) are selected for the three classes: hydrilla (red), vegetation (green), and water (blue), as shown in (figure 39).

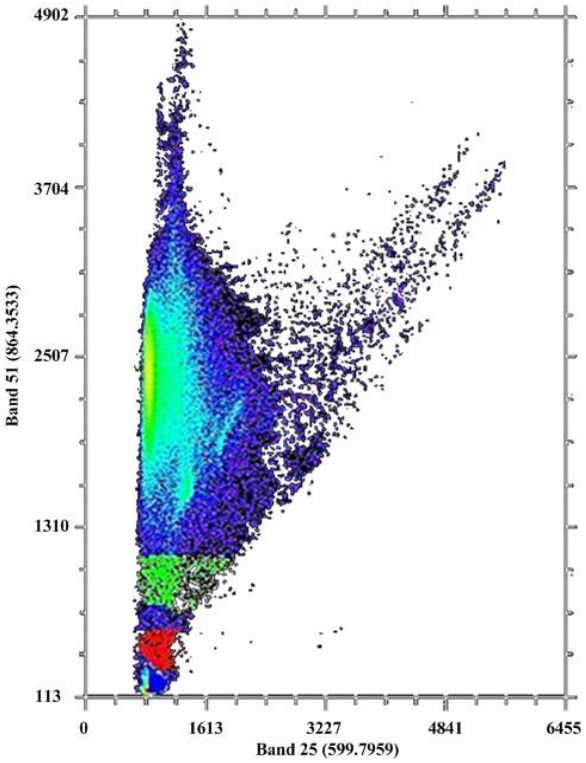

Figure 39 Two-dimensional scatter plot

5.3.6 Regions of Interest (ROI)

Once a set of pixels were defined using a scatter plot, each separate projection on the scatter plot, which corresponded to a pure end-member, was exported to a ROI from

the apparent reflectance data to act as end-members for spectral mapping **(**Kruse et al., 2003). The extracted end-members from the image were compared to the spectral library integrated in ENVI, which were collected on the water at the study site. A subset of identified end-member spectra that were extracted from the Hyperion image were used for spectral mapping techniques. Identified endmember spectra, including water and hydrilla, is shown in (figure 40). Figure 41 is the endmember collected spectra from the image in figure 40.

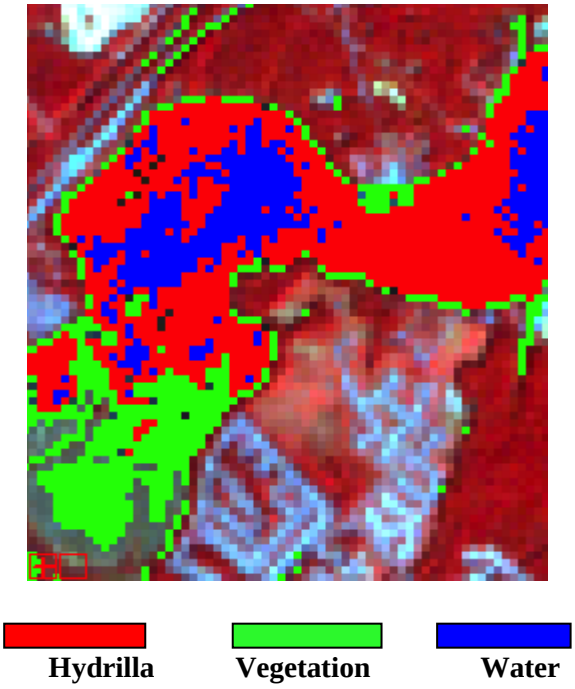

Figure 40 Regions of Interest

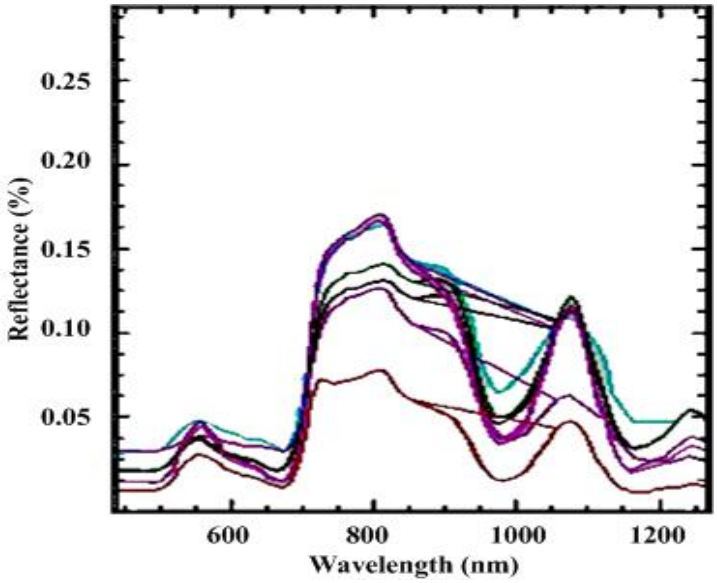

Figure 41 Endmember collection spectra of ROI

5.3.7 Spectral Angle Mapper (SAM)

The Spectral Angle Mapper (SAM) is a hyperspectral classification technique based on the method of matching spectral signatures. This classification technique matches the reference spectra from the spectral library and the pixels extracted from the remote sensing image for each pixel. This algorithm determines the spectral similarity between two spectra by computing the angle between them. It assumes that each spectrum can be described as a vector in n-dimensional space where n is the number of spectral bands. As such, it calculates the angle between the vector of the test pixel spectra and the vector of the reference spectra. The greater the difference between the test and reference spectra, the larger the resulting value. A threshold is set such that a pixel within the threshold is classified as the material being identified. An import feature in SAM is that it uses only the vector direction and not its length to calculate the spectral angle

between an input and a reference spectrum. This means that the method is not sensitive to spectra intensity changes and allows comparison between spectral signatures of different brightness levels. The algorithm derives from basic geometry; two vectors pointing in the same direction with different magnitudes have a zero degree angle difference. Relative image brightness acts as a scalar vector and will not change the reported angle between vectors. The spectral intensity could change due to changes in the inherent optical properties (IOP) in the water column, or due to atmospheric effects. If it is assumed that the IOP are constant for a given pixel, atmospheric and other environmental effects could be ignored. However, the accuracy of SAM is sensitive to the reference spectra.

SAM is applied to hyperspectral data for identifying spectral signatures of aquatic vegetation. The Spectral Angle Mapper (SAM) was applied to the image using ENVI version 4.8 for identifying potential areas of hydrilla. There were three bands selected for processing by SAM with NIR wavelengths ranging from 440 nm to 900 nm.

5.3.8 Spectrum extraction and analysis

There are several pixels extracted from the image of (figure 42) that show how the SAM algorithm was applied to the hydrilla mats. Image classification was performed using the Spectral Angle Mapper (SAM) in ENVI Version 4.8 in conjunction with the ground measurements collected on August 9, 2009 (Blanco et al., 2012). The SAM classified all 182 Hyperion bands for each pixel in the image set to determine the similarity between the spectral signatures developed from a pixel and that of a spectral signature from the spectral library.

Hydrilla Land Vegetation Water

Figure 42 SAM results

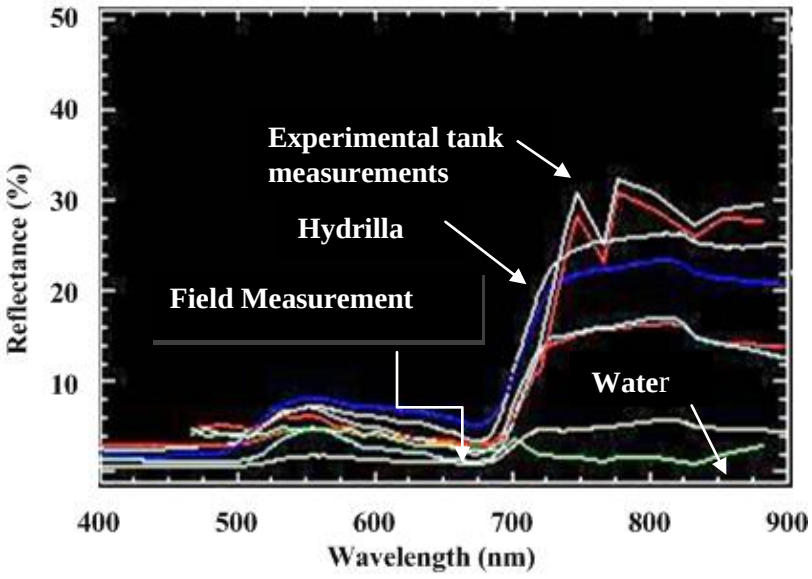

Figure 43 Spectral profile from SAM

The SAM results are shown in (figure 42) and the spectral library plots extracted from the SAM image are shown in (figure 43). Figure 42 shows the SAM classification map produced spectrally dominant hydrilla as clusters of red colored pixels using red band 201, green band 45, and blue band 23 corresponding to 2163 nm, 803 nm, and 579 nm respectively. Figure 43 shows the spectral library plots of hydrilla and vegetation end-member spectra extracted from the Hyperion image. The maximum reflectance of hydrilla was at twelve and seventeen percent at a wavelength of 810 nm.

5.4 Summary Results

The spectral signatures generated from the image using ENVI were similar to the spectral signatures collected at the OPC pier. A field survey done by the Maryland Department of Natural Resources (MDDNR) for the years 2008 thru 2011 confirmed that the dominant SAV species is hydrilla (Delgado 2011). Therefore, the spectral profile generated from the field measurements agree with the spectral profile generated from the Hyperion image. Bands were linearly transformed using the Minimum Noise Fraction (MNF) transformation and evaluated considering the eigenvalues. MNF component images show steadily decreasing image quality with increasing component number (Chen 2000). Higher eigenvalues have higher spectral values, as shown in Table 2, which shows the hydrilla footprint as a red color on the water. These potential end-member spectra were used in an n-dimensional (n-D) scatter plot and rotated in real time on the screen until extreme points on the scatter plot were exposed (Boardman 1993). Identified end-member spectrum of hydrilla is shown in (figure 43). These preliminary results prove that hyperspectral imaging techniques can be used for refining the results. Image

classification was performed using the Spectral Angle Mapper (SAM) in ENVI Version 4.8 in conjunction with the spectral library collected during the ground measurements on August 9, 2009 (Blanco et al., 2012). The SAM classifier examined the Digital Numbers (DN) of all 180 Hyperion bands for each pixel in the image set to determine the similarity between the spectral signatures developed from a pixel and that of a spectral signature from the spectral library. Figure 42 shows that the SAM classification map produced spectrally dominant hydrilla, as clustered of colored red pixels.

CHAPTER SIX: REMOTE SENSING TECNIQUES USING THE AISA SENSOR FOR MONITORING HYDRILLA

6.1 AISA sensor

The Airborne Imaging Spectrometer for Applications (AISA) sensor (Specim Corporation) is a compact airborne sensor whose charged-coupled device (CCD) array is sensitive to the VNIR wavelengths of the reflected spectrum. AISA was developed and tested in Finland in 1992 as a portable, cost effective, and programmable imaging spectrometer. AISA has a direct sight imaging spectrograph and high performance camera. It has a built in miniature global positioning system (GPS/INS) that allows for aircraft roll, pitch, and yaw information to be encoded for georeferencing (Jensen 2005). AISA is a push broom imaging spectrometer designed for airborne measurement although it can also be used for ground-based campaigns. AISA was flown on July 10, 2005 at 6:13 PM over the Otter Point Creek estuary at an altitude of 3.07 km. The AISA image was acquired onboard an aircraft managed by the University of Nebraska's Center for Advanced Land Management Information Technologies (CALMIT) remote sensing center. AISA has a spectral resolution of 2.5 m and a spatial resolution of 2.0 m. The AISA imagery acquired for this research has a spectral resolution of ninety-seven (97) bands with a range of 498 nm – 819 nm. The objective of using the AISA sensor is to determine if hydrilla could be identified and classified in a waterbody by analyzing the spectral profiles processed using hyperspectral imaging techniques in the ENVI software.

6.2 Hyperspectral imaging analysis

The AISA image shown on figure 44 was analyzed in ENVI for the selection of the spectral Z profile and collection of spectral signatures from random pixels on the raw image. The bands that were selected were 67 for the red band (912 nm), 35 for the green band (700 nm), and 8 for the blue band (536 nm), which resulted in a true color image (see Figure 42). The Z profile was created from the ENVI version 4.8 software. Figure 45 shows the spectral profile extracted from random pixels in the AISA image.

Figure 44 AISA True color image

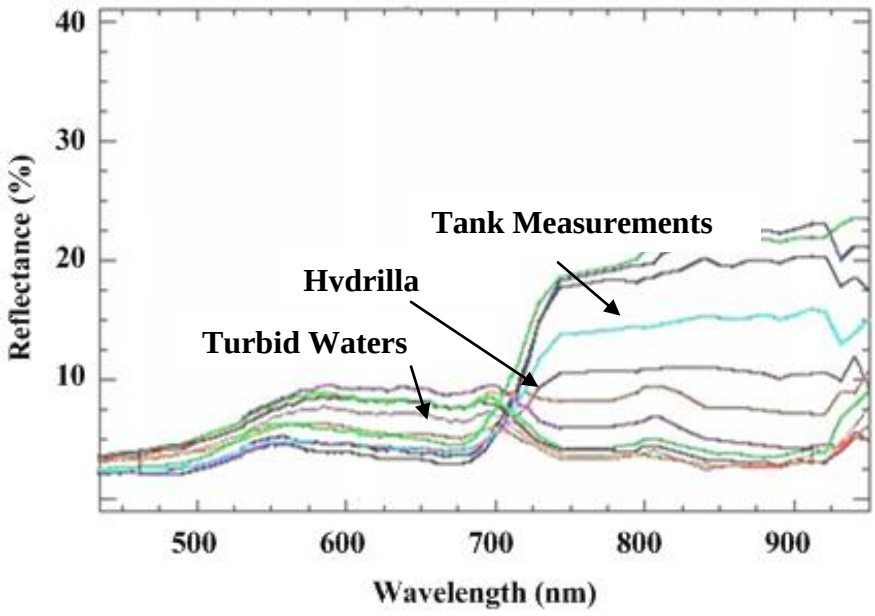

Figure 45 Spectral profile (Z) of true color image

6.3 Data preprocessing and analysis

6.3.1 Atmospheric correction

The conversion of radiance to reflectance for a hyperspectral image is necessary for atmospheric correction (Goetz et al., 2002). Atmospheric correction provides for more reliable results, especially the correction used with vegetation indices because the atmosphere introduces different levels of error into the bands that were used to create the indices. Moreover, data from different sensors, satellites, or aerial platforms can be substituted if the first selection is not available due to cloud cover, limitations of the orbit or technical issues. The AISA image was atmospherically corrected taking into consideration the solar irradiance, interaction of the electromagnetic energy with the atmospheric absorption, reflectance, scattering, and the sensor geometry. The AISA data set provided by the University of Nebraska, CALMIT, was corrected by the commercial package Fast Line-of-Sight Atmospheric Analysis of Spectral Hypercube, or FLAASH,

which is included in the ENVI Version 4.8 software. FLAASH corrects for atmospheric water vapor, oxygen, carbon dioxide, methane, ozone, and molecular and aerosol scattering. FLAASH also produces useful auxiliary information including a column water vapor image, a cloud map and a visibility value for the series (ENVI version 4.8 ITT-Exelis 2008). FLAASH is an atmospheric correction algorithm that covers the visible to the shortwave infrared (SWIR) hyperspectral data. FLAASH is a two-step process. The first step consists in the retrieval of atmospheric parameters. This is related to the aerosol type and its distribution, and water vapor. The second step then requires solving the radiation equation for the specific aerosol and water column and transformation to surface resistance. FLAASH uses the latest MODTRAN radiation transfer code to generate a unique solution for image (ENVI Tutorials 2008, ITT-Exelis Inc, Boulder, CO).

6.3.2 Spectral Hourglass Wizard procedure

The Spectral Hourglass Wizard process derives endmembers from the hyperspectral image. This process begins with calibrating the imaging spectrometer radiance data, converting the data to reflectance, reducing the spectral and spatial dimensions to a few key endmembers for identification purposes, and then using partial spectral unmixing to map the abundance and spatial distribution of the specific endmembers (Boardman and Kruse, 2011). The steps were previously shown in Figure 30. The Spectral Hourglass can extract spectral information without having previous knowledge or requiring the collection of ground data. The hourglass processing flow uses the spectrally over-determined nature of hyperspectral data to find the most spectrally

pure or spectrally unique pixels, called endmembers, within the dataset and to map their locations and sub-pixel abundances. This processing flow begins with reflectance or radiance input data. The data can be spectrally and spatially subset, visualized in n-D space and the purest pixels can be clustered into endmembers. When the endmembers are located, the Spectral Analyst is used to identify them and to review the mapping results. To perform an image classification several methods are integrated in the wizard and they are SAM, the Mixture Tuned Matched Filtering (MTMF) and the Linear Spectral Unmixing. Only the SAM method was used in this study, which produced a classified image based on the value specified for the Maximum Angle of 0.1.

6.3.3 Flow diagram of Spectral Hourglass Wizard

A flow diagram of hyperspectral imaging processes for the Spectral Hourglass Wizard was shown previously in Chapter 5, Figure 30.

6.3.4 Minimum Noise Fraction Transformation

The first step in the hourglass processing flow was the Minimum Noise Fraction, or MNF, rotation, a process that determined the inherent dimensionality of the data set, segregated noise in the data, and reduced the computational requirements for further processing (Boardman and Kruse, 1994). For example, this process determined the number of possible endmembers. The MNF transform in ENVI is modified from Green et al., 1998 and is essentially a double, or cascaded principal component transformation that results in a data space that can be divided into two parts, one part associated with a coherent signal, and a complementary part dominated by noise. Using only the coherent

portion in further processing, the noise was separated from the data, reducing the size of the data set, and improving the results. The MNF results indicated the true dimensionality of the dataset; the number of MNF bands containing a coherent signal is approximately equal to the number of unique endmembers in the dataset. The objective of the Minimum Noise Fraction Transform (MNFT) process is to reduce the spectral variances of the data that exist in the image so that it can be displayed in a minimized form without changing the original data (Keshara and Mustard, 2002). The magenta color delineates the hydrilla mat area in figure 46. The green color defines the algae-laden water. Figure 47 resulted in a typical spectral profile for very productive waters containing cyanobacteria (blue-green algae) in the visible region at 550 nm with a peak reflectance of 19 percent. This spectra profile is similar to the one from the Hyperion image (figure 35). At the "Red Edge", hydrilla peaked at a reflectance of 13 percent and at a wavelength of 710 nm. At 710 nm, hydrilla absorbs water, so the reflectance declines. Both spectra were selected from the same pixel location.

MNF reduced the data set to 10 bands as shown on Table 2 and then processed an estimate of the noise statistics. The higher order images will have larger eigenvalues and spatially coherent MNF images (Jensen 2005). The spectral profile shown a target spectra was collected from random pixels in the MNF image shown on figure 47.

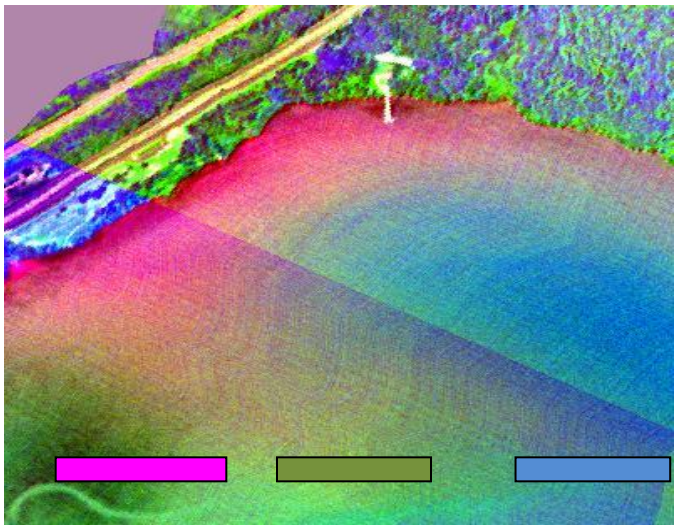

Hydrilla **Algae** **Water**

Figure 46 MNF image results

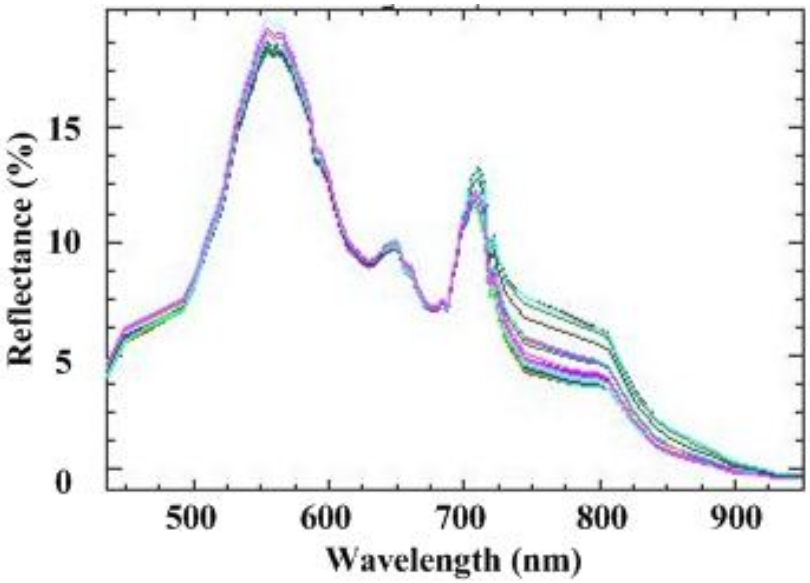

Figure 47 Target spectral profile collected from MNF image

The hydrilla spectra and the associated spectra in the image were examined for weighting using the high variance, or Eigen vector, portion of the spectra. Bands 1 – 10 have the highest eigenvalues as shown on Table 3 (250 to 2).

Table 3 AISA Eigenvalues

Eigenvalues (Bands)	Eigenvalues
1	250
2	200
3	150
4	50
5	12
6	10
7	8
8	6
9	4
10	2

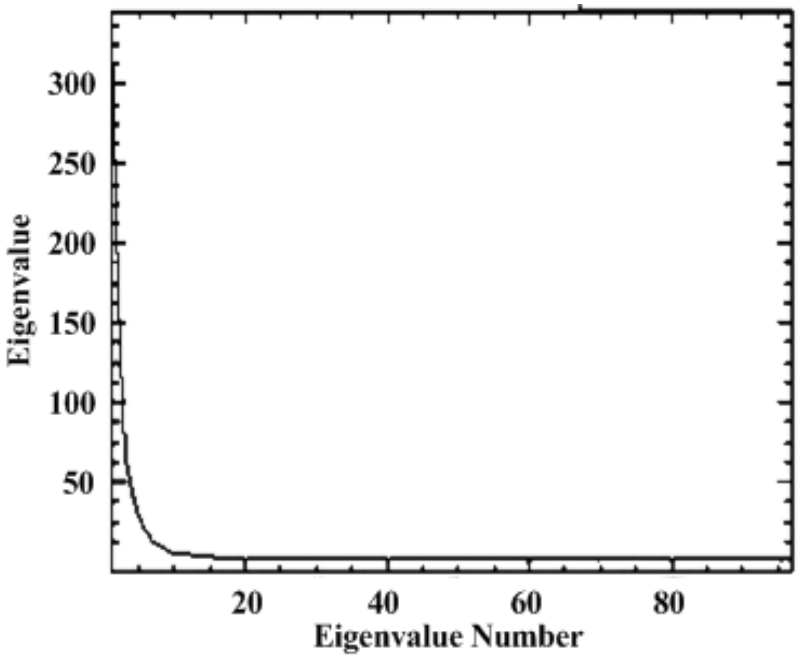

Figure 48 Plot of MNF

6.3.4.1 Minimum Noise Fraction Statistics

ENVI will generate statistical reports and display plots of histograms (frequency distributions), mean spectra, eigen values, and other statistical information. ENVI will calculate basic statistics and/or tabulated histogram information for single –band or multi-band images. The minimum, maximum, and mean spectrum was calculated for multi-band images (figures 49, 50). Similarly the covariance statistics, including the eigen vectors and a correlation matrix, was only calculated for multi-band images.

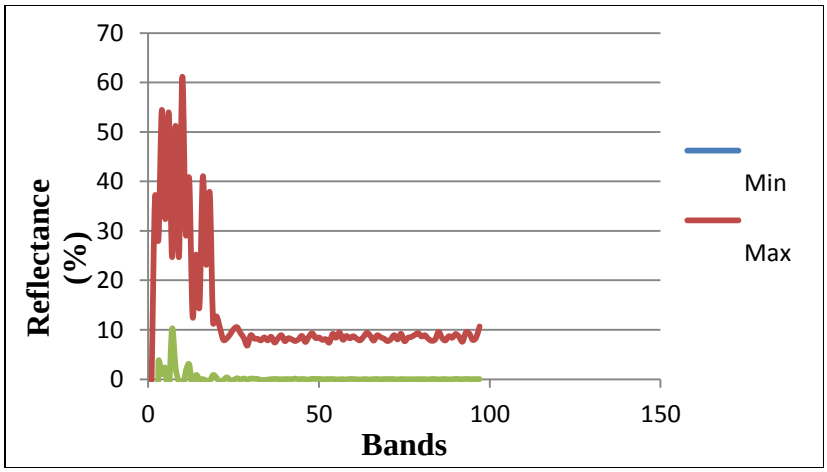

Figure 49 AISA Minimum Noise Fraction Statistics (Red)

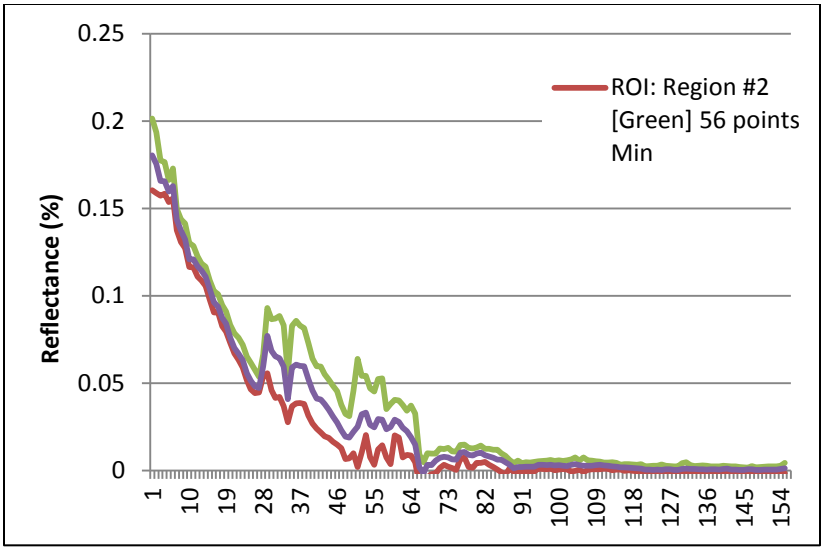

Figure 50 AISA Minimum Noise Statistics (Green)

6.3.5 Pixel Purity Index (PPI)

The PPI algorithm is integrated in ENVI Version 4.8 and it finds spectrally pure pixels in hyperspectral images. A PPI image was created from the MNF image dataset in which the digital numbers (DN) of each pixel represents the spectral pureness of the pixel. A threshold was placed in the PPI image for segregating the pixels with high PPI values, which identifies the location of spectrally pure pixels. PPI results show the number of iterations, 5000, and the cumulative number of pixels, 22,000, that have been found to be spectrally extreme. Once the iterations were completed, the PPI image was created in which the value of each pixel corresponds to the number of times that the pixel was recorded as spectrally extreme, as shown in figure 51.

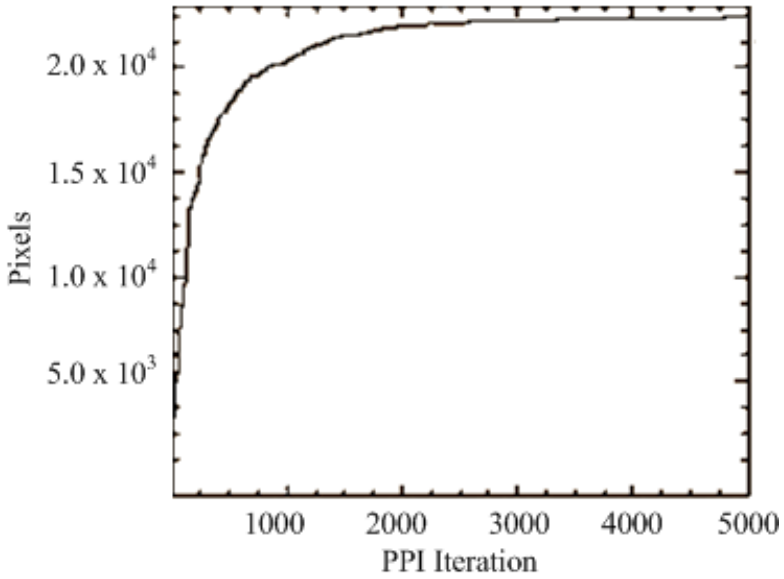

Figure 51 Pure Pixel Index

6.3.6 Two-dimensional scatter plot

The two-dimensional scatter plot shown on figure 52 was used for testing the image data. Two bands were selected for identifying the training sites, which included different classes such as water, and aquatic vegetation. These training sites were used to identify the hydrilla mat on the water surface. The 2D scatter plot method provides a two-band interactive classification of image data. Two bands, band 48 (803 nm) and band 104 (1184 nm), were selected with minimum correlation to show high scattering for pixels.

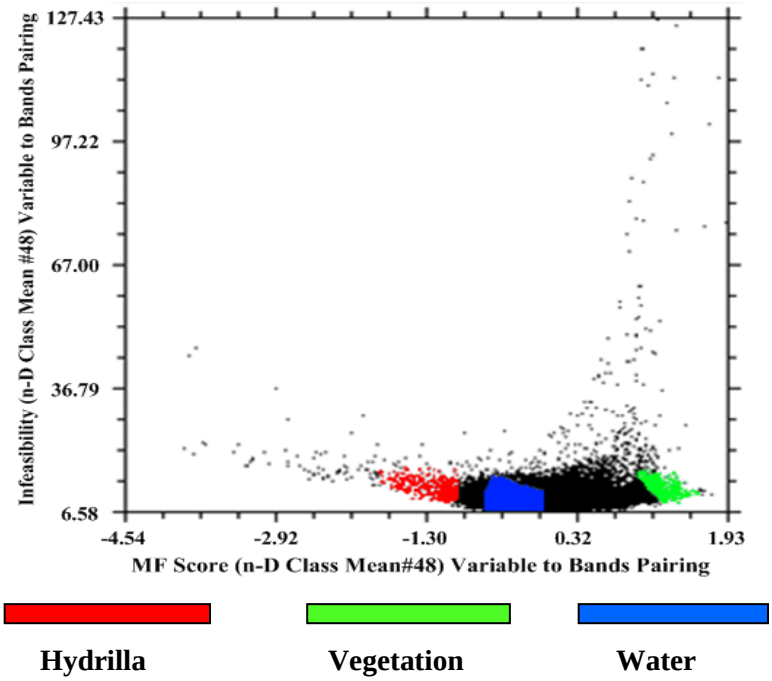

Figure 52 Two-dimensional scatter plot

The cursor is dragged over the scatter plot to mark pixels in color. The pixels corresponding to the pixels colored on the 2D scatter plot are highlighted in the image simultaneously. At the same time, the pictures and the composite image were used to identify the pixels that represent the class. A good separation is visible between hydrilla, land vegetation, and water. The density distribution shows how dense the cloud of pixels is at each location in the scatter plot. ROI's are selected for three classes: hydrilla (red), vegetation (green), and water (blue), as shown in figure 52.

6.3.7 n-Dimensional visualizer

The n-Dimensional Visualizer is an interactive tool for finding endmembers by locating and clustering the purest pixels in n-dimensional space. The spectra are points in

an n-dimensional scatter plot, and n is the number of MNF bands as shown on figure 53. The coordinates for cluster of pixels in n-space consist of “n” values that are simply the spectral radiance or reflectance values in each band for a given pixel.

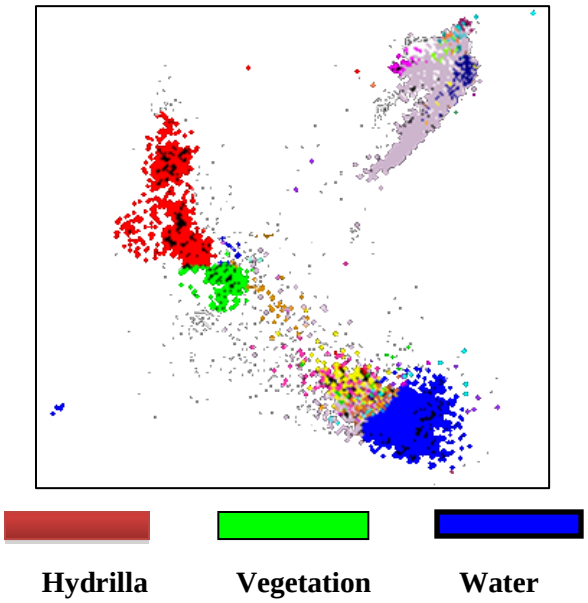

Figure 53 n-Dimensional Visualizer

The n-D Visualizer on figure 54 rotates the data cloud and colors draw a polygon on the image (figure 53) around a corner in the n-D Visualizer.T he position in the scatter plot conveys the same information in the spectrum for a single pixel. The best endmembers occur as vertices, or corners, of an n-Dimensional data cloud or mixing volume. A spectral profile is extracted from (figure 54) resulting on (figure 55) which is a typical vegetation spectra.

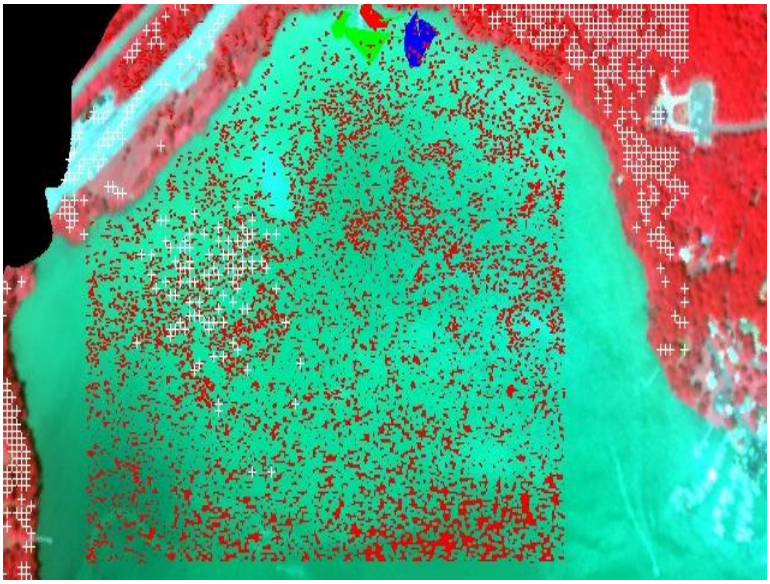

Figure 54 Regions of Interest

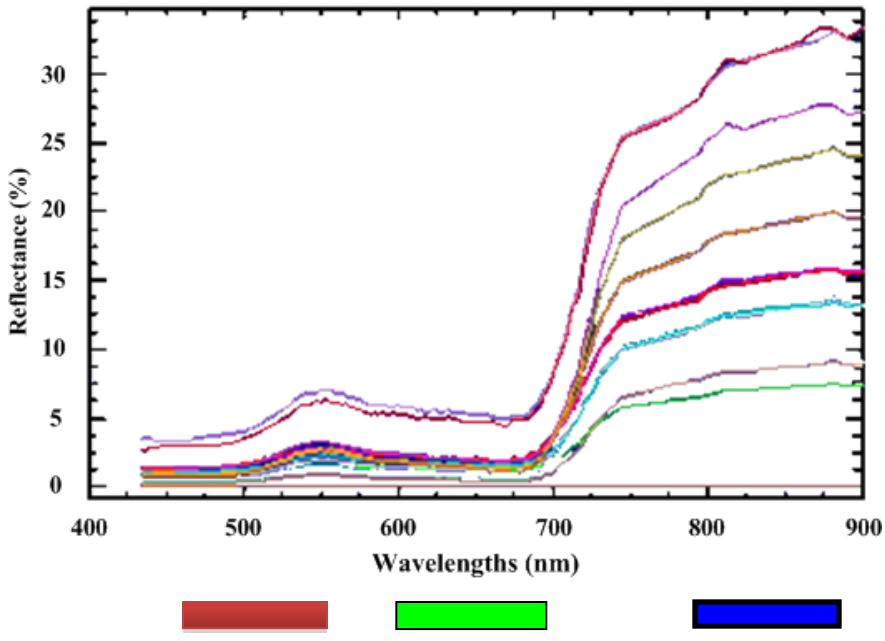

Figure 55 n-D Visualizer Endmember Spectra

6.3.8 Spectral Angle Mapper

A supervised classification using the SAM classifier was performed on an AISA image with the following three steps. First, the classification key was formulated consisting of the classes hydrilla, algae-laden water, and water. The classification scheme was partly based on the inspection of the classes present in the MNF results and the reference data collected on the water. Second, approximately 10 training sites were collected from the AISA imagery based on a random sampling. The training sites were carefully determined based on the homogenous nature of pixels with respect to tone, texture, association, etc., within a similar class. Their selection was guided by photo interpretation of the AISA image's very high spatial resolution imagery. Figure 56 illustrates the average hyperspectral spectra of the training sites collected for different classes. Using the training site data, the SAM classifier was processed using the ENVI version 4.8 software. SAM classifies the imagery based on the spectral similarity between image spectra and the reference spectra (Kruse et al., 1993). The spectral similarity is determined by calculating the angle between reference spectra and satellite image spectra when treating them as vectors in an n-dimensional space where 'n' is equal to the number of spectral bands of the sensor. Reference spectra can be generally taken either from laboratory or field measurements or can be equally extracted directly from the remote sensing imagery. In an n-dimensional multispectral space, a pixel vector has both magnitude (length) and an angle measured with respect to the axes that defines the coordinate system of the space. SAM is an automated method for comparing spectra of image pixels to the spectra of reference endmembers (also termed "Training Classes")

(CSES, 1992; Kruse et al., 1993). SAM treats each spectrum as a vector and determines the similarity between the unknown pixel spectrum and the reference spectrum by calculating the spectral angle between them. An example is shown in Figure 57 that uses a reference spectrum for Material A and an unknown spectrum from Material B with a data set of n spectral bands. The reflectance of each material can be plotted in a 2-D scatter plot for each combination of bands in the data set. A vector is extended from the origin to the point I-J reflectance for each material. The two band spectral angle for the reference and unknown pixels in the I-J data space is the angle between the two vectors. The color of a material is defined by the direction of its unit vector in n-dimensional spectral space. The length of the vector relates only to how fully the pixels are illuminated, not its absorption features. Because SAM uses only the direction of the spectrum, and not its length, all levels of illumination are treated equally. Poorly illuminated pixels fall closer to the origin, but still lie on the same vector as brightly illuminated pixels. Notice that the angle between the vectors is the same regardless of the length. In SAM, only the angular information is used for identifying pixel spectra, as the method is based on the assumption that an observed reflectance spectrum is a vector in a multidimensional space where the number of dimensions equals the number of spectral bands. A detailed description of the SAM algorithm is given in Kruse et al. (1993). The n-dimensional space for the SAM implementation was defined by the total number of AISA bands remaining after the implementation of the last pre-processing step. A single value of 0.1 radians was used as the maximum classification threshold value for all classes.

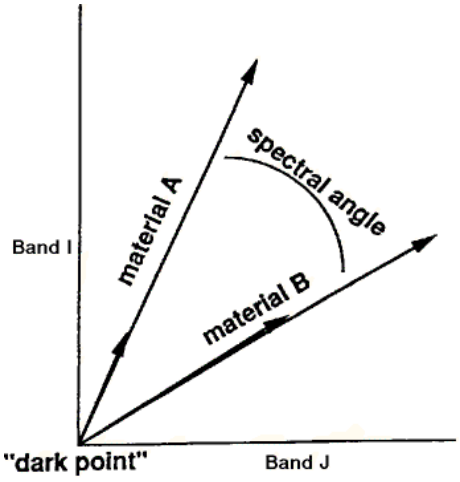

Material A – Hydrilla pixel spectra from reference data

Material B – Hyrilla pixel spectra from AISA sensor

Figure 56 Two-dimensional example of SAM (CSES 1992)

The SAM algorithm generalizes this geometric interpretation to n-dimensional space. SAM determines the similarity of an unknown spectrum "t" to a reference spectrum "R" by applying the equation shown in Equation 9 (CSES, 1992). In this equation, "nb" is the number of bands in the image. This technique was developed by J.W. Boardman and determines the spectral similarity between given reference spectra, "r" (image endmember) and the spectra found at each pixel, "t" (Kruse et al., 1992). The result of the comparison is reported as the angular difference in radians between the two spectra.

Equation 4 SAM Algorithm (CSES, 1992)

$$\alpha = \cos^{-1}\left(\frac{\vec{t} \bullet \vec{r}}{\left\|\vec{t}\right\| \bullet \left\|\vec{r}\right\|}\right)$$

$$\alpha = \cos^{-1}\left(\frac{\sum_{i=1}^{nb} t_i r_i}{\left(\sum_{i=1}^{nb} t_i^{\,2}\right)^{1/2}\left(\sum_{i=1}^{nb} r_i^{\,2}\right)^{1/2}}\right)$$

6.4 Summary Results

6.4.1 Spectral Angle Mapper (SAM)

SAM is the final step in the spectral hourglass wizard (SHW) procedure and is the best method for mapping Hydrilla. Past experience in other studies supports the selection of SAM as the most commonly used technique. The SAM output consists of a classification image as shown on (figure 57) and a set of rule images, which corresponds to the spectral angle, calculated between each image pixel and each endmember. The rule images are helpful if the SAM classification image does not show spatially coherent classes. They can be examined individually by loading each rule image into a display window. The SHW automatically reverses the color table and estimates a linear stretch of the image. The best matches are the small angles. In order to change the stretch maximum of the displayed rule image the desired value can be entered in the default

stretch max text box. The ENVI cursor location tool was used to look at SAM spectral angles for each pixel and identify a new SAM threshold, if necessary (ENVI Tutorials 2008. ITT-Exelis Inc, Boulder, CO). The threshold was set at 0.1 radian. Finally a SHW summary report is obtained which contains a summary of processing steps and a list of output files. SAM classified all 97 AISA bands for each pixel in the image set to determine the similarity between the spectral signatures developed from a pixel and that of a spectral signature from the spectral library.

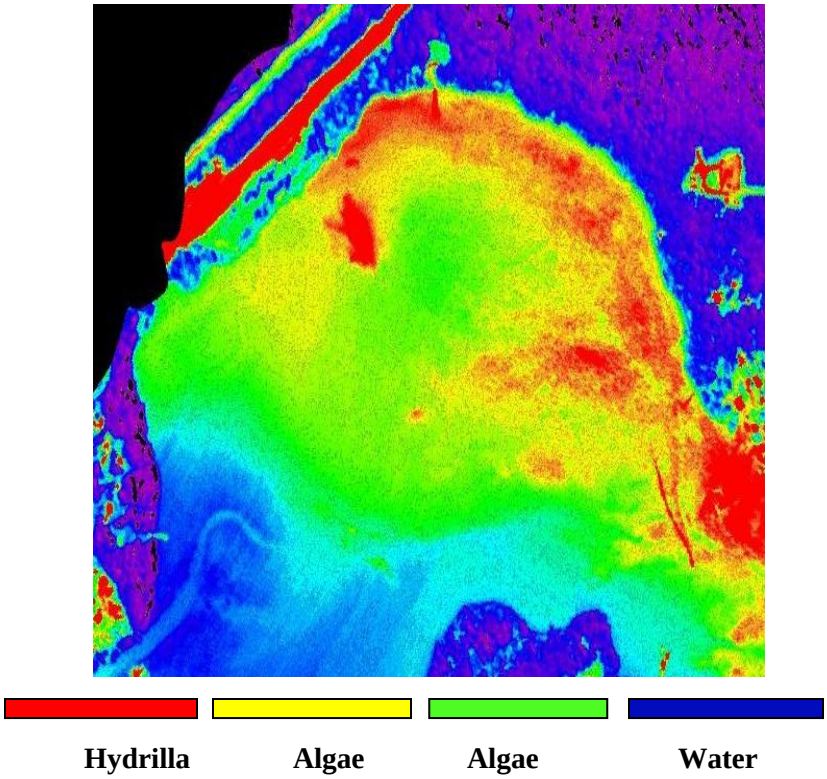

Figure 57 Spectral Angle Mapper Results

For mapping hydrilla, the SAM was selected and produced an image map showing the distribution and abundance of hydrilla. Figure 58 shows the spectral library plots of hydrilla and vegetation endmember spectra extracted from the Hyperion image.

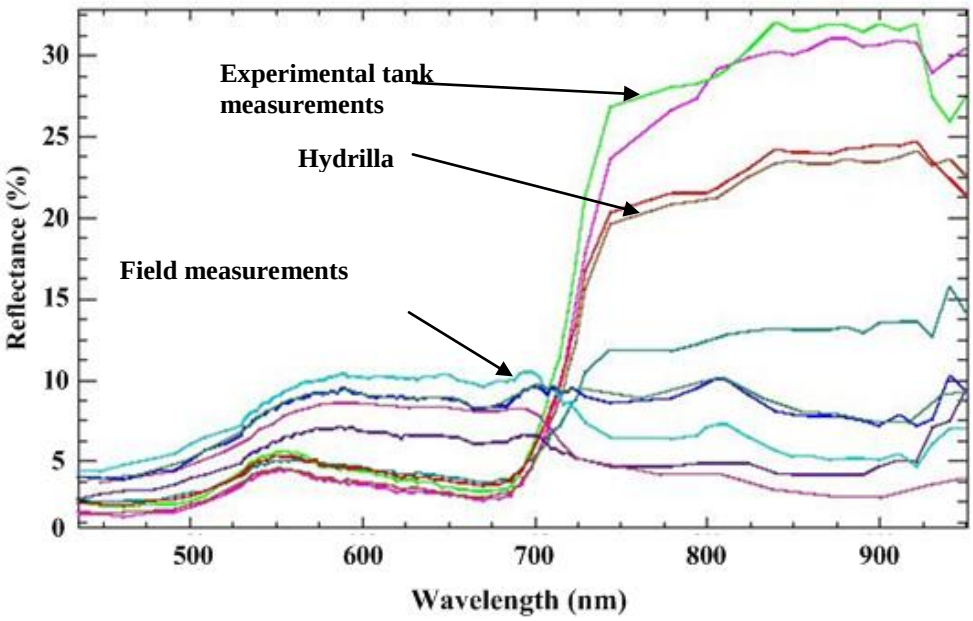

Figure 58 Spectral profile collected from SAM

The maximum reflectance of hydrilla is 17 percent at 810 nm, which approximately agrees with MNF results of about 19 percent. The user determines the spectral properties of the class by defining an ROI within an image and extracting the spectral information for that group of pixels. The types of classes defined by the user depend on the themes of interest within the image. The major thematic classes often used

for invasive plant species mapping are: invasive plant species versus background, primary vegetation groupings and disturbance.

Chlorophyll-a is represented by the yellow patches and the green may be algae. The aquamarine and blue cluster of pixels represent turbid conditions in productive waters. The turquoise and blue water are turbid and clear water. Hydrilla is dominant in the Otter Point Creek estuary. Therefore the spectral profile generated from the ground truth measurements are in agreement with the spectral profile generated for the spectral profile generated from the AISA image.

6.5 Accuracy assessments

Accuracy was empirically determined by selecting a sample of pixels from the thematic map and checking their labels against classes determined from the ground measurements. Accuracy assessments determine the quality of the information derived from remotely sensed data (Congalton and Green, 2009). Assessments can be either qualitative or quantitative. Qualitative assessments, a map is looked at to see whether the image is correct or not by comparing what is observed on the image with the ground. This analysis is very straightforward. Qualitative assessment attempts to identify and measure remote sensing-based error. In this assessment, the reference data is compared to thein-situ field measurements. The Confusion Matrix was calculated in ENVI using the ROI's. Adding up the number of pixels that are correctly classified and dividing it by the total number of pixels calculates the overall accuracy. The ground ROI defined the true class of the pixels. The Overall Accuracy for the AISA image was 49.35 5 AND A Kappa Coefficient of 0.36.

CHAPTER SEVEN: VALIDATION OF SATELLITE AND AIRBORNE HYPERSPECTRAL IMAGES WITH IN SITU FIELD MEASUREMENTS AND AERIAL PHOTOS

7.1 Validation of satellite and airborne with in - situ field measurements

The easiest way of validating the satellite and airborne hyperspectral measurements is to compare the spectral profile collected from the Hyperion and AISA images, MNF, and SAM, with the field measurements. The spectral signature profiles collected from the experimental hydrilla tank with the hydrilla canopy emergent generated a range of peak reflectance between 16 and 26% at a wavelength of 810 nm as seen on (figure 59) because the hydrilla canopy was emergent on the tank. The spectral profile from the estuary, as shown in (figure 60), generated a lower spectral reflectance between 4 and 7% at 810 n. At the time the field measurements were obtained on the water surface, the hydrilla canopy was submerged; therefore, this validates the spectral profiles on Figure 61. A reflectance of less than 10% generally indicates that the hydrilla is submergent.

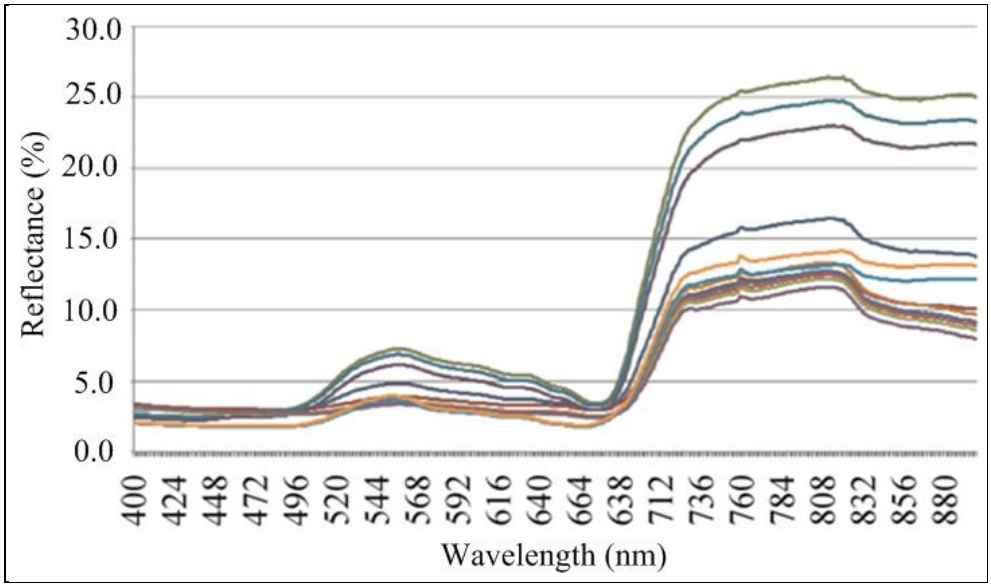

Figure 59 Experimental tank spectral profile of hydrilla

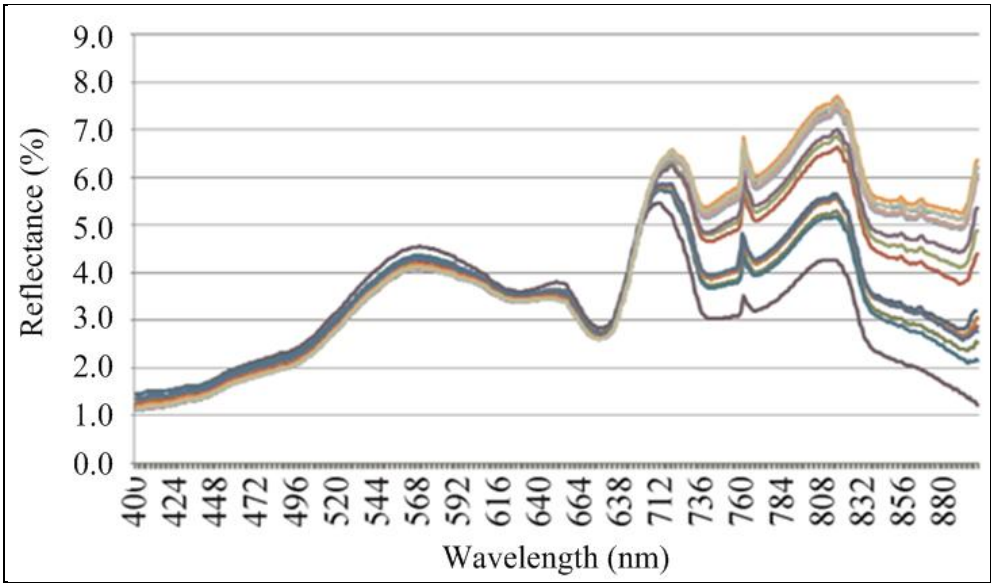

Figure 60 Reference field spectral profile

7.2 Validation of the Hyperion measurements

The image in Figure 61 was generated from a subset of a true color Hyperion image. The plot below is based on a collection of random pixels in the image. The spectral profile in the visible region of the electromagnetic spectrum declines from an average reflectance of 19% at 425 nm to 5% at 690 nm. At the "Red Edge"760 nm the spectral curve reaches a peak reflectance at 28 %. Oxygen is absorbed at 760 nm followed by water absorption at 820 and 935 nm. The trough on Figure 59 at 680 nm agrees with Figure 60, 690 nm at a surface reflectance of 3%. The peaks shown on Figure 60 reference field data at 765 nm are due to oxygen absorption.

Figure 61 Subset of raw Hyperion image after atmospheric correction

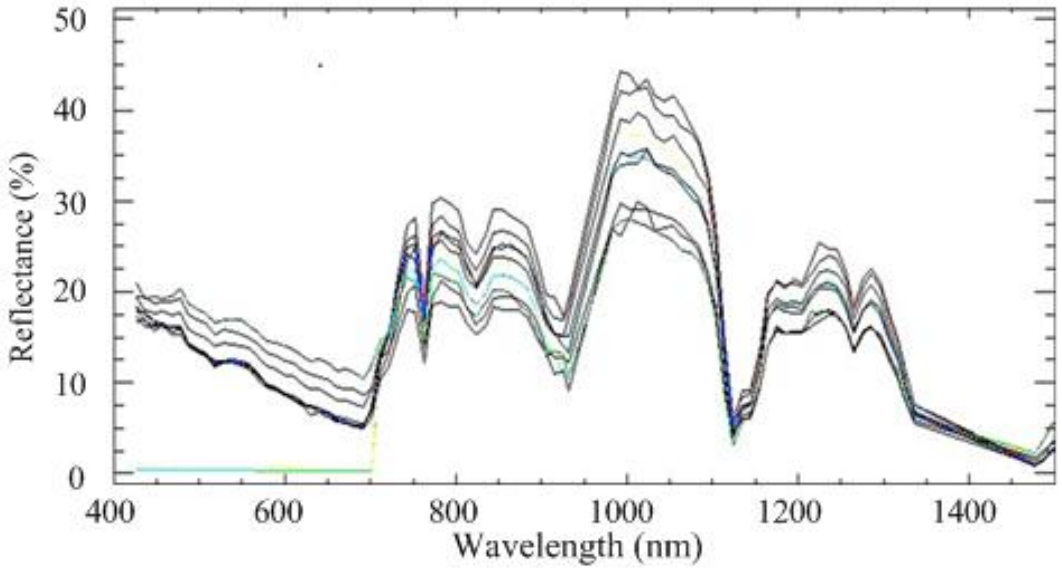

Figure 62 Spectral signature profiles of hydrilla collected from Figure 63

The spectral profiles from the Hyperion true image the "Red Edge" starts from to 760 nm with a peak reflectance of 28%, which validates Figure 62. The spectral library plots generated from the Spectral Angle Mapper (SAM) image Figure 62 resulted in a peak reflectance between 17 and 27% at a wavelength of 810 nm as shown on Figure 65. It is possible that the hydrilla canopy is floating at the higher reflectivity and submerged at less than 16% reflectance. This comparison of spectral results matches very well and validates the hydrilla canopy as floating.

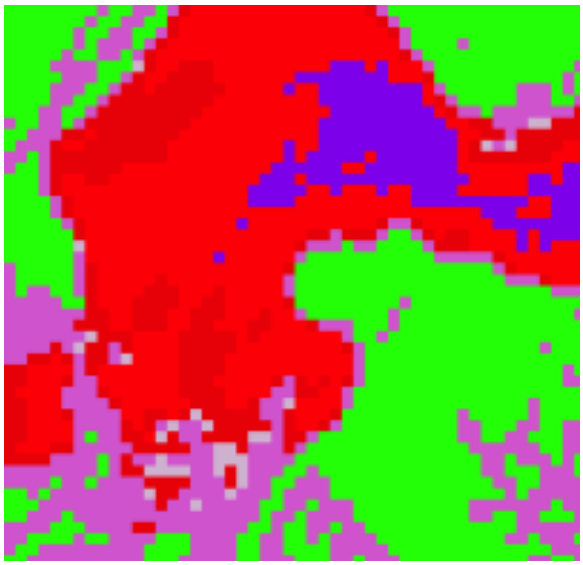

Figure 63 SAM results

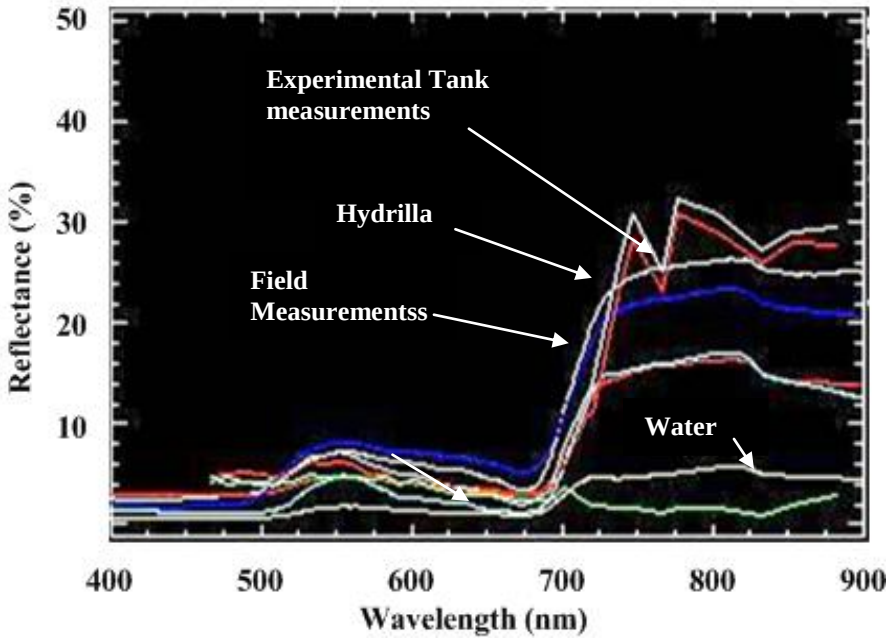

Figure 64 Spectral profile generated from the Spectral Angle Mapper

7.3 Validation of AISA measurements

Several random pixel locations were selected on the water surface of Otter Point Creek from the true color image shown on Figure 65. A spectral signature profile was processed in ENVI® version 4.8 for the AISA true color image resulting in a peak reflectance in the NIR of 11.5 to 18% at a wavelength of 730 nm as shown on Figure 66. This means that the hydrilla is floating. When we compared this spectral profile with the field reference data, we noted similarities. For instance, the profile shows two peak reflectances, one at the "Red Edge" 710 nm with a peak reflectance of 10% and 11% at 830 nm.

Figure 65 Subset of AISA true color image

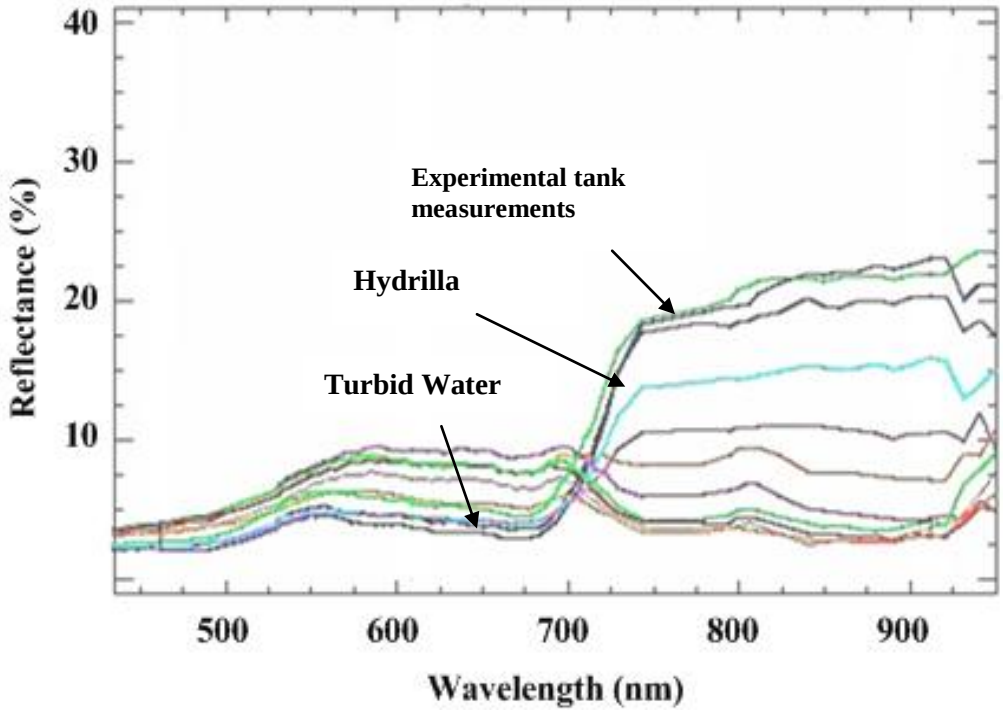

Figure 66 Spectral profile generated from true color AISA image

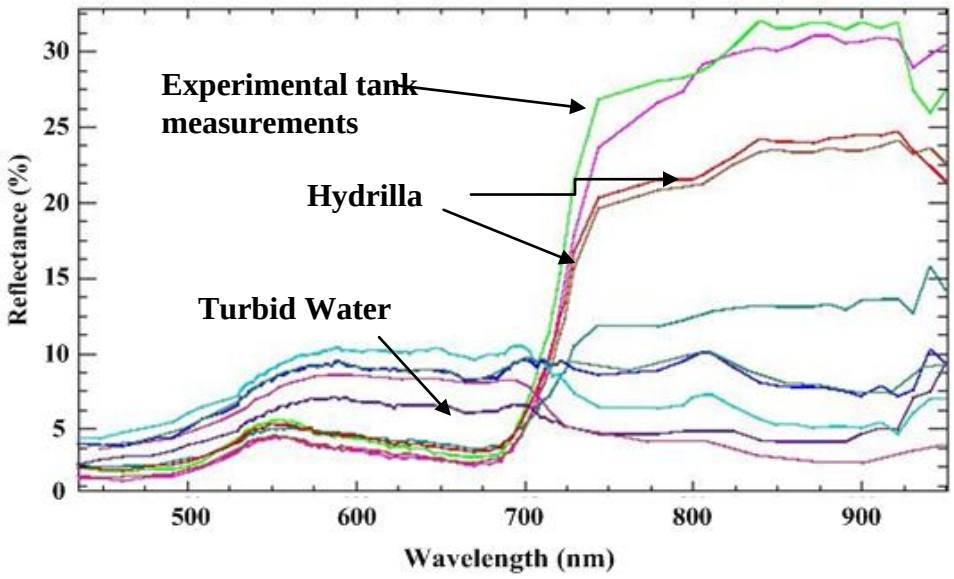

Figure 67 Spectral profiles generated from SAM image

7.4 Hyperion and AISA MNF results

The results from the processing of the MNF algorithm are compared for determining the extent of the hydrilla canopy. Figure 68 shows a bright red canopy inside a darker red canopy. This may be interpreted as the hydrilla canopy being partly submerged in water. Figure 68 is the MNF results from the AISA image. By visual analysis, the Hyperion sensor resulted in a more distinct hydrilla canopy than the AISA image.

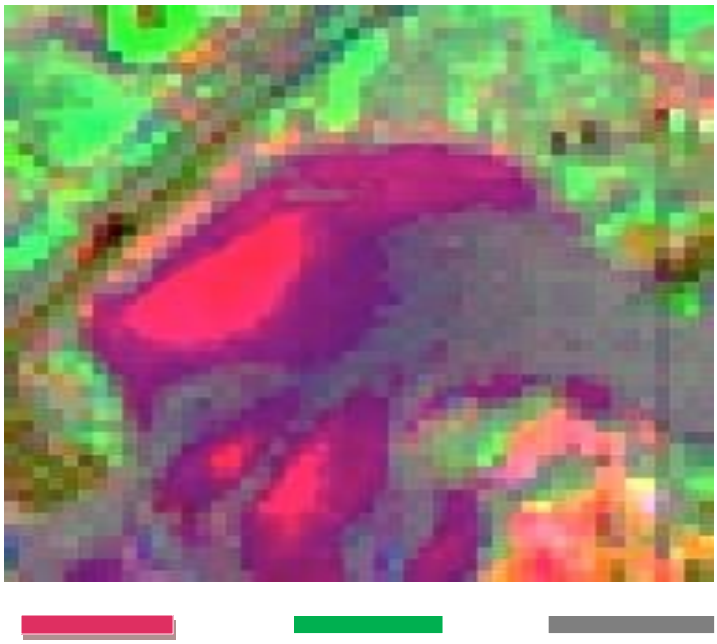

Figure 68 MNF results of Hyperion image

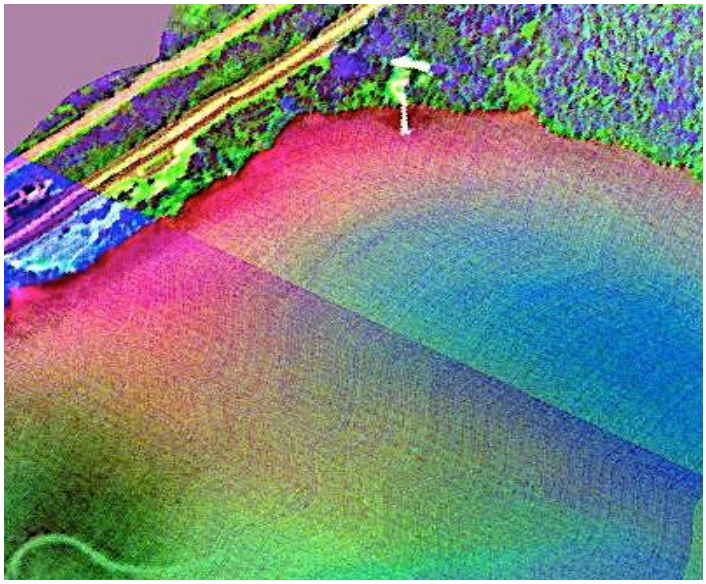

Hydrilla Vegetation Water

Figure 69 MNF results of AISA image

7.5 Validation of hydrilla canopy

Table 4 shows coverage in the area for four years and it can be concluded that no change in surface area for the hydrilla canopy occurred for those years. There were only two other SAV beds found in Otter Point Creek for those years. No SAV data was collected for the years 2006, 2009, and 2010.

Table 4 Surface area of hydrilla for 2005, 2007, 2008, and 2011 (Source: VIMS)

Year	Class of SAV	Area (m^2)	Density %	Source
2011	Hydrilla	470,297	70-100	VIMS
2008	Hydrilla	470,207	70-100	VIMS
2007	Hydrilla	470,207	70-100	VIMS
2005	Hydrilla	470,207	70-100	VIMS

7.6 Photo interpretation and bed delineation

The SAV beds were interpreted on-screen from the orthophoto mosaics shown on (figure 70) using ESRI ArcInfo GIS ® software. The identification and delineation of SAV beds by photo interpretation used knowledge of aquatic grass signatures on film, distribution of SAV in 2011 from aerial photography, 2011 ground survey information, and aerial site surveys. In addition to delineating SAV bed boundaries, an estimate of SAV density within each bed was made by visually comparing each bed to an enlarged crown density scale similar to those developed for estimating crown cover of forest trees from aerial photography (Paine 1981).

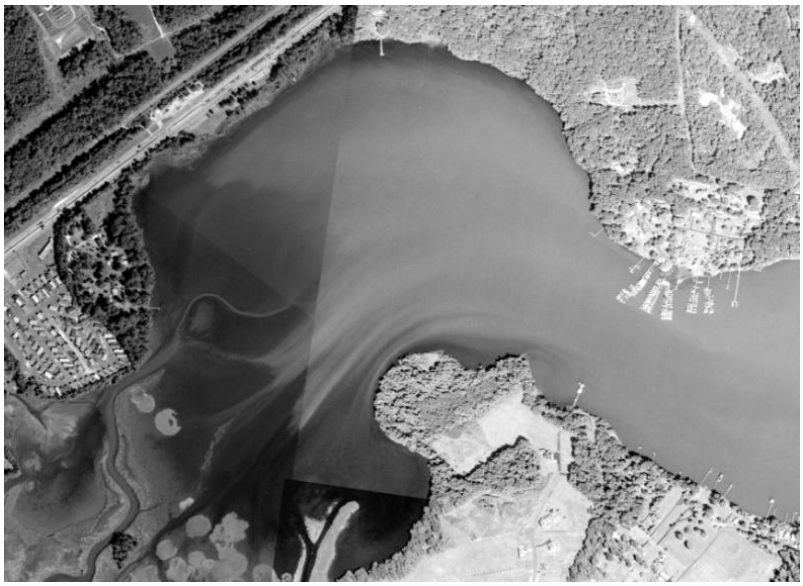

Figure 70 Aerial photo of Otter Point Creek
Note: Hydrilla canopy is shown as darker areas. (Source: VIMS , 2011)

Bed densities were categorized into one of four classes based on a subjective comparison with the density scale. These were: 1, very sparse (<10% coverage); 2, sparse (10-40%); 3, moderate (40-70%); or 4, dense (70-100%) (Wilcox et al., 2009). Figures 70 and 71 show the aerial photos taken of the study area showing submerged SAV as dark areas on the water.

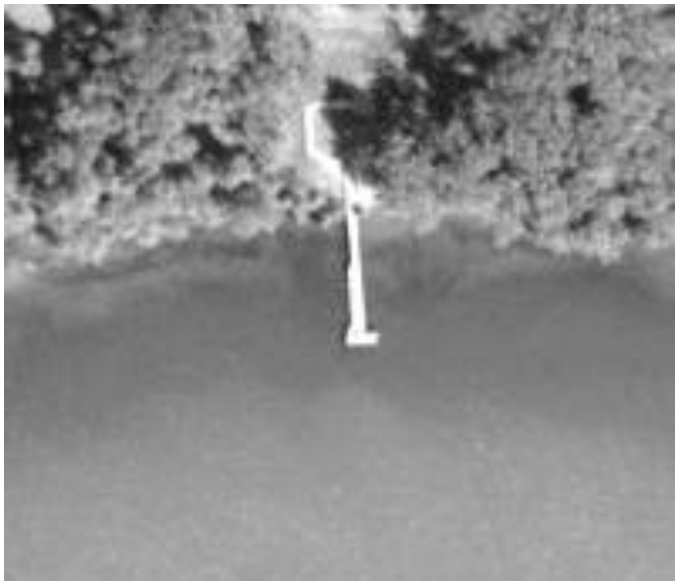

Figure 71 Subset of the aerial photo showing the fishing pier where in situ field measurements were collected. (Source: VIMS, 2011)

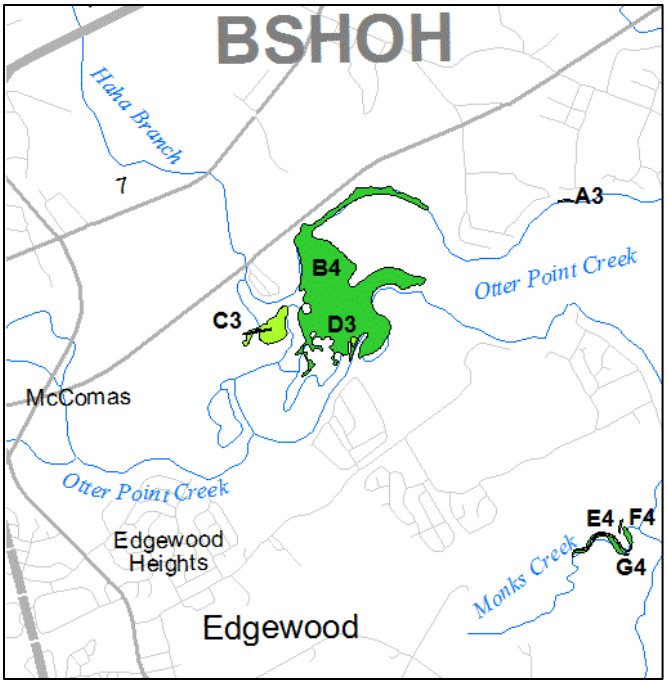

Figure 72 Subset of Otter Point Creek showing in detail the location of the hydrilla canopy as D3 and D4 (Source: VIMS 2005)

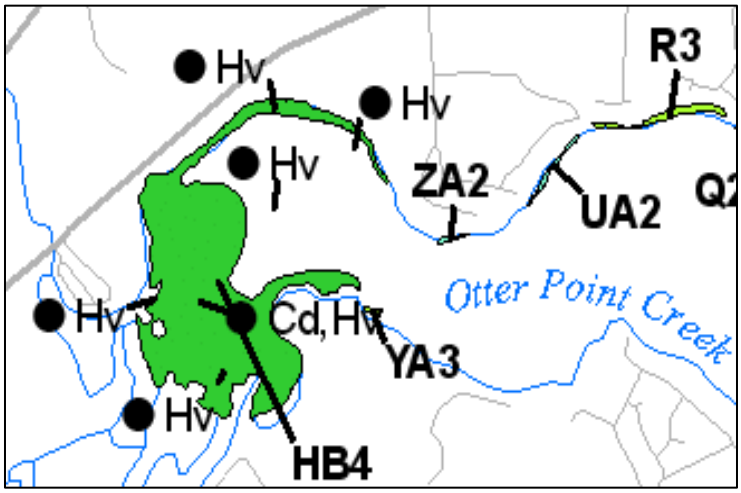

Figure 73 Subset of Otter Point Creek showing in detail the location of the hydrilla canopy indicated by HB4. HV- hydrilla, Cd -Elodeas Canadensis, Nm- Najas Minor (VIMS 2005)

Maryland Department of Natural Resources has collected reference values of aquatic species in the Otter Point Creek from 2007 to 2011. The dominant species at OPC has been hydrilla. Few other species were present during the data collection effort (Delgado 2011).

7.8 Accuracy assessment of Hyperion and AISA images

Accuracy is determined empirically by selecting a sample of pixels from the thematic map and checking their labels against classes determined from the ground measurements. From these checks, the percentage of pixels from each class in the image labeled correctly by the classifier can be estimated along with the proportions of pixels from each class erroneously labeled as other classes. Accuracy assessments determine the quality of the information derived from remotely sensed data (Congalton and Green, 2009**)**. Assessments can be either qualitative or quantitative. For qualitative assessments, a map is visually looked at to see whether the image is right or not by comparing what is seen on the image with the ground. This analysis is done in a very straightforward way. Qualitative assessment attempts to identify and measure remote sensing-based error. In this assessment, the reference data is compared to the ground truth data.

ENVI® Version 4.8 calculated the Confusion Matrix using the ground truth image or ground truth ROI's. Adding up the number of pixels that are correctly classified and dividing it by the total number of pixels calculate the Overall Accuracy. The ground truth image or ground ROI's define the true class of the pixels. The pixels that were correctly classified are found along the diagonal of the Confusion Matrix table that lists

the number of pixels that were classified into the correct ground truth classes. The Producer's Accuracy relates to the probability that a reference sample photo is correctly mapped and measures the error of omission. This User's Accuracy indicates the probability that a sample from a map actually matches the reference data (photo) and measures the error of commission (Congalton and Green, 2009). Another measure of classification accuracy is the Kappa Coefficient (k) which is calculated by multiplying the total number of pixels in all the ground measurement cases by the sum of the Confusion Matrix diagonals, subtracting the sum of the ground truth pixels in a class multiplied by the sum of the classified pixels in that class. The Overall Accuracy of the Hyperion image using ENVI classification image was 54.36 % with a Kappa Coefficient of 0.27 and the Overall Accuracy of the AISA image was 49.35% with a Kappa Coefficient of 0.36.

7.10.5 Summary Results of Hyperion and AISA images

The Hyperion classification image had Overall Accuracy of 54.36% and a Kappa value of 0.27. For classification of the Hyperion image, the only classification method realistic enough to quantify with an accuracy assessment was the SAM classification using MNF transformed bands. The AISA classification image had Overall Accuracy of 49.35 % and a Kappa value of 0.36. For classification of the AISA image, the only classification method realistic enough to quantify with an accuracy assessment was the SAM classification using MNF transformed bands. The Hyperion accuracy was

influenced by noise, which is considered a tradeoff for minimizing the risk of committing an error of omission.

CHAPTER EIGHT: CONCLUSIONS AND DISCUSSIONS FOR THEINSITU FIELD MEASUREMENTS, HYPERION SENSOR, AND AISA SENSOR

8.1 Conclusions

This study arrived at several conclusions first of all that the spectral signatures collected in situ from the experimental hydrilla tank and the field settings can be utilized to determine whether the hydrilla canopies resulting from the identification and classification using the hyperspectral sensors are either floating or submerged. The spectral library was necessary to approximately match the spectral signatures from the tank and the field measurements with the spectra collected from the remote sensors.

The Spectral Hourglass Workflow in ENVI performed very well thru the different algorithms and classification method for the Hyperion and the AISA sensor. The spectral profile resulting from the SAM classification determined that the Hydrilla canopies were floating on the water surface since the reflectance of the mat was higher than the established threshold of 10% surface reflectance. During the processing of the Minimum Noise Fraction Transform it was concluded that the spectral profile was compared with results from other researchers and it was determined that a Cyanobacteria (blue-green algae) was present in the algae-laden waters. The accuracy assessment showed that hydrilla had a close overall accuracy for the Hyperion image and the AISA image.

Results from this study demonstrate that spaceborne and airborne hyperspectral imagery can be very useful data sources for distinguishing homogenous canopies of

hydrilla. The Spectral Hourglass Wizard can be used for mapping other invasive and non-invasive aquatic species. The Minimum Noise Fraction Transform with spatially coherent MNF bands is sufficient for identifying the location of hydrilla in the image. The SAM classification and spectral profile performed well, but these results are dependent only for Case 2 waters such as in coastal estuaries that have very productive waters.

It was also concluded that the spectral profiles from the AISA and Hyperion images matched closely with the spectral signatures collected from the experimental hydrilla tanks. Cyanobacteria (blue –green algae) was identified from the MNF spectral profile from both remote sensors. Therefore, the Hyperion and AISA sensors can identify not only algae blooms, but also hydrilla canopies in productive waters.

Validation of the satellite and airborne hyperspectral images with in situ field measurements, aerial photos, and ground surveys verified and valida the extent and the location of the hydrilla canopy at Otter Point Creek estuary. The SAM classification images from the Hyperion and AISA sensors when validated with surface area collected by VIMS and the surveys from the MDDNR for the years 2005 to 2011 concluded that hydrilla was the dominant aquatic vegetation in the estuary.

This research for the first time collected Hydrilla signatures from a satellite sensor, an airborne sensor, a ground truth site and aerial photography over the same site. Hydrilla spectral signatures were also collected at an experimental research tank in the immediate area. This provided a unique opportunity to compare and analyze these signatures and other sources of information about hydrilla in this area of Chesapeake Bay. The spectral

signatures that were taken and analyzed in this study are included in the spectral library that was also developed under this research and is housed at George Mason University.

8.2 Discussion

Hyperspectral imaging techniques are an important tool for identifying and classifying submergent or emergent aquatic vegetation. Hyperspectral imaging can assess the environmental and ecological impacts by non-native aquatic vegetation because changes in climate can be detected.

A very interesting finding during the image processing was the collection of endmember spectra, which resulted in the identification of cyanobacteria (blue-green algae). The analysis determined that the cyanobacteria curve had a higher reflectance of 19% than the hydrilla canopy of 14% for the Hyperion and AISA images. The spectral Z profiles of the Hyperion true color image was compared to the AISA image for determining that the spectra reflectance declined as the wavelength increases which could be interpreted as the hydrilla canopy being submerged. Once the light penetrates the water column it attenuates and reaches the submerged aquatic vegetation the reflectance increases. This is a typical reflectance curve in algae-laden waters. Algae-laden waters spectra behave similarly to the cyanobacteria curve at a wavelength of 550 nm. However, the AISA spectral profile derived different spectral signatures with higher surface reflectance of 20% in the NIR. The hydrilla canopy was emergent at low tide conditions. The SAM results from the Hyperion sensor generated a reflectance of over 20% at the "Red Edge" (680 – 760 nm), which compares very favorably with the spectral profiles

extracted from the AISA image. Both SAM results were compared with the spectral library plots from the reference data in the experimental tank and from the estuary and it can be concluded that the spectral signatures match with some slight differences in the NIR (15 to 26 %). From these results, it can also be concluded that the homogenous hydrilla canopy was emergent at the time the sensor flew over the site. Both sensors validated the spectral signatures of the tank and field measurements, which was one of the main objectives of this research.

Accuracy assessment was performed for both images using the Confusion Matrix or Error Matrices. The AISA image gave an Overall Accuracy of 49% with a Kappa Coefficient; however, the Hyperion image was not as accurate as the AISA image, with Overall Accuracy of 54.36% and a Kappa Coefficient of 0.27. Hydrilla had very good accuracies because of the uniformity of the canopies and because the training pixels were homogenous. The blue-green algae detected could have been confused spectrally with hydrilla in the Hyperion image resulting in lower accuracy. The water column exerts a strong effect in the signal where absorption and scattering water column is higher. With the AISA sensor all of the 97 bands were usable with very little noise; however, the Hyperion image did have calibration issues, and noise so the accuracies were lower than the AISA image. Hyperion flies at a higher altitude than the AISA which affects the signal to noise ratio.

The spatial-temporal differences were due to several factors which controlled the timing between the collection of the in situ measurements and the satellite and airborne flyovers:

The NASA flight schedule for the Hyperion sensor was not controllable because the satellite needed to be tasked by GSFC at a time with no cloud cover.

The image over the study area needed to be acquired under low tides and calm surface conditions and when the sun angles are low enough to avoid sunglint.

The spectrometer provided was not calibrated, so another calibrated instrument needed to be obtained from USGS and it needed to be operated by experienced personnel. The personnel were not always available and it took two (2) years to secure the instrument.

There were problems with the weather and the flyover by Hyperion. The flyover needed to be tasked by NASA weather permitting. Different dates had to be coordinated with NASA.

The only airborne image collected of the study area was in July 13, 2005 by the University of Nebraska

Since hydrilla has the same basic spectral characteristics because all vegetation are composed of the same types of biochemical pigments, water, cellulose, etc. Leaf spectra are dominated by the influence of four (4) variables: photosynthetic pigments, water, dry matter, and structural parameter related to leaf thickness. The phenological characteristics do not change from year to year.

The results from this study should be of interest to many scientists and water resource managers that have an interest in using cost effective techniques to identify and map hydrilla infestation in the aquatic environments, as well as alarming environmental agencies of possible harmful algae blooms.

The author recommends several areas for future work:

- Incorporate bathymetric measuring system such as LIDAR for determining depth with spectral reflectance
- Develop a spectral library for different aquatic vegetation species in the study areas at different times during the growing season.
- Synchronize the field measurements with hyperspectral sensor's overpass of the study area.
- Determine changes in hydrilla using historical aerial images from VIMS and collecting hyperspectral images for the same period in order to detect changes in the shallow and the deeper areas of the study area.
- Focus on the selection of sample types in the design of the sampling study in order to capture a substantial amount of variability in environmental conditions.

The best classification methods identified for one site may not perform the best for other sites. Therefore, it is always necessary to evaluate different image processing and classification techniques in order to obtain the best classification results. It is important to know that the ground spectra collected by the ASD instrument collects true pixels as it is held close to the hydrilla mat.

The next step is to test the feasibility of the ENVI software using other classification techniques such as Mixture Tuned Match Filtering, Linear Unmixing Spectral Feature Fitting (SFF), Linear Spectral Unmixing, and Matched Filtering covering different aquatic species over a large spatial area. Reference spectra should be collected at the same time of the sensor flyover. Reference spectra should be collected at

different times, place and solar conditions for examining several factors that can influence the spectral characteristics of other aquatic species.

Future work should evaluate other ENVI Workflows such as Target Detection Wizard and THOR, as well as other subpixel analysis techniques.

REFERENCES

Agrawal, G. and J. Sarup. "Comparison of QUAC and FLAASH atmospheric correction modules on EO-1 Hyperion data of Sanchi." *International Journal of Advanced Engineering Sciences and Technologies* 4 (2001): 178– 186.

Analytical Spectral Devices. "Spectral Solutions." Boulder, Colorado. *ASD, Inc*, 2011. Web. 12 February 2013 <http://www.asdi.com/>.

Armstrong, R. "Remote sensing of submerged vegetation canopies for biomass estimation." *International Journal of Remote Sensing* 14 (1993): 621–627.

Asner, G. P., and K. B. Heidebrecht. "Spectral unmixing of vegetation, soil and dry carbon cover in arid regions: comparing multispectral and hyperspectral observations." *International Journal of Remote Sensing* 23 (2002): 3939−3958.

Batiuk, R., P. Heasley, R. Orth, K. Moore, J. Capelli, J. C. Stevenson, W. Dennison, L.Staver, V. Carter, N. Rybicki, R. E. Hickman, S. Kollar, and S. Bieber. *Chesapeake Bay submerged aquatic vegetation habitat and restoration goals: a technical synthesis*. Annapolis, Maryland: U.S. Environmental Protection Agency Chesapeake Bay Program Report, 2000.

Becker B. L., D. P. Lusch, and J. Qi. "Identifying optimal spectral bands from in- situ measurements of Great Lakes costal wetlands using second derivative analysis." *Remote Sensing of the Environment* 97 (2005): 238-248.

Blackburn, R. D., L. W. Weldon, R. R. Yeo, and T. M. Taylor. "Identification and distribution of certain similar appearing submersed aquatic weeds in Florida." *Hyacinth Control Journal* (1969).

Blanco A. F., J. J. Qu, and W. E. Roper. "Spectral signatures of hydrilla from a tank and field setting." *Frontiers of Earth Science* 6 (2012): 453-460.

Boardman, J. W. "Automated spectral unmixing of AVIRIS data using convex geometry concepts: in summaries." *Fourth JPL Airborne Geoscience Workshop* (1994).

Boardman, J. W., and Kruse, F. A., 1994, Automated spectral analysis: A geological example using AVIRIS data, northern Grapevine Mountains, Nevada: in Proceedings, Tenth Thematic Conference, Geologic Remote Sensing, 9-12 May 1994, San Antonio, Texas, p. I-407 - I-418.

Boardman, J. W., and Kruse, F.A., 2011, Analysis of Imaging Spectrometer Data Using N-Dimensional Geometry and A Mixture-Tuned Matched Filtering (MTMF) Approach: in Special Issue on Spectral Unmixing of Remotely Sensed Data, Transactions on Geoscience and Remote Sensing (TGARS), IEEE, 2011.

Bukata R. P. "Satellite monitoring of inland and coastal water quality, retrospection, introspection, and future directions." National Water Research Institute. Ontario, Canada: Taylor and Francis, 2005: 53.

Bukata. R. P., J. H. Jerome, K.Y. Kondratyo, and D. V. Pozdrvehov. *Optical Properties and Remote Sensing of Inland and Coastal Waters*. New York: CRC Press, 1995: 362.

Carter, G. A. "Response of leaf spectral reflectance to plant stress." *American Journal of Botany* 80, 3 (1993): 2310-243.

Carter, G. A., W. G. Cibula, and R. L. Miller. " Narrow band reflectance imaging compared with thermal imagery for early detection of plant stress." *Journal of Plant Physiology* 148 (1996): 515-522.

Carter, V., C. J. Johannsen, ed., and J. L. Sanders, ed. "Application of remote sensing to wetlands." *Remote Sensing in Resource Management,* Soil Conservation Society of America (1982): 284–300.

Center for the Study of Earth from Space (CSES) SIPS User's Guide, The Spectral Image Processing System, v.11. University of Colorado, Boulder: 2002: 74.

Chadwell, T. B. and K. Engelhard. **"**Effects of pre-existing submerged vegetation and propagules pressure on the invasion success of *Hydrilla verticillata*." *Journal of Applied Ecology* 45 (2008): 515–523.

Chauvaud, L., F. Jean, O. Ragueneau, and G. Thouzeau. "Long-term variation of the Bay of Brest ecosystem: benthic-pelagic coupling revisited." *Marine Ecology Progress Series* 200 (2000): 35-48.

Chen, C.M. "Comparison of principal component analysis and minimum noise fraction transformation for reducing the dimensionality of hyperspectral imagery." *Geographical Research* 33 (2000): 163–178.

Chesapeake Bay Submerged Aquatic Vegetation Water Quality and Habitat-Based Requirements and Restoration Targets: A Second Technical Synthesis. Chesapeake Bay Program, August 2000.

Ciraolo, G., E. Cox, G. La Loggia, and A. Maltese. "The classification of submerged vegetation using hyperspectral MIVIS data." *Annals of Geophysics* 49, issue 1 (2003): 287-294.

Congalton, R.G.; Green, K. *Assessing the accuracy of remotely sensed data: principles and practices*. Boca Raton, FL: CRC Press: 2009: 177.

Dekker, A. G., V. E. Brando, J. M. Anstee, N. Pinnel, T. Kutser, H. J. Hoogenboon, S. W. M. Peters, R. Pasterkamp, R. J. Vos, C. Olbert, and T. J. Malthus. *Imaging Spectrometry: Basic Principles and Prospective Applications IV*. Dordrecht: Kluwer Academic Publishers (2001): 307-359.

Delgado, P. "Chesapeake Bay Maryland National Estuarine Research Reserve." *Maryland Department of Natural Resources* 2 (2011): 47.

Dennison, W. C., R. J. Orth, K. A. Moore, J. C. Stevenson, V. Carter, S. Kollar, P. W. Bergstrom, and R. A. Batiuk. "Assessing water quality with submerged aquatic vegetation requirements as barometric of Chesapeake Bay health." *Bioscience* 43, issue 2 (1993): 87–94.

Dierssen, H., R. Zimmerman, R. Leathers, T. Downes, and C. Davis. "Remote sensing of seagrass and bathymetry in the Bahamas banks using high-resolution airborne imagery." *Limnology Oceanography* 48 (2003): 444–455..

DiPietro, D., S. L Ustin, E. C. Underwood, K. Olmstead, and G. J. Scheer. "Mapping the invasive riparian weed arundo donax (giant reed) using AVIRIS." *The Eleventh Annual JPL Airborne Visible Infrared Imaging Spectrometer (AVIRIS) Workshop* (2002). Jet Propulsion Laboratory, Pasadena, California.

ENVI Tutorial. *ITT Exelis* Boulder, Colorado, USA. ENVI, 2008.

EPA-903-R-07-005, Ambient Water Quality Criteria for Dissolved Oxygen Water Clarity and Chlorophyll for the Chesapeake Bay , CBP/TRS 288/07, Nov. 2007

Everitt, J. H., C. Yang, and C. J. Deloach. "Comparison of Quickbird and SPOT 5 satellite imagery for mapping giant reed." *Journal of Aquatic Plant Management* 46 (2008): 77-82.

Executive Order 13112 on Invasive Species. *Federal Register: Presidential Documents.* 64(25), (1999): 6183-6186.

Felde, G. W., G. P. Anderson, T. W. Cooley, M. W. Matthew, S. M. Adler-Golden, A. Berk, and J. Lee. "Analysis of Hyperion data with the FLAASH atmospheric correction algorithm." *IEEE Transactions on Geoscience and Remote Sensing* (2003): 90–92.

Gausman, H. W., W. A. Allen, R. Cardenas. "Reflectance of cotton leaves and their structure." *Remote Sensing of the Environment* 1 (1969): 110-22.

Gitelson, A. A. "The Peak Near 400 nm on Radiance Spectra of Algae and Water: Relationships of its magnitude and position with chlorophyll concentration." *International Journal of Remote Sensing* 13 (1992): 3367-3373.

Gitelson, A. A., J. F. Schalles, D. C. Rundquist, F. R. Schiebe, and Y. Yacobi. "Comparative reflectance properties of algal cultures with manipulated densities." *Journal of Applied Phycology* 11 (1999): 345-354.

Gitelson, A., Y. Yacobi, J. Schalles, D. Rundquist, L. Han, R. Stark, and D. Etzion. "Remote estimation of phytoplankton density in productive waters." *Archives of Hydrobiology: Advances in Limnology* 55 (2000): 121-136.

Goetz, A.F.H., Ferri M., Kindel, B., Qu, Z. Atmospheric correction of Hyperion data and techniques for dynamic scene correction. In 2002, IEEE International Geoscience and Remote Sensing Symposium and the 24th Canadian Symposium of Remote Sensing, Toronto, Canada, June 24-28, 2002.

Green E. P., P. J. Murphy, A. J. Edwards, and C. D. Clark. *Remote Sensing Handbook for Tropical Coastal Management*. France: UNESCO, 2000.

Green R. O., M. L. Eastwood, C. M. Sarture, T. G. Chrien, M. Aronsson, B. J.Chippendale, J. A. Faust, B. E. Pavri, C. J. Chovitt, M. Solis, M. R. Olah, and O. Williams. "Imaging spectroscopy and the airborne visible/infrared imaging spectrometer (AVIRIS)." *Remote Sensing Of The Environment* 65,3 (1998): 227-248t.

Haller, W.T. "Hydrilla goes to Washington." *Aquatics* 4, issue 4 (1982): 6-7.

Han, L., and D. Rundquist. "The spectral responses of *Ceratophyllum demersum* at varying depths in an experimental tank." *International Journal of Remote Sensing* 24,4 (2003): 859-864.

Han, L. “Spectral reflectance of *Thalassia testudinum* at varying depths.” *IEEE* (2002): 2123-2125.

Holcombe, R. G., ed. *15 Great Austrian Economists*. Auburn, Ala: Ludwig von Mises Institute (1999).

ITT-Exelis Inc., The Environment for Visualizing Images. ENVI Users Guide, Version 4.8, 2008.

ITT Visual Information Solutions, (2007), Environmental Research Systems Institute

Jakubauskas, M., K. Kindscher, A. Fraser, D. Debinski, and K. P. Price. “Close range remote sensing of aquatic macrophyte vegetation cover.” *International Journal of Remote Sensing* 21,18 (2000): 3533-3538.

Jakubauskas, M. E., D. L. Peterson, S. W. Campbell, F. deNoyelles, S. D. Campbell, and D. Penny. “Mapping and monitoring invasive aquatic plant obstructions in navigable waterways using satellite multispectral imagery.” *FIEOS 2002 Conference Proceedings.*

Jensen, John R. *Remote Sensing of the Environment, an earth resource prospective*. Prentice Hall Series in Geographic Information System, 1995. ISBN-10: 0131453610

Jensen, J. R., M. Hodgeson, and E. Christensen. “Remote sensing inland wetlands: a multispectral approach.” *Photogrammetric Engineering and Remote Sensing* 52, issue 1 (1986): 87-100.

Jensen, John. “Introductory digital image processing.” *A Remote Sensing Perspective, 3rd edition*. Prentice Hall, 2005.

Junk, W. J., ed. *The Central Amazon Floodplain: Ecology of a Pulsing System*. Springer, Berlin: 147–186.

Jupp, D. L., B. Datt, J. Lovell, S. Campbell, and E. King. “Discussions around Hyperion data: background notes for the Hyperion data users workshop.” *CSIRO Office of Space Science and Applications, Earth Observation Center.* Canberra, Australia. (2002).

Jupp, D. L., K. K. Mayo, D. A. Kuchler, D. V. Classen, R. A. Kenchington, and P. R. Guerin. “Remote Sensing for Planning and Managing the Great Barrier Reef of Australia.” *Photogrammetria* 40, issue 1 (1985): 21-42.

Kemp, M. W., R. Batleson, P. Bergstrom, V. Carter, C. L. Gallegos, W. Hunley, L. Karrh, E. W. Koch, J. M. Landwehr, K. A. Moore, L. Murray, M. Naylor, N. B. Rybicki, S. J. Court, D. Wilcox. "Habitat requirements for submerged aquatic vegetation in Chesapeake Bay: water quality, light regime, and physical-chemical factors." *Estuaries* 27 (2004): 363–377.

Keshara, N. and J. F. Mustard. "Spectral Unmixing." *IEEE Signal Processing Magazine* 19 **(**2002): 44–57.

Kim, M.S., C. S. T. Daughtry, E. W. Chapelle. The use of high spectral resolution bands for estimating absorbed photosynthetically active radiation (Apar.). In: *Proceedings of the Sixth Symposium on Physical Measurements and Signatures in Remote Sensing.* January 17–21, Val D' Isure, France (1994): 299.

Kirk, Jto. *Light and photosynthesis in aquatic systems.* 2nd edition. Cambridge: Cambridge University Press (1994): 528.

Klaver, C. C. *A/Moral Economics: Classical Political Economy and Cultural Authority in Nineteenth-Century England*. Columbus: Ohio State University Press (2003).

Kutser, T. "Quantitative detection of chlorophyll in cyanobacteria blooms by satellite remote sensing." *Limnology and Oceanography* volume 49, issue 6 (2004): 2179-2189.

Kruse, F. A., W. Boardman, J. F. Huntington. "Evaluation and validation of EO-1 Hyperion for mineral mapping." *IEEE Trans. Geosci. Remote Sensing* 41 (2003): 1388-1400.

Kruse, F. A., J. W. Boardman, A. B. Lefkoff, K. B. Heidebrecht, A. T. Shapiro, P. J. Barloon, A. F. H. Goetz. "The spectral image processing systems (SIPS) interactive visualization and analysis of imaging spectrometer data." *Remote Sensing of the Environment* 44 (1993): 145–163.

Labsphere Spectralon. "Labsphere, Inc. Homepage." Web. 2013. <http://www.labsphere.com>.

Laba, M., R. Downs, S. Smith, S. Welsh, C. Neider, S. White, M. Richmond, W. Philpot, and P. Baveye. "Mapping invasive wetland plants in the Hudson River National Estuarine Research Reserve using quickbird satellite imagery." *Remote Sensing of Environment* 112 (2008): 286-300.

Langeland, K.A. Hydrilla verticillata (L.F.) Royle (Hydrocharitaceae), "The perfect aquatic weed". *Castanea* 61 (1996): 293-304.

Lathrop, R. G., P. Montesano, and S. Haag. "A multiscale segmentation approach to mapping seagrass habitats using airborne digital camera imaging." *Photogrammetry Engineering Remote Sensing* 72 (2006): 665-675.

Lass, L. W., T. S. Prather, N. F. Glenn, K. T. Weber, J. T. Mundt, and J. Pettingill. "A review of remote sensing of invasive weeds and example of early detection of spotted knapweed (*Centaurea maculosa*) and baby breath (*Gypsophila paniculata*) with a hyperspectral sensor." *Weed Science* 53 (2005): 242–251.

Lillesand, T. and R. Kiefer. *Remote Sensing and Image Interpretation 4th Edition*. John Wiley & Sons Inc., 1999. ISBN 0-471-25515-7.

Lillesand, T. M., R. W. Kiefer, and J. W. Chipman. *Remote Sensing and ImageInterpretation, 6th edition*. John Wiley and Sons, New York, NY, USA, 2008.

Lin, Y. and Z. Liquan. "Identification of the spectral characteristics of submerged plant Vallisnera spiralisis." *Acta Ecologia Sinica* 26 (2006): 1005-1011.

Lobo, F. L., C. C. Barbosa, E. M. M. L. Novo, and J. S. Yunes.Mapping potential cyanobacterial bloom using Hyperion/EO-1 data in Patos Lagoon estuary. *Acta Limnology*. Bras, Vol. 21, No. 3 (2009): 299-308.

Madden, M. "Remote Sensing and Geographic Information System Operations for Vegetation Mapping of Invasive Exotics." *Weed Technology* 18 (2004): 1457-1463.

Marshall, T., and P. F. Lee. "Mapping aquatic macrophytes through digital image analysis of aerial photographs: an assessment." *Journal of Aquatic Plant Management* 32 (1994): 61-66.

Maryland Department of Natural Resources DNR Pub: 12-723 2006 Water Quality Newsletter Bush River, MD 2007-230 August 2007.

Malthus T. J., and D. G. George. "Airborne Remote Sensing of Macrophytes in Cefni Reservoir, Anglesey, UK." *Aquatic Botany* 58, 3-4 (1997): 317-332.

Moore K. A., R. J. Orth, and D. Wilcox. *Assessment of Submersed Aquatic Vegetation (SAV) Communities in the Chesapeake Bay*. Gloucester Point ,VA: Virginia Institute of Marine Science, College of William and Mary (2009): 233-257.

Moore K.A., R. J. Orth, and D. Wilcox. *Analysis of the Abundance of Submersed Aquatic Vegetation Communities in the Chesapeake Bay, Estuaries* 23 (2000): 115-127.

Mumby, P., E. Green, A. Edwards, C. and Clark. "Measurement of Seagrass Standing Crop Using Satellite and Digital Airborne Remote Sensing." *Marine Ecology. Progress Series* 159 (1997): 51–60.

Naylor M., N. B. Rybicki, J. Court Stevenson, D. J. Wilcox. "*Habitat requirements for submerged aquatic vegetation in Chesapeake Bay: water quality, light regime, and physical-chemical factors*." Estuaries 27, 3 (2004): 363–377.

Nelson, S. A. C., K. S. Cheruvelil, and P. Soranno. "Satellite Remote Sensing of Freshwater Macrophytes and the Influence of Water Clarity." *Aquatic Botany* 85 (2006): 289-298.

Nikolakopoulos G. K., D. A. Vaiopoulos, and G. A. Skianis. "A Preliminary approach on the use of Satellite hyperspectral data for geological mapping." *Proceedings of the 11th International Congress*. Athens: Bulletin of the Geological Society of Greece, 2007.

Olmanson, L. G., M. E. Bauer, and P. L. Brezonik. "Aquatic Vegetation Surveys Using High-Resolution IKONOS Imagery." *FIEOS 2002 Conference Proceedings*.

Onaindia. M., B. G. Bikuna, I. Benito. "*Aquatic Plants in Relation to Environmental Factors in Northern Spain.*" Journal of Environmental Management 47, 2 (1996): 123–137. doi.org/10.1006/jema.1996.0041

Orth, R. J. and K. A. Moore. "Submerged Vascular Plants: Techniques for Analyzing Their Distribution and Abundance." *Marine Technology Society Journal* 17, 2 (1983): 38-52.

Orth, R. J., K. A. Moore, and H. H. Gordon. *Distribution and Abundance of Submerged Aquatic Vegetation in the Lower Chesapeake Bay, Virginia*. Final Report to U.S. EPA, Chesapeake Bay Program, Annapolis, MD: 1979. EPA-600/8–79–029/SAV1

Ozesmi, S. L., and M. E. Bauer. "Satellite Remote Sensing of Wetlands." *Wetlands Ecology and Management* 10 (2002): 381- 402.

Paine, D. P. "Aerial photography and image interpretation for resource management." New York: John Wiley & Sons, 1981.

Pasternack G. B., and L. A. Hinnov. "Hydrometeorological controls on water level in a vegetated Chesapeake Bay tidal freshwater delta." *Estuary Coastal Shelf Science* 58, 2 (2003): 367–387

Pearlman, J. S., P.S. Barry, C. C. Segal, J. Shepanski, D. Berso, and S. L. Carman. "Hyperion a space based imaging spectrometer.*" IEEE Trans Geoscience Remote Sensing* 41 (2003): 1160–1173.

Personal Communication February 15,2011 from Richard Perk CHAMP Program Manager CALMIT Hyperspectral Airborne Monitoring Program, University of Nebraska, Center for Advanced Land Management Information Technologies (CALMIT).

Pengra, W. Bruce, Carol A. Johnston, Thomas R. Loveland. "Mapping an Invasive Plant, Phragmites Australis, in Coastal Wetlands Using the EO-1 AVIRIS Hyperspectral Sensor." *Remote Sensing of the Environment* 108 (2007): 74-81.

Peñuelas, J., J. A. Gamon, K. L. Griffin, and C. B. Field. "Assessing Community Type, Plant Biomass, Pigment Composition and Photosynthetic Efficiency of Aquatic Vegetation from Spectral Reflectance." *Remote Sensing of the Environment* 46 (1993): 110-118.

Peterson, D.L., and S. W. Running S.W. "Applications in Forest Science and management." *Theory and Applications of Optical Remote Sensing*. New York: John Wiley & Sons (1989): 4210-473.

Pimentel, D., L. Lach, R. Zuniga, and D. Morrison. "*Environmental and economic costs of nonindigenous species in the United States.*" Bioscience 50 (2000): 53-65.

Pinnel, N., T. Heege, and S. Zimmermann. "Spectral Discrimination of Submerged Macrophytes in Lakes Using Hyperspectral Remote Sensing Data." *SPIE Proceedings Ocean Optics XVII* (2004). 1-15.

Richardson, L. L. "Remote sensing of algal bloom dynamics." *BioScience* 46 (1996): 492-501.

Rouse J. W., R. H. Haas, J. A. Schell, D. W. Deering, J. C. Harlan. Monitoring the Vernal Advancements and Retrogradation of Natural Vegetation. In: *NASA/GSFC,Final Report*. Greenbelt, USA (1974): 1–137.

Rowan, K. S. *Photosynthetic Pigments of Algae.* Cambridge: Cambridge University Press, 1989.

Rulon E. Simmons, Stephanie Vermillion, and James Coss. *Water Quality Monitoring with Hyperspectral Imaging, Final Report*. Contract NAS13-98080.

Rundquist, D. C., L. Han, J. F. Schalles, and J. S. Peake. "Remote measurement of algal chlorophyll in surface waters: the case for the first derivative of reflectance near 690 nm." *Photogrammetric Engineering & Remote Sensing* 62 (1996): 195-200.

Rundquist, D.C., J.F. Schallis and J.S. Peake. "The response of volume reflectance to algae concentration above bright and dark bottom at various depth in an experimental pool." *Geocarta International* 10 (1995): 5-14.

SAV in Chesapeake Bay and Coastal Bays. "Monitoring 2011 Report." Virginia Institute of Marine Science. *William and Mary*, 2011. Web. 12 February 2013 <http://web.vims.edu/bio/sav/sav11/quads/ed007th.html?svr=www>.

Sawaya, K. E., L. G. Olmanson, N. J. Heinert, P. L. Brezonik, and M. E. Bauer. "Extending Satellite Remote Sensing to Local Scales: Land and Water Resource Monitoring Using High-Resolution Imagery." *Remote Sensing of Environment* 88 (2003): 144-156.

Schalles, J. F., and Yacobi, Y. Z. "Remote detection and seasonal patterns of phycocyanin, carotenoid and chlorophyll pigments in eutrophic waters." *Archive for Hydrobiologie Special Issues Advancements in Limnology* 55 (2000): 153-168.

Schmidt, K. S. and A. K. Skidmore. "Spectral Discrimination of Vegetation Types in a Coastal Wetland." *Remote Sensing of the Environment* 85 (2003): 92-108.

Schmitz, D. C., B. V. Nelson, L. E Nall, and J. D. Schardt. "Exotic aquatic plants in Florida: a historical perspective and review of the present aquatic plant regulation program." In: *Proceedings of the Symposium on Exotic Pest plants*. T.D. Center, R.F. Doren, R.L. Hofstetter, R.L. Myers and L.D. Whittaker, eds. US Department of the Interior /National Park Service, Denver. (1991): 387.

Sheppert P, Introduction to Hyperspectral Images, http://www.microimages.com/getstart/pdf/hyprspec.pdf

Shuman, C. S., and R. F. Ambrose. "A Comparison of Remote Sensing and Ground-Based Methods for Monitoring Wetland Restoration Success." *Restoration Ecology* 11,3 (2003): 325-333.

Silva S. F. T, Costa P.F. M, Melack J.M, Novo M.L.M. E. "Remote sensing of aquatic vegetation: theory and applications." *Environmental Monitoring Assessment* 140 (2008): 131-145.

Staenz K., and P. M. Teillet. "Effects of spectral, spatial and radiometric characteristics on remote sensing vegetation indices Canada Centre for Remote Sensing." Ontario, Canada: Williams MacDonald Dettwiler and Associates Ltd.

Underwood, E., S. Ustin, and D. DiPietro. "Mapping Nonnative Plants Using Hyperspectral Imagery." *Remote Sensing of Environment* 86 (2003): 150-161.

Underwood, E., M. J. Mulitsch, J. A. Greenberg, M. L. Whiting, S. L. Ustin, and S. C. Kefauver. "Mapping Invasive Aquatic Vegetation in the Sacramento-San Joaquin Delta Using Hyperspectral Imagery." *Environmental Monitoring and Assessment* 121 (2006): 47-64.

Underwood, Nelson S. A. C., K. S. Cheruvelil, and P. Soranno. "Satellite Remote Sensing of Freshwater Macrophytes and the Influence of Water Clarity." *Aquatic Botany* 85 (2006): 289-298.

The U.S. Geological Survey, Digital Spectral Library: Version 1: 0.2 to 3 Microns. In: U.S. Geological Survey Open File Report 93–592, U.S. Geological Survey, Reston, USA. <http://speclab.cr.usgs.gov>

U.S. Geological Survey. "Earth Observing Mission 1." *NASA*, 2004. Web. 12 February 2013. <http://earthexplorer.usgs.gov>

U.S. Geological Survey. "EarthExplorer." *USGS Earth Resources Observation and Science Center*, 2012. Web. 12 February 2013. <http://earthexplorer.usgs.gov>.

Valta-Hulkkonen, K., A. Kanninen, and P. Pellikka. "Remote Sensing and GIS for Detecting Changes in the Aquatic Vegetation of a Rehabilitated Lake." *International Journal of Remote Sensing* 25,24 (2004): 5745-5758.

Valta-Hulkkonen, K., A. Kanninen, R. Ilvonen, and J. Leka. 2005. Assessment of aerial photography as a method for monitoring aquatic vegetation in lakes of varying tropic status. *Boreal Environment Research.* 10: 57-66.

Van, T. K. Wheeler G. S., and T. D. Center, Competitive Interactions between Hydrilla (Hydrilla verticillata) and Vallisneria (Vallisneria americana) as Influenced by Insect, 1998, Herbivory. Biological control 11, 185–192.

Vane G., R. O. Green, T. G. Chrien, H. T. Enmark, E. G. Hansen, W. M. Porter. "The Airborne Visible/Infrared Imaging Spectrometer (AVIRIS)." *Remote Sensing of the Environment* 44, 2-3 (1993): 127-143.

Valta-Hulkkonen, K., A. Kanninen, R. Ilvonen, and J. Leka. "Assessment of Aerial Photography as a Method for Monitoring Aquatic Vegetation in Lakes of Varying Tropic Status." *Boreal Environment Research* 10 (2005): 57-66.

Vincent, R. K., X. Qin, R. M. McKay, J. Miner, K. Czajkowski, and J. Savino. "Phyocyanin detection from Landsat TM data for mapping cyanobacteria blooms in Lake Erie." *Remote Sensing of the Environment* 89 (2004): 381-392.

Vis, C., C. Hudon, and R. Carignan. "An Evaluation of Approaches Used to Determine the Distribution and Biomass of Emergent and Submerged Aquatic Macrophytes Over Large Spatial Scales." *Aquatic Botany* 77 (2003): 187-201.

Washington Suburban Sanitary District, photo provided by Walter Bailey.

Werdell, J. P., and C. S. Roesler. "Remote Assessment of Benthic Substrate Composition in Shallow Waters Using Multispectral Reflectance." *Limnology and Oceanography* 48, Part 1 and 2 (2006): 557-567.

Wilcox, J. D., J. R. Orth, R. J. Whiting, K. A. Kenneth, L. A. Owens, and S. L. Nagey. "Final Report: Evaluation of color imagery and direct referencing for mapping submersed aquatic vegetation in Chesapeake Bay." *Virginia Institute of Marine Science*. December 2009.

Williams, D. J., N. B. Rybicki, A. V. Lombana, T. M. O'Brien, and R. B. Gomez. "Preliminary Investigation of Submerged Aquatic Vegetation Mapping Using Hyperspectral Remote Sensing." *Environmental Monitoring Assessment* 81 (2003): 383-392.

Williams, A.P., and E. R. Hunt Jr. "Estimation of Leafy Spurge Cover From Hyperspectral Imagery Using Mixture Tuned Matched Filtering." *Remote Sensing of the Environment* 82 (2002): 445-456.

Wolter, P. T., C. A. Johnston, and G. J. Niemi. "Mapping Submerged Aquatic Vegetation in the US Great Lakes Using Quickbird Satellite Data." *International Journal of Remote Sensing* 26, 23 (2005): 5255-5274.

Wu C. Y., Z. Niu, W. Tang. "Estimating chlorophyll content from hyperspectral vegetation indices: Modeling and validation." *Agriculture for Meteorology*, 148 (2008): 1230–1241.

Zhang, Y. “Surface Water Quality Estimation using Remote Sensing in the Gulf of Finland and the Finnish Archipelago Sea.” Report 55 (2005): 10.

Zhu, B., D. G. Fitzgerald, S. B. Hoskins, L. G. Rudstam, C. M. Mayer, and E. L. Mills. “Quantification of Historical Changes of Submerged Aquatic Vegetation Cover in Two Bays of Lake Ontario with Three Complementary Models.” *Journal of Great Lakes Research* 33 (2007): 122–135.

Yuan and Zang. “Mapping Large-scale Distribution of Submerged Aquatic Vegetation Coverage Using Remote Sensing.” *Ecological Informatics* 3, 1 (2007): 245–251.

CURRICULUM VITAE

Alfonso Blanco, P.E., is an Environmental Engineer with 38 years of domestic and international experience on Water, Wastewater, Drainage, and Flood Control projects. Mr. Blanco graduated with an Associate Degree in Mechanical Design Engineering from Wentworth Institute, Boston, Mass (1969), and a B.S. in Civil Engineering from Merrimack College in North Andover, Massachusetts (1972) concentrating in Civil and Sanitary Engineering. He obtained his Master's of Science Degree with concentration in Environmental Engineering from Tufts University in Medford, Massachusetts (1981). He has worked for nineteen years at EPA, Office of Water. He has also worked for 20 years in domestic and international consulting in the areas of planning, design, and construction management of water, wastewater, stormwater, solid, hazardous waste and bioremediation projects. He has worked throughout Latin-American countries assisting governmental entities dealing with technology transfer and loan programs for waer,wastewater, solid and hazardour wastes.

Mr. Blanco is a Ph.D Candidate at George Mason University in Fairfax, Virginia concentrating on remote sensing techniques applied to surface water quality and aquatic vegetation. Mr. Blanco has published in several journals, such as Frontiers of Earth Science, Water Environment Federation, and International Association of Environmental Applications. He is a Peer Reviewer for the Journal of Applied Remote Sensing (JARS). He has made presentations on remote sensing for the Tufts University School of Conservation Medicine and Graduate Engieneeing school, the US Army Aberdeen Proving Grounds, Water Environment Federation Technical Conference, International Association of Environmental Applications, and NASA Workshops. He is a Registered Professional Engineer in Massachusetts and Puerto Rico and also a Diplomate in Water Resources from the American Academy of Water Resources Engineers.